University of Alberta

Grid-free Facies Modelling of Inclined Heterolithic Strata in the McMurray Formation

by

Rahman Mohammad Hassanpour

A thesis submitted to the Faculty of Graduate Studies and Research
in partial fulfillment of the requirements for the degree of

Doctor of Philosophy

in

Mining Engineering

Civil and Environmental Engineering

Fall 2013
Edmonton, Alberta

To my lovely wife Shima, with love and admiration

Abstract

The McMurray Formation contains complex geological features that were partially formed in a fluvial-estuarine depositional environment. These geological features that are interrelated to each other exist with different shapes, patterns, and sizes. The inclined heterolithic strata (IHS) formed as part of kilometer scale channels contain continuous centimeter scale features that are important for flow characterization of Steam Assisted Gravity Drainage (SAGD) recovery processes. Modelling the detailed facies in such depositional systems requires a methodology that integrates the shape and size of geological architectures and reflects heterogeneity over many scales. Object-based and event-based modelling provide the framework to integrate geological architectures into geostatistical facie models however, representation of geological architectures with discretized grid would result in the loss of small scale heterogeneity. This dissertation presents algorithms and workflows on grid-free modelling that allows modelling of multi-scale geological features without relating them to a grid system. The contributions of this work include 1) the development of a stochastic object-based algorithm for modelling of tidal channelized systems, 2) the development of a grid-free object-based algorithm that allows modelling of multi-scale geological features in the McMurray Formation, and 3) the construction of a grid-free training image library for the application of McMurray Formation facies modelling. The details of algorithms and workflows are discussed. The performance of the proposed methodology is compared to conventional geostatistical modelling techniques through thermal flow simulations.

Acknowledgements

First, I would like to thank my supervisor, Dr. Clayton Deutsch, for his invaluable guidance and support throughout this work. Without him this project could not have been completed. I also gratefully acknowledge the guidance and support of Dr. Michael Pyrcz and Dr. Murray Gingras throughout my research.

Furthermore, I would like to thank my colleagues at the Centre for Computation Geostatistics (CCG) for their friendship and support on the way. I would specially like to thank Hadi, Mehdi, Behrang, Olena, Sahyun, and Yupeng.

I would like to thank the sponsors of the CCG and Enerplus Corporation for providing the financial support needed to complete this dissertation.

I would like to thank my parents, Reza and Parvaneh who supported me in all my pursuits. Most importantly, I would like to thank my wife Shima for her love, support and friendship.

Contents

List of Tables

List of Figures

Abbreviations and Nomenclatures

BR	breccia
CHF	channel fill
CSOR	cumulative steam oil ratio
CSS	cross stratified sand
DEV	Devonian Formation top
FMI	formation micro imager
GFM	grid-free modelling
IHS	inclined heterolothic stratification
m	meters
mD	millidarcy
MCM	McMurray Formation top
MPS	multiple point statistics
NTG	net-to-gross ratio
OBM	object-based modelling
PBS	point bar sand
SAGD	steam assisted gravity drainage
SGS	sequential Gaussian simulation
SH	shale drape
SIS	sequential indicator simulation
SNESIM	single normal equation simulation
SOR	steam oil ratio
SVG	scalable vector graphic

TI	training image
TGS	truncated Gaussian simulation
VAPEX	vapor extraction process
Vsh	volume of shale
VTK	visualization toolkit

A	area
α	dip angle
$B(s)$	channel half width function
b_i	relative location of IHS set half width
c_i	variable related to the curvature of initial channel
$C(s)$	curvature function
$C(\mathbf{h})$	covariance function
d_{drape}	shale drape horizontal extension
δx	discretization distance in x direction
δy	discretization distance in y direction
$\epsilon(s)$	disturbance value
Ea	expected value of variable a
F	cumulative distribution function
ϕ	porosity
$g(y)$	Gaussian distribution function
$\gamma(\mathbf{h})$	variogram function
$\mathbf{h}$	distance or lag vector
h	dampening factor
h	IHS thickness
h_{drape}	shale drape vertical extension
I	indicator variable
k	primary wavelength
K	number of categories
L	IHS length
$\lambda_\alpha, \lambda_\beta$	simple kriging weights
m_b	slope of sigmoidal surface at the bottom

m_t	slope of sigmoidal surface at the top
m_Z	stationary mean
ν_α, ν_β	ordinary kriging weights
p_k^*	indicator kriging estimate
$p_0, \cdots, p_6$	IHS and shale drape control points
s	intrinsic length
σ	standard deviation
σ^2	variance
S_w	water saturation
T	thalweg ratio
t_{drape}	shale drape top thickness
θ	tangent angle
$\mathbf{u}$	spatial position vector
Var	variance
W_0	opening width of IHS set
W_m	width of IHS set in the middle
$W(z)$	channel fill width function in vertical direction
$Y(\mathbf{u})$	standard normal residual variable
Y^*	kriging estimate
$Y_s(\mathbf{u})$	simulated value
Z	random variable
Z^*	kriging estimate

Chapter 1

Introduction

Reservoir heterogeneity description is required for hydrocarbon flow simulation, future reservoir performance prediction, establishing development plans and making business decisions.

Characterization of petroleum reservoir heterogeneity is a challenging task due to limited information available from the subsurface. Reservoir rock properties are commonly sampled at sparse well locations. Although, the correct reservoir description may be known at the well locations uncertainty about the distribution of rock properties will exist at unsampled locations.

This ambiguity about the true distribution of subsurface rock properties suggests a stochastic modelling approach. The main idea of a stochastic approach is to generate multiple equally probable realizations of the rock properties, rather than one deterministic description. It is based on incorporating a random component that describes the variability overlaying a deterministic trend (Deutsch, 2002; Gómez-Hernández, 2005).

Geostatistics provides stochastic approaches to integrate data at different scales and quantify the uncertainty at unsampled locations. Incorporation of more input data leads to a more "accurate" reservoir model and reduces the uncertainty. The core and well log data from wells are the most commonly used data for geostatistical modelling. Most of the geostatistical algorithms are able to appropriately integrate core and well log data. The seismic data

are generally integrated into the model as a secondary information to improve prediction of petrophysical properties. Integration of dynamic production data such as pressure and temperature measurements as a function of time leads to a more accurate reservoir model that accounts for the production history. Integrating dynamic data is not straightforward, but there are a number of inverse modelling techniques available for this purpose (Gómez-Hernández et al., 1997; Capilla et al., 1997; Wen et al., 2005; Evensen, 2009).

One important source of information that is difficult to consider completely in the geostatistical techniques is that related to the size, shape and orientation of geological architectural elements. The architectural elements are defined as rock bodies within the depositional system that have distinct facies content (Miall, 1985). These bodies, that are formed as a result of sediment accumulation have specific geometries defined by bounding surfaces. Each depositional environment has unique architectural elements. For example, fluvial systems contain crevasses and levees that may not exist in turbidite systems; if they do exist, they are likely of different size and shape.

Conventional geostatistical techniques mostly rely on two-point statistics represented by variogram models, and are therefore unable to reproduce complex geological architectural elements that are generally non-linear. As a result, the stochastic models generated by these techniques often appear unrealistic and lack in adequate geometric representation of geological features. Recent developments in facies modelling techniques such as object-based and event-based modelling address this issue to some extent by mimicking the interpreted geological geometries and/or physical processes. These techniques are usually developed for a specific geological depositional environment (e.g. fluvial environment) and may not be useful for other geological settings. This is due to the uniqueness of architectural elements in each depositional environment.

This dissertation develops a stochastic object/event based facies modelling algorithm for the estuarine environment of the McMurray Formation in Northern Alberta. The methodology integrates details of geological features and typi-

cal architectural elements in an estuarine system. It also provide a framework to model multi-scale geological features without relating them to a specific 3D grid system. Storing the geometric and geological parameters of architectural elements without saving to a 3-D cell-based grid system will permit quantification at any required scale for subsequent flow modelling. Section 1.1 explains the motivation of this research as well as challenges involved in the characterization of oil sand deposits. Section 1.2 describes the grid-free facies modelling approach that is used in this dissertaion to integrate multi-scale architectural elements in the McMurray Formation. The outline of this dissertation is summarized in Section 1.3.

1.1 Alberta Oil Sands

Oil sand is a naturally developed amalgamation of sand, clay minerals, shale, water, and bitumen. Bitumen is a type of heavy oil with API gravity of around 8.5 and very high viscosity of more than 10,000 cPo that could not flow at room temperature (Government of Alberta, 2008).

Oil sands deposits can be found in several locations around the world. Northern Alberta oil sand deposits, encompassing the Athabasca, Peace River and Cold Lakes areas, are the largest oil sands deposits in the world that cover a surface area of about 142,000 km^2 with an estimated initial oil in place of 1,800 billion barrels (ERCB, 2012). Figure 1.1 shows the location map of oil sands deposits in Alberta. The Athabasca oil sands deposits is the largest bitumen reservoir within the Alberta oil sands deposits with estimated reserve of 1,500 billion barrels (ERCB, 2012).

Only around 10% (180 billion barrels) of the Alberta's oil sand reserve is estimated to be economically recoverable with the current technologies and oil price (ERCB, 2012). Bitumen can be produced either by mining or by various in-situ techniques involving heating up the oil and allowing it to flow to the surface through a well. Surface mining may be used to produce 20% of the total

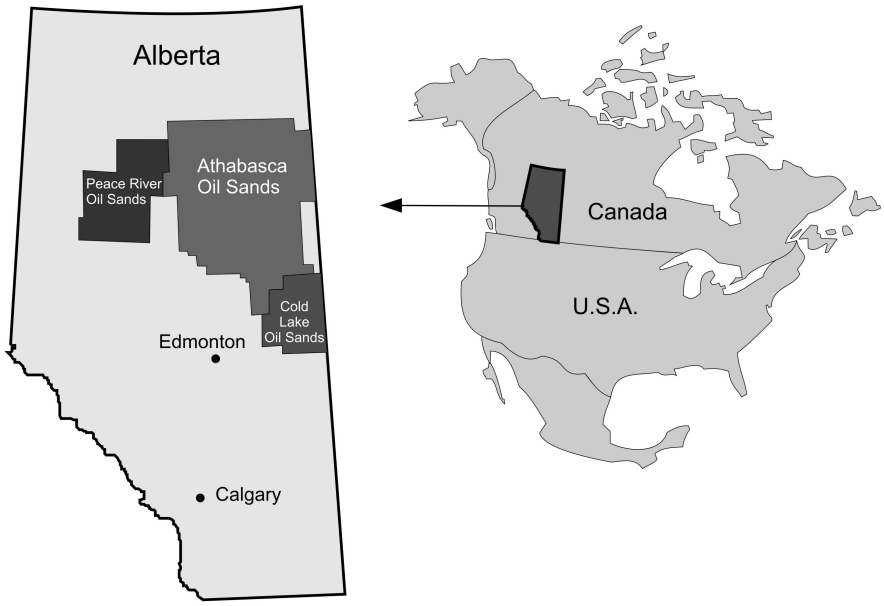

Figure 1.1: Location Map of Alberta Oil Sand Deposits (image from: `http://www.ags.gov.ab.ca/energy/oilsands/alberta_oil_sands.html`

recoverable oil sands deposits of Alberta (Government of Alberta, 2008). The remaining oil sands may be produced by thermal in-situ methods such as In-situ combustion, Steam Assisted Gravity Drainage (SAGD), or Vapor Extraction Process (VAPEX).

The SAGD in-situ recovery method (Butler et al., 1994) has emerged as an effective technology for the recovery of oil from oil sands deposits that are too deep to be produced by surface mining (generally more than $65m$). In this process, two horizontal wells up to $1000m$ long are drilled one well above the other and separated by a vertical distance (usually $5m$) near the bottom of oil bearing formation (Figure 1.2). The top well is used to inject steam into the oil sands and the bottom well is utilized to produce the oil. As the steam heats up the reservoir, the viscosity of the bitumen is reduced and it can flow by gravity into the producing well.

Performance of the SAGD process depends on the development of a steam chamber. The steam chamber is a cone-shape volume that is affected by the

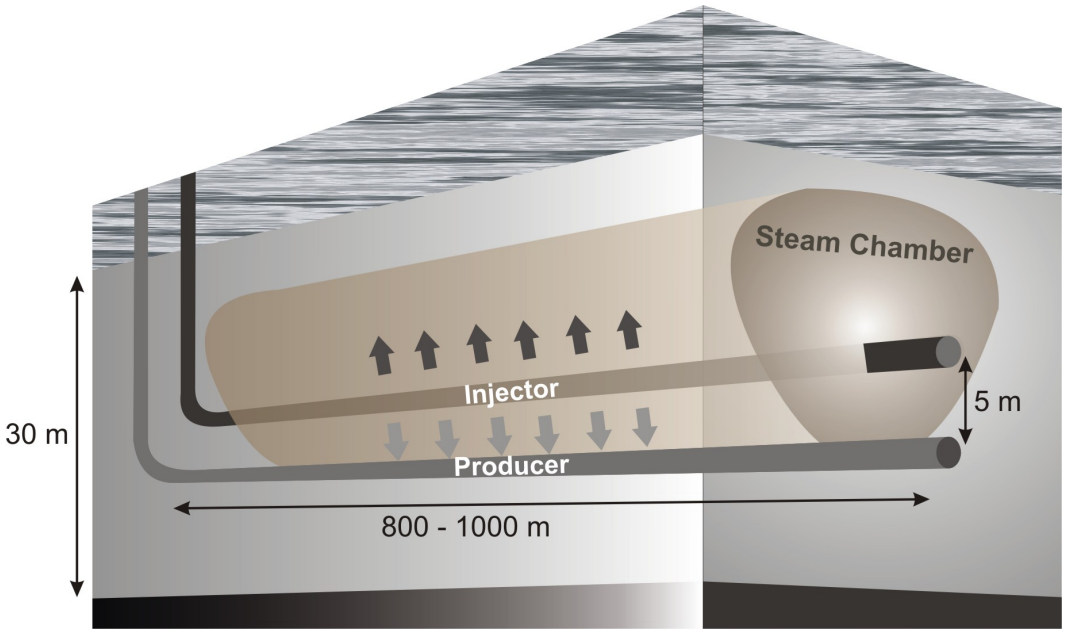

Figure 1.2: Steam Assisted Gravity Drainage, the most common in-situ oil sand recovery technique. Two horizontal wells and the steam chamber are shown.

high temperature of the injected steam (Figure 1.2). The steam chamber volume is a measure for the performance evaluation of the SAGD process. Another representative parameter for evaluating the performance of a SAGD is steam-oil-ratio (SOR) that is defined as the equivalent amount of steam needed to produce one barrel of oil. The lower the SOR, the more efficient the SAGD process.

A challenge in SAGD reservoir characterization is to define how the steam distributes in the formation. Other challenges include finding the optimum horizontal well pair location, identifying the flow barriers and water and gas saturated zones and defining the best injection pressure. Geological heterogeneity plays an important role in the performance of in-situ production processes.

1.1.1 Geological Heterogeneity

In the Athabasca oil sand deposits, the majority of the in-place bitumen is trapped within the Lower Cretaceous McMurray Formation. The McMurray

Formation contains complex geological features that were formed in a fluvial-estuarine depositional environment.

Many architectural elements, that have particular geometry and lithofacies, are detected in the fluvial-estuarine system of the McMurray Formation (Thomas et al., 1987; Ranger and Gingras, 2003; Bailleul et al., 2006). Some examples of these elements are tidal meandering channels, tidal bars, point bars, inclined heterolithic stratification (IHS) sets, and shale drapes.

These architectural elements exist at different scales. Tidal networks are developed over hundereds of square kilometers. Meandering channels are common and interrelated over many square kilometres. The IHS sets deposited as part of meandering channels contain metre to centimetre scale features such as shale drapes. Figure 1.3 shows heterogeneity of inclined heterolithic stratification, one of the main facies in the McMurray Formation, at three different scales.

Both large scale elements (channels, tidal bars) and small scale features (shale drapes) have impact on the flow of steam and bitumen in an oil sand reservoir. Tidal bars and point bars are considered as main reservoir and shale drapes and mud-filled channels are acting as barriers. Neglecting these multi-scale features in a reservoir model may result in an inaccurate reservoir performance assessment.

1.1.2 Facies Modelling

An appropriate facies modelling technique for characterization of an oil sand reservoir in the McMurray Formation should reproduce complex geological features of the McMurray Formation by integrating the size and shape of architectural elements. This is a challenging task with the currently available object-based facies modelling techniques considering the multi-scale architectural elements that exist in the McMurray Formation. In almost all modelling techniques, facies are populated on a cell based grid. In the traditional object-based modelling approach either a template of cells is utilized to represents the geo-object in the model or a parametrized geometry is immediately rasterized to

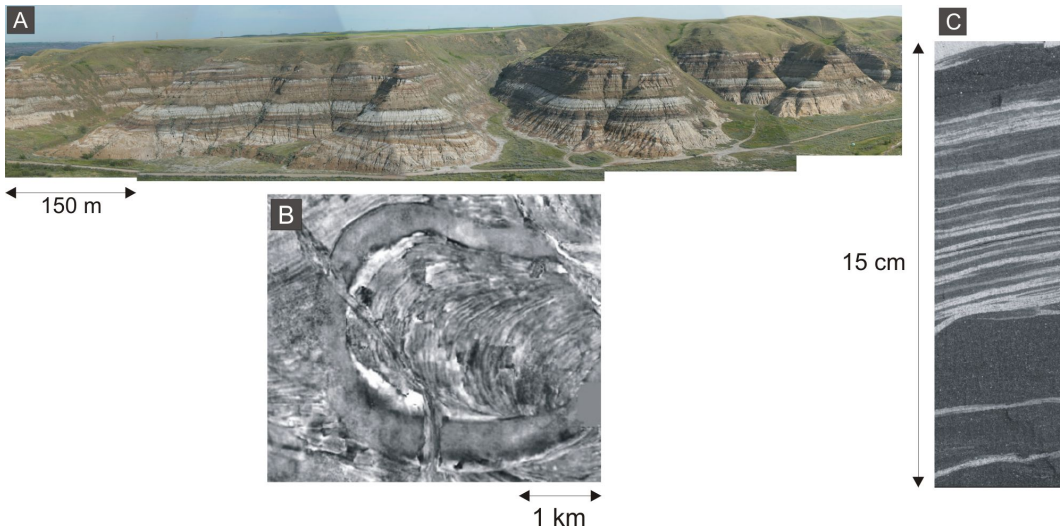

Figure 1.3: Geology complexity of IHS facies at different scales. A) an outcrop near Drumheller, Alberta shows IHS deposit extended over hundereds of meters . B) seismic time slice of a single IHS set extended over 4 km (modified from Hubbard et al. (2011)). Abandoned channel and accretion surfaces within the IHS facies can be detected, C) a core sample from IHS facies (dark color shows oil stained sand and light color shows centimeter scale shale drapes).

the grid. This limitation entails that heterogeneities that exist at scales smaller than the modelling cell cannot be explicitly represented.

Consider modelling a typical SAGD drainage volume of $1200m$ by $800m$ by $50m$. A grid cell size of $5\,m$ by $5\,m$ by $1\,m$ is normally considered as a small grid size in a geostatistical reservoir modelling applications. Each cell in this grid represents a $25\,m^3$ volume of rock. It is clear that small scale geological features such as shale drapes cannot be properly represented with this grid considering that only one facies code is assigned to each cell. Although a smaller grid size could be chosen to account for small geological features, this may lead to an unreasonably large number of grid cells and consequently excessive computational time.

1.2 The Approach

The grid-free approach developed in this dissertation allows for a representation of geological objects as surfaces and parametric shapes that are not linked to any particular grid system. This is similar to the concept of vector graphics where visual objects are represented with mathematical functions and not with sets of pixels as in raster graphics. Figure 1.4 illustrates this concept by showing a pixel-based image and its equivalent vector image. When the objects are represented with mathematical functions it is possible to introduce both centimetre scale shale drapes and the kilometre long channels in the same model.

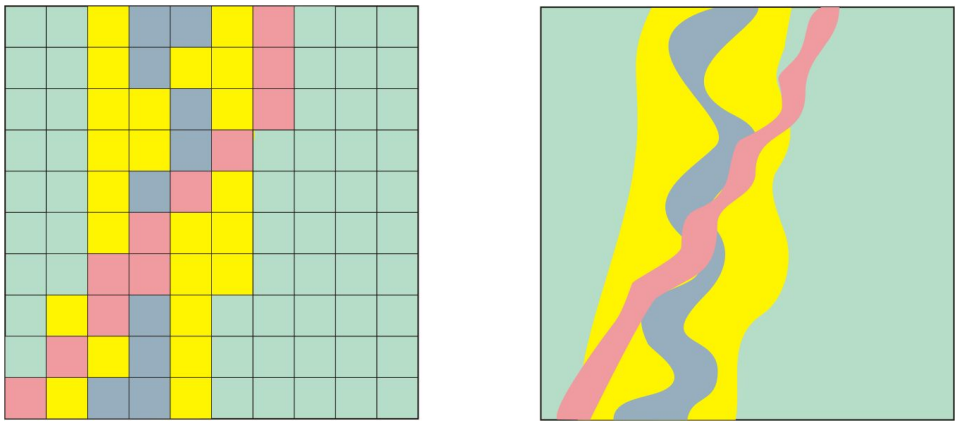

Figure 1.4: A pixel-based image (left) and as equivalent vector image (right), equivalent to conventional and grid-free facies modelling, respectively.

With traditional object-based methods the limits of a template or immediate rasterization results in the loss of important information. The grid-free, object-based facies modelling technique addresses this issue by preserving the parameterized geometric representation of the objects and saving them to allow the user to visualize them and apply any gridding scheme for local grid refinement, exact down scaling and upscaling, within facies trend models. In addition, various additional parameters related to the object geometries may be stored and eventually interpolated to the reservoir grid to improve the heterogeneity model. These may include local measures of properties within objects,

curvature, azimuth, thickness, thalweg, coordinates schemes and distance from object edge that may be applied for within object modelling (Pyrcz and Strebelle, 2008; Schafmeister et al., 2010).

The methodology involves development of three main components: geological object database, simulation engine, and rasterization engine. The geological database is a general library that contains the parameters of the geological architectural elements as objects. Each geo-object is defined by a series of parameters, properties and a unique code. A simulation engine is a stochastic object-based or event-based algorithm that generates the grid-free geological model by following the geological rules and using objects from the geological object database. The rasterization engine is a tool to transform the grid-free geological model to a gridded model for purpose of further petrophysical properties modelling, flow simulation, or visualization.

An important contribution of this dissertation is a grid-free facies modelling technique that accounts for the multi-scale architectural elements of the McMurray Formation. The required computer programs (one for stochastic simulation and one for rasterization) that provide tools for grid-free modelling of McMurray Formation are developed. Different applications of grid-free models are discussed. An estuarine training image library is generated using the developed computer programs. This training image library will be used for different applications including multiple-point geostatistics.

1.3 Dissertation Outline

Chapter 2 explains the basic concepts behind this research and reviews the related literature. An introduction to estuarine depositional systems is provided. The geology of the McMurray Formation is explained in detail to better understand the complex features that have significant effects on production performance. The general reservoir modelling workflow is explained and available facies modelling techniques are described in detail.

Chapter 3 develops a methodology for generating complex geological features of the estuarine system. An event/object-based modelling is presented to model tidal channels network of estuarine deposit.

Chapter 4 presents the grid-free facies modelling technique. First, the general framework of the grid-free facies modelling and details of its main components are described. Then, the implementation details of the grid-free facies modelling of IHS in the McMurray Formation is discussed. Unconditional and conditional simulation algorithms are described and the developed software tools are introduced.

Chapter 5 shows the application of grid-free facies modelling in two parts. The first part introduces two programs that are generated to implement the proposed methodology. All input parameters and the implementation algorithms are explained. The second part covers steps related to development of grid-free training image and specifications of the estuarine training image library.

Chapter 6 develops an extended example comparing the proposed grid-free facies modelling methodology to the conventional facies modelling techniques(sequential indicator simulation). Both methodologies are applied to a real McMurray Formation data set and the generated models are processed through a transfer function (thermal flow simulation). The two methodologies are compared based on the flow simulation outputs.

Finally, **Chapter 7** summarizes the methodology presented in this dissertation and presents the conclusions and recommendations for future research directions.

Chapter 2

Background

This chapter explains the required geological and theoretical background related to the methodology developed in this dissertation.

Section 2.1 explains the scales of geological heterogeneity and their importance in reservoir modelling. Section 2.2 discusses the reservoir modelling workflow, avaialble data for modelling, geostatistics, and available facies modelling methodologies. Section 2.3 describes the main characteristics of the estuarine depositional environment. Finally, Section 2.4 describes the geology of the McMurray Formation.

2.1 Multiscale Geological Heterogeneity

Geological heterogeneity exists at all scales and influences the flow of fluids in the reservoir; there is heterogeneity at multiple scales, from pore structures to bedding structures, litho-facies, and fault blocks. Haldorsen and Lake (1984) and Slatt (2006) classified the heterogeneity with respect to the scale. Figure 2.1 illustrates this classification. The smallest heterogeneity in the reservoir is called the microscopic scale that is related to the mineralogy and arrangement of grains and pores. This small scale heterogeneity is important for fluid flow by having a direct impact on the permeability and capillary pressure behaviour of reservoir rock (Bakke and Øren, 1997; Øren and Bakke, 2002).

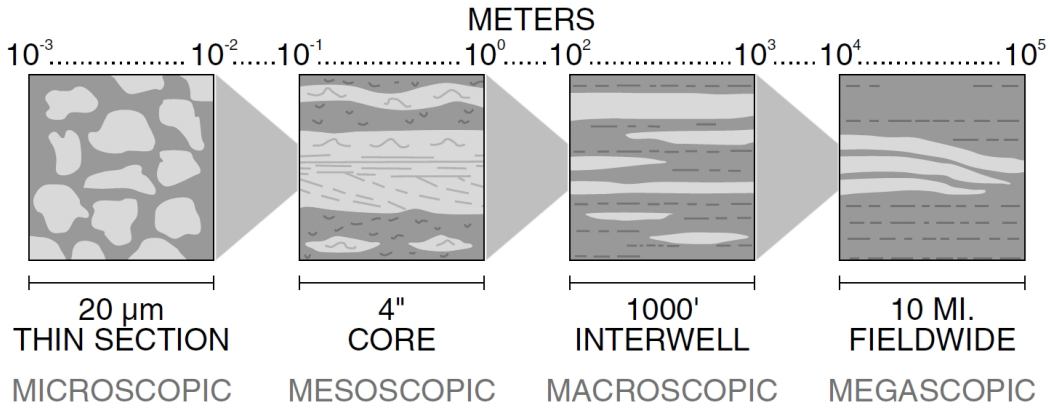

Figure 2.1: Classification of the scales of geological heterogeneity in reservoirs (from Slatt (2006)).

The heterogeneity observed in core and well logs is called the mesoscopic scale; the lithological type and bedding stratification can be observed at this scale.

The macroscopic heterogeneity is seen at the interwell scale and is related to the lateral bed continuity and stratigraphic unit discontinuity. This heterogeneity is the most difficult heterogeneity scale to infer because most subsurface geological data are sampled from sparse vertical wells. A representative outcrop or a high resolution seismic image would aid in better understanding details of the macroscopic geological heterogeneity.

The megascopic heterogeneity scale is related to the overall geometry and architecture of the geological setting that is controlled by the geological processes and events in a depositional environment.

All four heterogeneity scales are hierarchically related to each other (Miall, 1985; Slatt, 2006). For example, in an estuarine depositional system such as much of the McMurray Formation, distributary tidal channel's architectures (macroscopic) are highly related to the main estuarine channel development (megascopic). Consequently, development of estuarine point bars (macroscopic) and mesoscopic shale drapes are controlled by the tidal channel's geometry

(Thomas et al., 1987; Ranger and Gingras, 2003; Lettley, 2004). The deemed relevant geological heterogeneity and their hierarchical relations should be reproduced in a quantitative reservoir models for reservoir management.

2.2 Reservoir Modelling

Numerical reservoir modelling is an essential part of reservoir engineering. Reservoir models are used for different purposes including resource estimation, reservoir performance prediction and determining the optimal location of future wells. In general, the term "reservoir model" refers to two related models: the geological model and the simulation model. The geological model is a numerical description of reservoir rock properties based on geological and geophysical observations. The reservoir simulation model utilizes the geological model to predict the flow of fluids in the porous media. In this dissertation, the focus is on the geological model.

2.2.1 General Workflow

A common reservoir modelling workflow begins by collecting all available information. A complete analysis on the gathered data is then performed to check the quality of the data and understand the sampled data population. This includes statistical and spatial data analysis. Defining the key structural features, such as relevant horizons and fault blocks is the next step. In this step a container for the reservoir property population is generated. This volume is then discretized by a grid network that is aligned with the geological horizons and major faults. The next step is to transform the reservoir coordinate system to the depositional coordinate system. This step includes stratigraphic data transformation. The available data are then upscaled to the grid system. Geological facies are populated on the grid using the statistical and spatial characteristics of the sampled data. The petrophysical properties, such as porosity and permeability, are then characterized within the defined facies using the static data.

Then, the dynamic data are integrated by performing flow simulation several times on the geo-models (Figure 2.2). This step is an iterative process in which the geological model is adjusted to match the production data.

2.2.2 Available data

Reservoir models are generated based on available data. There are different types of data available for reservoir modelling. Each one has its own measured property, error content, and scale of measurement. Some data provides direct measurements of reservoir properties such as core and well log data. Some data provides indirect measurement of reservoir properties such as seismic. Although these data are indirect, they are closer to being direct because they are measured with relatively low error content and with a high correlation to the real rock properties. Some data (such as geological interpretation) is a qualitative representation of reservoir properties while other data is quantitative (e.g. well log or seismic). The most common data for reservoir modelling are summarized below.

Geological Interpretations

Geological interpretations provide information about the reservoir at all scales ranging from the megascopic to the microscopic scale. This includes information about the depositional environment, architectural elements, stratigraphy and sedimentology. This information is often descriptive or qualitative and may be quantified through the variogram or 3D training images (see the following section for a detailed description). This information may also be used to determine large scale trends in facies proportions or other rock properties.

Dynamic Production Data

This information is generally provided by field measurements of pressure, flow rates, or temperature during the production phase. Production data provide important information about the interwell connectivity, flow barriers, boundary

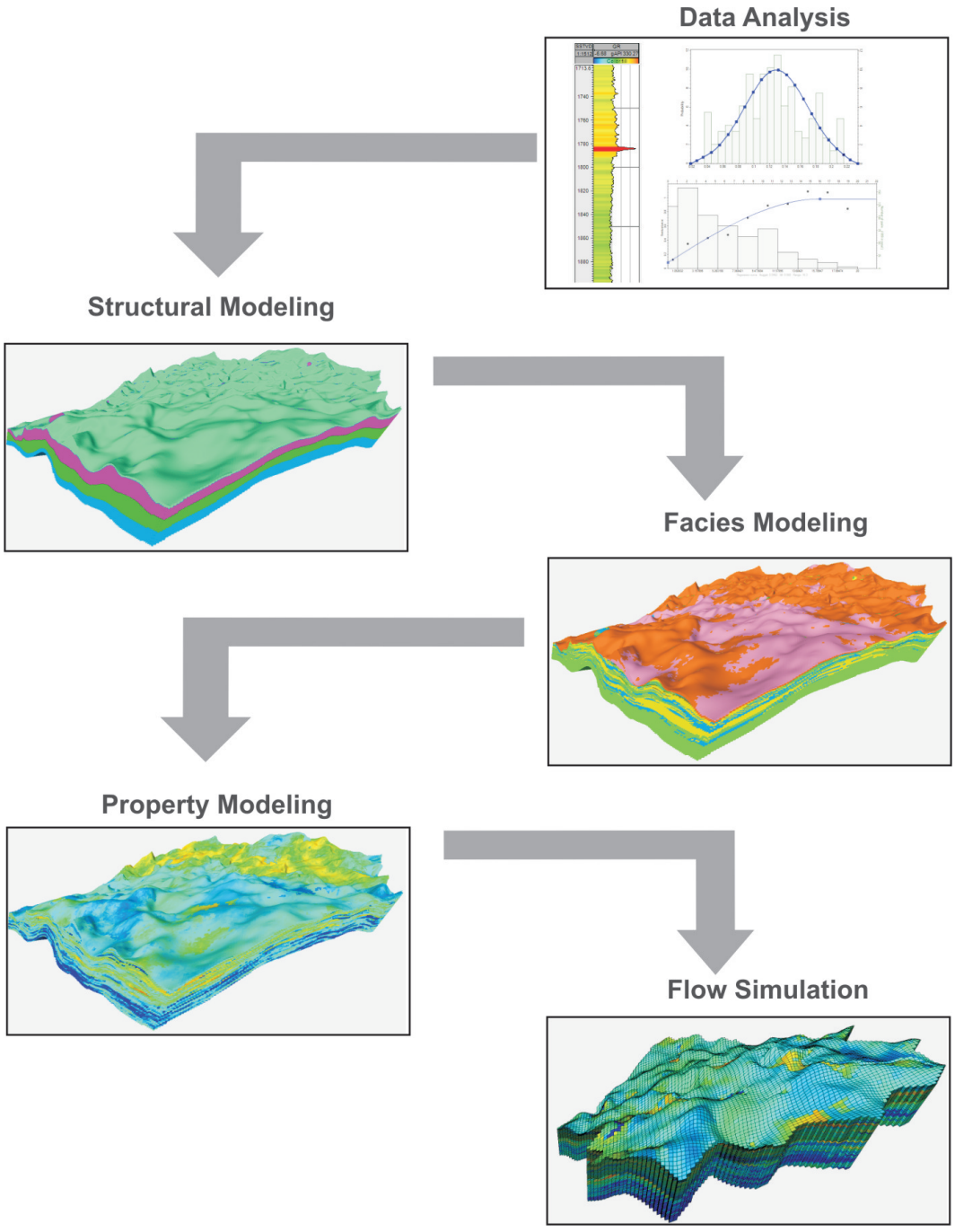

Figure 2.2: Reservoir Modelling Workflow. The cartoons are schematic "postage stamp" sized graphical depictions of a numerical model.

of reservoir and effective reservoir permeability. Some of the typical production data are drawdown/build up test, production logs, pressure and temperature readings at each well, fractional flowrates and well tracers observed at production wells.

4D seismic is another source of dynamic reservoir data that contains information about changes in subsurface rock and fluid properties at different times. Multiple 3D seismic images taken at different times provides information on changes in pressure, temperature and saturations as a result of hydrocarbon production. Seismic images are sensitive to spatial variations in both geology and dynamic fluid flow properties. When two or more seismic images taken at different times are compared to each other, it may be possible to distinguish changes in dynamic flow properties due to geological heterogeneity.

Seismic Data

This data provides extensive lateral coverage but with limited vertical resolution. Seismic attributes do not directly measure the reservoir properties. They are typically correlated with petrophysical data and used as a secondary data in reservoir modelling or as additional information to determine the horizontal variograms (Doyen 1988). Seismic impedance is a function of bulk density and incident wave velocity. Bulk density is a function of the porosity and facies distribution while wave velocity is a complex function of the saturation and facies distribution (Aki and Richards, 1980). Seismic amplitude data are used to delineate the reservoir boundaries and stratigraphic surfaces.

Petrophysical Well Logs and Core Data

Well log data are the most commonly used data in reservoir modelling and treated as hard data. Conventional well logs measure the electrical, radioactive and acoustic properties of reservoir rocks (Rider, 1986). The petrophysical properties such as porosity, water saturation and volume of shale are calculated from these well log readings. The well logs have high resolution along the well

bore (about 10 to 15 cm) but only provide information a limited distance around the wellbore. The log data scale is sometimes referred to as a point scale or quasi-point scale.

It is reasonably common to sample the subsurface rock during the drilling of a well. The core is a cylindrical section of rock that can be measured for important information about the geology of reservoir. Core plugs are small cylindrical samples taken from the large cores for more detailed analysis. They are normally 2.5 to 4 cm in diameter and 5 cm long. The core plugs are tested in a laboratory and the rock and fluid properties are measured. Using core plug data is a major challenge in geostatistical reservoir modelling because they may be biased and are normally sampled from the good quality portion of the reservoir.

Core plug data and well log data are the smallest data typically available for conventional reservoir modelling. The well log data provides porosity, water saturation and volume of shale at every 10 to 15 cm vertically. Facies may be defined at the same resolution of well logs by using the multivariate analysis of conventional logs or based on the volume of shale. Core plugs that sample specific portions of the reservoir provide measured porosity, permeability and water saturation. Facies are normally identified in cores and classified based on the microscopic and small scale features such as lithology, grain size, texture, sedimentary structure and color (Coll et al., 1999).

Image logs

There are a variety of image log tools including the Formation Micro Imager (FMI). It measures the micro-resistivity of the formation throughout the borehole and generates an electrical image that has a vertical resolution of about 5 millimeters. FMI logs can be used as an alternative to coring in order to reduce drilling costs and coring risks. The application of FMI logs is to define important reservoir geometries and petrophysical reservoir parameters. They can also be used to identify anisotropic features that could be barriers to fluid

flow.

Core Photographs

Cores are usually analyzed, inspected, and photographed. The digitized core photographs provide interesting information about micro-scale features and lamina that may have a large impact on fluid flow. High resolution core photographs usually have a pixel size equal to or smaller than a millimeter. The application of core photographs to micro-modelling of permeability and fine-scale facies determination is well documented (Hosseini et al., 2008; Deutsch, 2010; Boisvert et al., 2012).

Possible Additional Data

There may be additional data available that is less commonly used for reservoir modelling purposes. Thin cross sectional slices of cores are usually sampled and prepared for micro scale analysis. CT scans of cores provides information at micrometer scales. This information allows improved understanding of the flow phenomena at a microscopic level.

2.2.3 Geostatistics

Geostatistics is an important part of the reservoir modelling workflow. It is a branch of applied statistics that accounts for the geological context of data and is useful tool to model spatial variability. Geostatistics was first initiated by Krige (1951) for estimation of ore reserves at unsampled locations. Later, Matheron (1962) formulated this estimation technique and called it *kriging*. Since then, many different geostatistical algorithms and techniques have been developed.

Concept of Random Function

Most Geostatistical algorithms are built on the theory of random functions and a spatial distribution related to those random functions (Deutsch and Journel,

1998). A Random variable RV, denoted as Z, is a variable that can take a series of possible values described as a probability distribution function (pdf) or a cumulative distribution function (cdf). This probability distribution characterizes the uncertainty about the unsampled value z. The primary goal of a geostatistical technique is to model the random variable probability distribution. Since a RV is location dependent, it is denoted as $Z(\mathbf{u})$, where $\mathbf{u}$ is a location within the domain. The cdf of a continuous RV is defined as:

$$F(\mathbf{u}; z) = Prob\{Z(\mathbf{u}) \leq z\} \tag{2.1}$$

For a categorical random variable that can take any value from K outcomes $k = 1, ..., K$, the distribution function is defined as:

$$F(\mathbf{u}; k) = Prob\{Z(\mathbf{u}) \in \text{category k}\} \tag{2.2}$$

A random function (RF) is a set of dependent random variables over the study domain. One of the main applications of a RF is to predict statistics at unsampled locations using statistical measures from the sampled data. This relies on the decision of *stationarity*. This means that the statistics of the limited sampled data can be extended to the entire domain of interest. In geostatistics, first order stationarity implies location independence of the mean and variance:

$$E\{Z(\mathbf{u})\} = m, \textit{ for all } \mathbf{u} \textit{ in } A \tag{2.3}$$

$$E\{[Z(\mathbf{u}) - m]^2\} = \sigma^2, \textit{ for all } \mathbf{u} \textit{ in } A \tag{2.4}$$

Second order stationarity refers to the covariance that is the measure of spatial similarity between two locations in the space. The covariance between two locations that are separated by a lag separation vector of $\mathbf{h}$ is defined as:

$$C(\mathbf{h}) = E\{[Z(\mathbf{u}) - m] \cdot [Z(\mathbf{u}+\mathbf{h}) - m]\} \tag{2.5}$$

The semi-variogram, often called the variogram, is used as a measure of variability or dissimilarity between two points in the space:

$$2\gamma(\mathbf{h}) = E\{[Z(\mathbf{u}) - Z(\mathbf{u}+\mathbf{h})]^2\} \tag{2.6}$$

Under first and second order stationarity, the covariance is related to the variogram:

$$C(\mathbf{h}) = C(\mathbf{0}) - \gamma(\mathbf{h}) \tag{2.7}$$

where $C(\mathbf{0})$ is equal to the stationary variance (σ^2).

Kriging

The kriging algorithm, mentioned above, estimates the value at an unsampled location. It provides a weighted moving average of data with minimum error variance. Consider n data sampled at locations $\mathbf{u}_\alpha, \alpha = 1..., n$, the kriging estimate at locations $\mathbf{u}$ is defined as:

$$Z^*(\mathbf{u}) = \sum_{\alpha=1}^{n} \lambda_\alpha \cdot [Z(\mathbf{u}_\alpha) - m_Z] + m_Z \tag{2.8}$$

where m_Z is the stationary mean and λ_α are kriging weights that are calculated using the covariance function:

$$\sum_{\beta=1}^{n} \lambda_\beta \cdot C(\mathbf{u}_\beta, \mathbf{u}_\alpha) = C(\mathbf{u}, \mathbf{u}_\alpha) \quad \alpha = 1, \cdots, n \tag{2.9}$$

The linear estimator in Equation 2.8 is called "simple kriging" that relies on the stationary mean. In a case where there is a local trend in the data and the mean is not constant throughout the area, a more robust estimator called "ordinary kriging" could be applied:

$$Z^*(\mathbf{u}) = \sum_{\nu=1}^{n} \nu_\alpha Z(\mathbf{u}_\alpha) \tag{2.10}$$

where the ordinary kriging weights (ν_α) are defined as:

$$\begin{cases} \sum_{\beta=1}^{n} \nu_\beta \cdot C(\mathbf{u}_\beta, \mathbf{u}_\alpha) + \mu = C(\mathbf{u}, \mathbf{u}_\alpha) \quad \alpha = 1, \cdots, n \\ \sum_{\beta=1}^{n} \nu_\beta = 1 \end{cases} \tag{2.11}$$

where μ is the Lagrange parameter. As defined in Equation 2.11 the ordinary kriging weights sum to one.

In summary, the kriging algorithm provides a weighted moving average of the data and, as a result, the extreme values are smoothed out. This smoothing effect results in a smaller variance of estimated values than the data-based stationary variance. Thus, this algorithm is not suitable for generating reservoir property models such as permeability because high and low permeability values are often essential for an unbiased forecasting of the fluid flow response.

Geostatistical Simulation

Geostatistical simulation incorporates a random component in order to capture spatial variability that cannot be described by the kriging estimate. This provides a better representation of reservoir properties such as permeability by correcting the smoothing effect of kriging. As a result, the variance of simulated values is equal to the variance of the sample data. This process also allows building equally probable realizations of the spatial distribution. An assessment of uncertainty is then obtained by the multiple realizations of reservoir properties.

There are many geostatistical simulation techniques available. Sequential Gaussian simulation (Isaaks, 1990) is the most popular geostatistical simulation technique that is used for modelling continuous variables such as porosity and permeability. In this technique, each variable is simulated sequentially by drawing from a conditional cumulative distribution defined by kriging. The conditioning data include original data and all previously simulated values. When the original data is used in the simulation, it is called *conditional simulation* and when it is not used in the simulation, it is called *unconditional simulation.*

A normal score transformation of input data are required. The probability density function of a standard normal or Gaussian distribution with mean $m = 0$ and standard deviation $\sigma = 1$ is defined as:

$$g(y) = \frac{1}{\sqrt{2\pi}} \cdot exp(-\frac{1}{2}y^2) \tag{2.12}$$

All original data and all previously simulated values are used as conditioning

data. Considering a standard normal residual variable defined as:

$$Y(\mathbf{u}_\alpha) = Z(\mathbf{u}_\alpha) + m \quad \alpha = 1, \cdots, n \tag{2.13}$$

the simulated value at location $\mathbf{u}$ is defined as:

$$Y_s(\mathbf{u}) = Y^*(\mathbf{u}) + R(\mathbf{u}) \tag{2.14}$$

where $Y^*(\mathbf{u})$ is the kriging estimate and $R(\mathbf{u})$ is the random component that follows a normal distribution with mean of 0.0 and a variance equal to the kriging variance.

The model generated by the Gaussian simulation technique reproduces the input statistics and variogram model.

2.2.4 Facies Modelling

The term *facies* is related to a specific rock or sediment volume that is different from others based on lithological, structural, and organic aspects (Teichert, 1958; Anderton, 1985). Facies are often descriptive and indicative of a depositional process and a specific sedimentary environment. They may also represent diagenetic alteration that took place after deposition. The vertical and horizontal arrangement of several facies that describe a depositional environment are called *facies association* (Anderton, 1985).

Facies are important in reservoir modelling because the petrophysical properties of interest are highly correlated with facies type. Geostatistics permits heterogeneity modelling within a stationary domain and since the facies model fundamentally defines these stationary zones, the petrophysical distribution within a facies is considered stationarity.

There are a number of different techniques for modelling geological facies. Four main approaches include variogram-based modelling, object-based modelling, event-based modelling, and most recently, multiple point geostatistics using training images. Choosing the best approach for facies modelling is highly dependent on the application (Deutsch, 2002).

Variogram-based Facies Modelling

Variogram-based facies techniques rely on the two-point variogram statistic to capture spatial correlations. Indicator and truncated Gaussian methods are common in this class of techniques. This type of facies modelling is a more popular technique because the sample data is explicitly reproduced in the final model and calculation of the variogram is relatively straightforward (Deutsch, 2002).

The facies can be modelled by indicator values. Indicators are widely used in modelling categorical variables because the distribution of uncertainty can be estimated directly (Journel, 1983). The categorical facies data are transformed into a binary variable via the following transform:

$$I(\mathbf{u}_\alpha; k) = \begin{cases} 1 & \text{If facies } k \text{ exists at } \mathbf{u}_\alpha \quad \alpha = 1, \cdots, n \\ 0 & \text{Otherwise} \end{cases}$$

where $k = 1, \cdots, K$ facies, and $\mathbf{u}_\alpha$ represents a location in domain A. The mean and variance are then defined as:

$$E\{I(\mathbf{u}; k)\} = p_k$$

$$Var\{I(\mathbf{u}; k)\} = p_k(1 - p_k)$$

where p_k is proportion of facies k within the domain.

Inference using indicators can be performed in one of two modes: estimation and simulation. Indicator kriging (IK) yields the estimated probability of each facies at unsampled locations:

$$p_k^*(\mathbf{u}) = \sum_{\alpha=1}^{n} \lambda_\alpha [i(\mathbf{u}_\alpha; k) - p_k] + p_k \tag{2.15}$$

where λ_α is the weight to the indicator value at location $\mathbf{u}_\alpha$.

Sequential indicator simulation (SIS) permits global and local uncertainty to be assessed on the reservoir model (Journel and Alabert, 1989). Note that the estimation of indicators results in a continuous estimate (a probability), while

SIS results in realizations that consist of categorical values that represent the specific facies. SIS is widely used for diagenetically controlled facies because the results have high variability and yet correct anisotropy and variogram measures of spatial correlation (Deutsch, 2002)

Truncated Gaussian simulation (TGS) is another variogram-based facies modelling technique proposed by Matheron et al. (1987). In this method, the spatial distribution of facies is modeled using a continuous multi-Gaussian random function. Truncation is applied at a series of thresholds to create categorical facies realizations. The thresholds can be defined by the target global (or local) proportions for each facies. The advantage of this technique is the clear ordering of the facies appearance that is a direct result of the facies being generated by the truncation of an underlying continuous variable. The Truncated Gaussian simulation may work well for clearly ordered facies. Figure 2.3 shows examples of facies models generated by SIS and TGS. The model generated with the TGS technique reproduces the input facies proportion as well as the facies ordering. For example, red facies always appears beside to the yellow facies. However, this feature is not reproduced in the SIS realization.

Truncated pluri-Gaussian simulation (Galli et al., 1994; Le Loch and Galli, 1997) is an extension of truncated Gaussian simulation that allows simulation of more complex geometry of lithofacies. More variables are simulated by considering multiple random functions and then the multivariate distribution is truncated.

Object-based Modelling

Object-based modelling (also known as boolean simulation or a marked point process) is suitable for reproducing geometry of geological features. For example, in the object-based model shown in Figure 2.4, the shale content of a sandstone reservoir is represented as ellipsoids. The geological models generated with object-based modelling (OBM) reproduce complex geological features and are often visually attractive and can perform better when used in complex

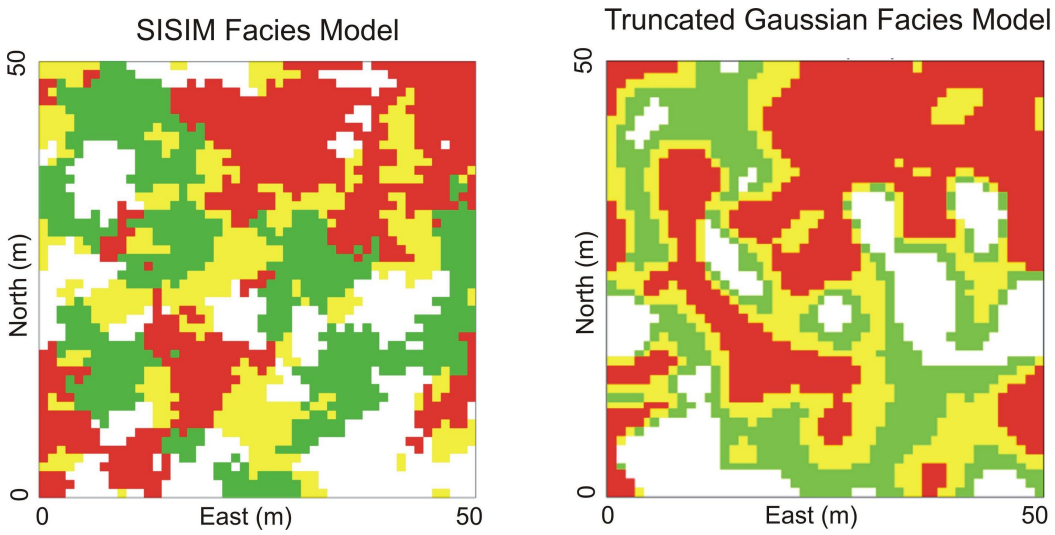

Figure 2.3: Schematic 2-D slices of 50 by 50 m facies models generated by Sequential Indicator Simulation (left) and Truncated Gaussian Simulation (right).

transfer functions such as flow simulation (Journel et al., 1998; Hu and Jenni, 2005).

Object-based modelling was first introduced by Haldorsen and Lake (1984) and Haldorsen and MacDonald (1987) where shale barriers were modelled as rectangular objects. Their work inspired others to adopt this technique and improve it for more complicated geological settings. The fluvial setting is a common example of reservoirs which has been modelled with the object-based techniques (Ømre, 1992; Georgsen and Omre, 1993; Hatloy, 1995; Deutsch and Wang, 1996; Holden et al., 1998; Viseur et al., 1998; Shmaryan and Deutsch, 1999). Miall (1985) classified fluvial architectural elements based on their scales, bounding surfaces, texture, and internal geometries. Examples of geo-objects in a fluvial reservoir are channels, levees, and crevasses splays. FLUVSIM (Deutsch and Tran, 1998) and ALUVSIM (Pyrcz, 2004) are two object-based algorithms for building stochastic fluvial facies models. These methods produce visually attractive and realistic facies models and successfully reproduce long range curvilinear connectivity that cannot be captured by variogram-based facies methods, but these methods are inefficient at reproducing a realistic level of conditioning

data (Viseur et al., 1998; Shmaryan and Deutsch, 1999; Pyrcz et al., 2009).

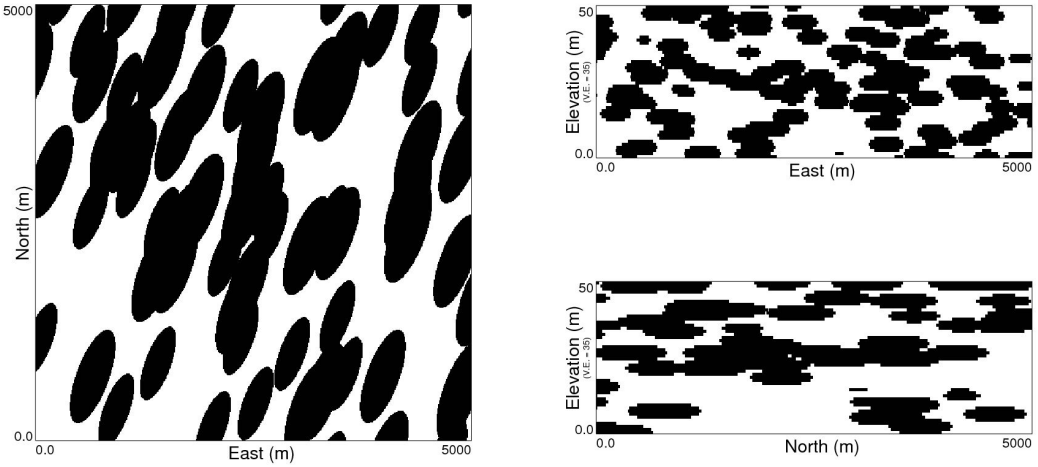

Figure 2.4: An example of a 5000 by 5000 by 50 m 3-D object-based model in which shale barriers are represented as ellipsoids (generated by `ellipsim` program of GSLIB (Deutsch and Journel, 1998)).

Although object-based modelling is mostly used in fluvial modelling applications, it can also be used for modelling other depositional setting where the geometry of geological architectures are well understood and can be represented by parametrized geometries. Deutsch and Tran (1999) developed an object-based algorithm to model deepwater turbidite sand bodies. In their LOBESIM algorithm, 3D sand bodies are represented with lobe geometries. Hosseini and Deutsch (2010) proposed a methodology for modelling the distribution of mega-karst features in the carbonate Grosmont Formation. In their approach, shape and size of sinkholes are parameterized as a semi-ellipsoid with the length of major radius, horizontal and vertical aspect ratios and the azimuth of major radius.

Parameterization

One of the earliest steps in any OBM algorithms is to mimic the geometry of possible geo-objects. Objects should be represented well enough to mimic the real heterogeneity of the study area.

In the traditional OBM a template of cells, that are coded as a particular facies inside the objects, is utilized to represents the geo-object in the model. For example, in the work of Maharaja (2008), crevasse splays are defined with the template shown in Figure 2.5. Using the template reduces the computational time; however, this may lead to lack of small scale geological feature reproduction when the features are smaller than the resolution of the grid.

In cases where the geometry of the geo-object is simple, the objects can be represented by simple geometric shapes. For example, in an early work of Haldorsen and Lake (1984), shale components in the sandstone reservoir were represented as rectangles that are parameterized by length and thickness.

For more geometrically complex geological object such as deepwater lobes where a simple geometric shape cannot be utilized, objects are parameterized by mathematical functions (Deutsch and Tran, 1998, 1999; Pyrcz, 2004). In some cases the geometry of geological objects is so complex and cannot be characterized by a simple mathematical function. An example of these complex objects is meandering channel geometry which irregularly undulates along its main stream axis.

Mallet (2002) in his Geomodeling book presented a variety of useful tools for modelling complex geological features with the discrete spline interpolation technique. Complex objects are represented by sets of discrete points which are connected together with interpolation functions. With this method, both the geometry and the physical properties of objects are assigned to the discrete points, simultaneously. Cubic spline is an example of interpolator which has been used to generate the complex pattern of meandering channels (Pyrcz 2004).

Simulation Algorithm

Object-based modelling is a boolean simulation where parameters of geological objects (geo-objects) are drawn from pre-specified distributions and then stochastically populated within the model. A typical object-based simulation involves the following main steps:

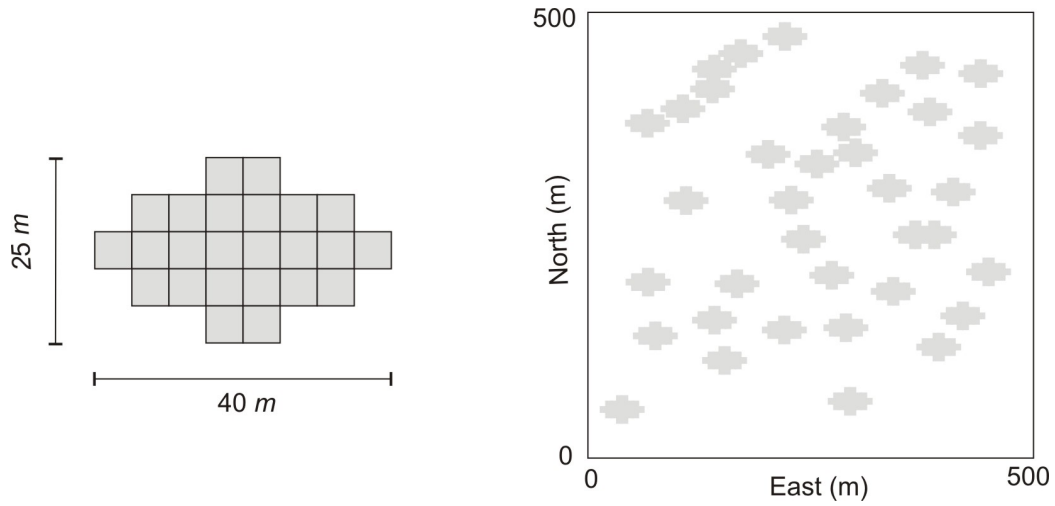

Figure 2.5: An ellipse template used to represent shale (left), and object-based model generated with the template (right).

- *Choosing shape, size, and orientation parameters of the geo-objects*: this is often done by drawing from pre-specified distributions. Common distribution models for the geo-object parameters include the triangular distribution that is chracterized by a minimum, maximum, and middle values and the normal distribution that is characterized by a mean and standard deviation.

- *Positioning geo-object in the modelling area*: this can be done in different ways. In the Poisson point process, objects are randomly placed in the area of interest. An intensity trend may be used in the Poisson process to provide more control on the location of the objects in a non-stationary domain. If well conditioning is considered, objects are placed in a way to match well data. In some cases, objects are placed relative to the other objects in the model. For example, in the LOBESIM algorithm lobe shaped sand are attached to the end of turbidite channel objects. In the event-based modelling (next section), objects are placed in the modelling area based on geological sequences and rules.

- *Rasterizing objects to grid*: rasterization is the process of finding cells that are inside each object. Each object is rasterized after its parameters and location are determined. An indicator variable is defined as follow:

$$I(\mathbf{u}; k) = \begin{cases} 1 & \text{if } \mathbf{u} \text{ is inside object } k \\ 0 & \text{Otherwise} \end{cases}$$

  where $\mathbf{u}$ is centre point of each grid cell in the modelling domain.

Conditioning

Conditioning the object-based models to the well data can provide models that are both geologically and statistically valid. There are several methods available for conditioning an object-based model to the well data (Tetzlaff, 1990; Shmaryan and Deutsch, 1999; Lopez et al., 2001; Oliver, 2002; Pyrcz, 2004; Pyrcz et al., 2005; Hauge et al., 2007).

A typical conditioning approach for object-based modelling is a rejection algorithm. In this method, objects are generated and compared against the conditioning data. If the generated object conforms to the well data, it is accepted; otherwise, a new object is generated and the procedure is repeated. One drawback for this method is that it may be computationally time consuming for dense conditioning data.

The other approach is to modify the objects until they match the conditioning data. Modification can be achieved by either moving the object or altering the grid cell after the object is rasterized (Pyrcz et al., 2009). In the annealing simulation techniques, an objective function is defined so the alteration and moving of objects is performed iteratively.

Viseur et al. (1998) proposed direct conditioning of objects to the well data. In this method, the generated objects are directly placed in locations corresponding to the well data. Shmaryan and Deutsch (1999) developed a fast conditioning algorithm similar to the work of Viseur et al. (1998). In this technique channel centerlines and shape parameters are generated by Sequential Gaussian

simulation (SGS). This method is efficient for channels with low sinuosity but cannot be used in high sinuosity or meandering channels.

In summary, the presence of many conditioning wells can be problematic and remains a long-standing challenge to the object-based approaches (Deutsch, 2002).

Event-based Modelling

Event-based modelling, also known as process-mimicking modelling, is an extension of object-based modelling in which the objects are placed in the model in a temporal sequence with rules to mimic the geologic processes associated with their deposition (Sun et al., 1996; Xie et al., 2001; Pyrcz, 2004; Cojan et al., 2005; Pyrcz et al., 2012). The result is more complex models of heterogeneity and object inter-relationships.

Event-based modelling has been used to generate realistic models of fluvial systems (Pyrcz, 2004). The basic building block of event-based modelling for the fluvial system is the channel centerline. This entails simulating channel centerlines to represent the central axes of channels. The centerlines are then modified and operated on to create further architectural elements of the depositional system such as abandoned channel fill, crevasse splays, and levees.

The event-based technique had been also used to produce the lateral accretion point bar of the McMurray Formation (see Figure 2.6). (Pyrcz and Deutsch, 2004), proposed a stochastic event-based methodology that generates fluvial point bar models based on the lateral migration of meandering channels adopting the bank retreat model of Howard (1992). Mud drapes that are part of tidal point bars are modelled separately and incorporated into the model. This method provides a realistic model but there is no control on the output configuration and distribution of the point bars and channel architectures in the model. This makes it more difficult to condition the model to a well data especially with the modification technique discussed earlier.

Wen (2004) presented a methodology that represents the complex channel-

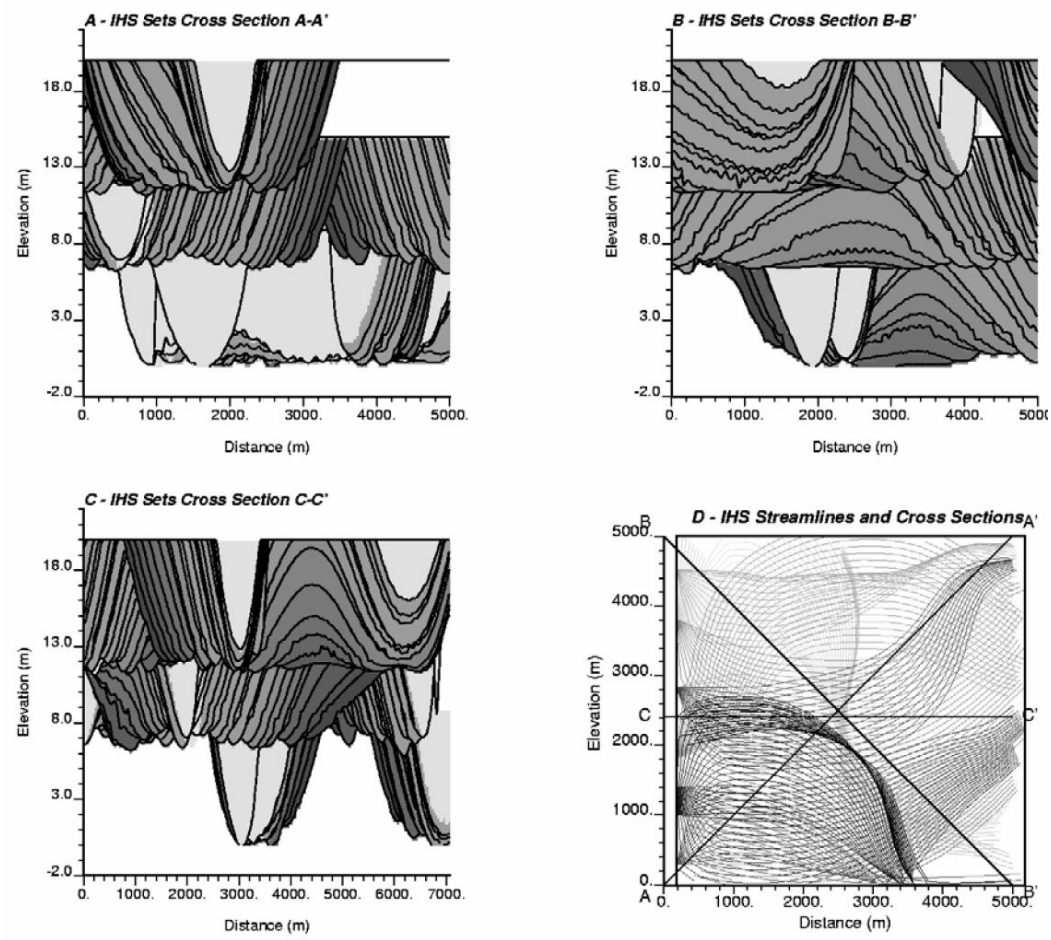

Figure 2.6: Example of event-based facies modeling for generation of IHS sets (Pyrcz and Deutsch, 2004). The areal section (lower right) shows lateral migration of several channel centerlines over kilometres scale. Vertical cross-sections show generation of IHS and accretionary surfaces as a result of channel migration over 20 metre scale. Vertical sections are exaggerated.

ized system of the McMurray Formation by surfaces. Surface or flow-based events have also been used for the application of deepwater depositional systems (Pyrcz, 2004; Pyrcz et al., 2005). The algorithm proceeds by generating stochastic flow events characterized by bounding surfaces. These flow events have geometries based parameter distributions from conditioning and analogue information. Successive surfaces representing sedimentary accumulations are

simulated by stochastically choosing the source location for the flow events, the path for the deepwater flow, and the geometry of the individual events. The resulting surface architecture is used to assign facies such as turbidite lobes and shales.

Multipoint Geostatistics

The Variogram-based facies modelling techniques rely on two-points statistics and therefore are unable to directly reproduce curvilinear geological features. Multiple point geostatistics has received much attention recently and relies on extracting multiple point statistics derived from training images (TI). A TI is a fully-populated model that is representative of the conceptual geology of the area under study, and can be viewed as the prior model of spatial structure (Journel and Zhang, 2006).

This technique was first proposed by Journel and Alabert (1989) and then used in simulation by Deutsch (1992); Strebelle and Journel (2000); Lyster (2009). Single normal equation simulation (SNESIM) is an efficient multiple-point geostatistical algorithm which was first proposed by Guardiano and Srivastava (1993) and then improved by Strebelle (2002).

The main idea is to select a template of n-points that coincides with the local data around an unsimulated location and then calculate the conditional probabilities of an outcome by scanning the template over the training image. The method does not require a variogram model. The variogram and histogram are implicitly extracted from the training image. Figure 2.7 shows a training image and a facies realization that is generated with then SNESIM technique based on that training image.

The multipoint geostatistical methods can reproduce non-linear geological features, but the validity of the resulting model relies heavily on the representativity of the training image.

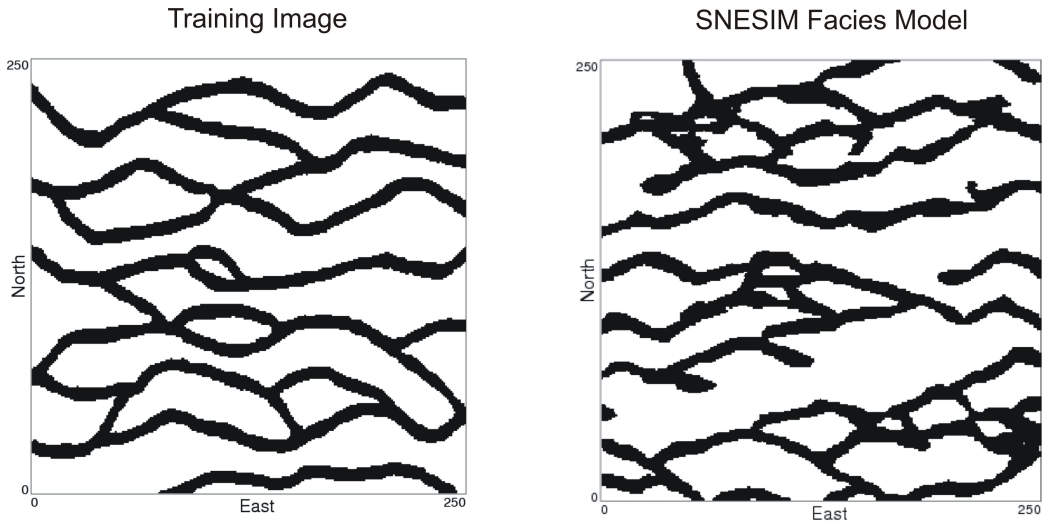

Figure 2.7: Example of facies model generated with multipoint geostatistics (right) using a conceptual geological model (training image) (left) (Lyster, 2009).

2.2.5 Multiscale Modelling

Reservoir models are conventionally populated on discretized volumes called grid cells. A grid cell is the smallest component of a numerical model that represents a specific reservoir property. The size of the modelling grid cell is called the modelling scale. The reservoir modelling scale mainly depends on the scale of available data, modelling application and computing resources. Choosing an appropriate modelling scale is especially important in the characterization of the McMurray Formation where there is a significant scale variation in the estuarine geological setting, the reservoir modelling scale, and the available data (see Figure 2.8). For example, a typical SAGD flow simulation grid ($10^2 m^3$) is seven orders of magnitude bigger than a core plug data ($10^{-5} m^3$). In the other words, about 10 million core samples are required to fill a flow simulation grid cell. This scale variation should be carefully considered in the reservoir modelling.

The geological modelling scale is typically larger than the core, well log, and seismic data scale and smaller than the flow simulation grid size. Calculating ef-

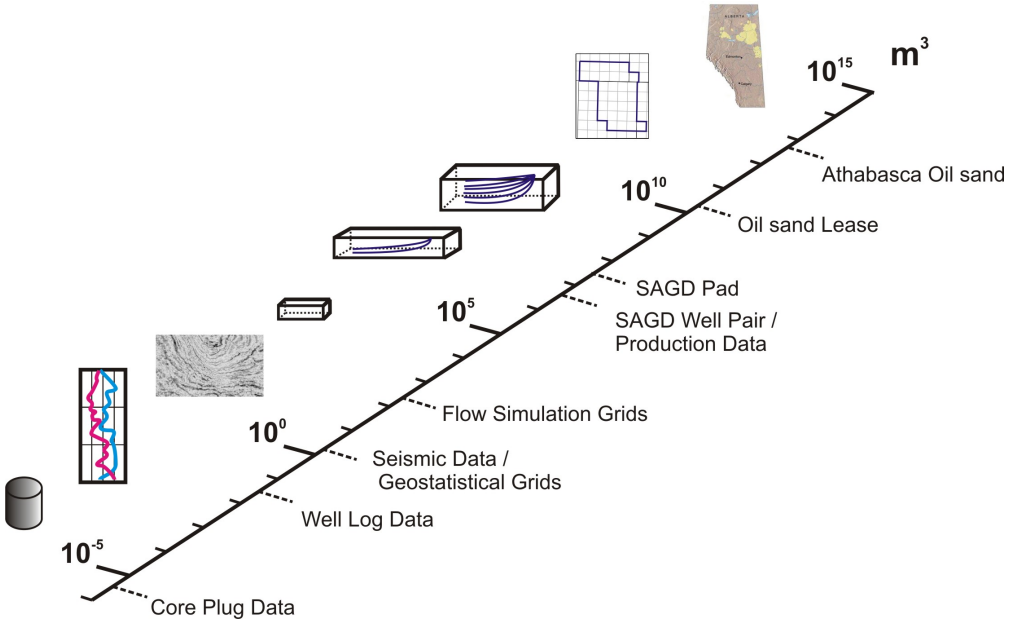

Figure 2.8: Variation of scale in available data and possible modelling scale for the McMurray Formation. An average thickness of 50 m is assumed for the oil sand lease and the Athabasca oil sands.

fective reservoir properties for flow simulation grid involves two upscaling steps; upscaling of data to the geological modelling cell, and upscaling of geological cells to the flow simulation scale after properties are populated. Upscaling for most reservoir properties such as porosity and fluid saturations is straightforward because there is a linear relation between those properties at different scales. However, permeability and facies proportions do not average linearly and have more complex relationship at different scales.

Permeability micro-modelling (Hosseini et al., 2008; Deutsch, 2010; Boisvert et al., 2012) and mini-modelling (Waite et al., 2004; McLennan et al., 2006; Deutsch, 2010) techniques account for the permeability scale variation and ensure that small scale heterogeneities are appropriately transferred to the flow simulation grid size. In the micro-modelling techniques, micro scale geological features that are extracted from 2D digital core photos and FMI logs are used as conditioning data to generate micro-models of facies, permeability, and

porosity at cubic $1-5$ millimetre grid cells. The size of a typical micro-model is about $0.1\,m$ x $0.1\,m$ x $0.1\,m$. The effective properties of each micro-model are calculated and calibrated with core sample data. A single-phase flow simulation is run for the micro-model to determine the horizontal and vertical permeability. The main goal of mini-modelling is to address the scale change from the decimetre scale to the scale of geological modelling. In this technique, results of micro-modelling, core analysis date, and well logs are used to generate mini-models ($1\,m$ x $1\,m$ x $0.5\,m$) at the decimetre grid cells. Effective properties are then calculated for mini-models and a relationship between porosity and permeability at the representative flow simulation grid size is established. This hierarchical modelling scheme resolves the scaling of permeability.

In general, reservoir models are often built at different scales to capture scale dependent geological heterogeneity. For example, 2D property maps that are generated over a large area (entire hydrocarbon pool) are suitable for integrating large scale geological features and trends. These maps are used for resource estimation and future drilling planning applications. High resolution 3D models are usually built over an area of interest. These models are suitable for flow simulation purposes.

2.3 Estuarine Environment

An estuary (Figure 2.9) is defined as the seaward portion of a drowned valley system which receives sediment from both fluvial and marine sources and which contains facies influenced by tide, wave and fluvial process (Dalrymple et al., 1992). If the sediment is supplied mostly from the fluvial part the site called as a delta and if the sediment is delivered to the area only by marine process the environment is known as a prograding coast. Dalrymple et al. (1992) divided the estuaries into two major groups of wave-dominated and tide-dominated estuaries based on the relative influence of waves and tides.

Figure 2.9: Example of a modern estuary. South Alligator River Estuary, Australia (image from Google Earth).

In the wave-dominated estuaries, tidal influence is small and the mouth of the system is dominated by relatively high wave energy which pushes sediments to move alongshore or onshore into the mouth of the estuary and develop a sub-aerial barrier. This distribution of energy generates a three-fold lithofacies within a wave-dominated estuary. A marine sand body deposits at the estuary mouth. It mainly contains transgressive sub-tidal washover deposits. Coarse grain sand is also deposited at the head of estuary by the river. The middle part of wave-dominated estuaries contains extensive salt marshes and is crossed by tidal channels (Dorjes and Howard, 1975). Figure 2.10 shows the plan view and cross sectional view of wave and tide dominated estuaries.

Tide-dominated estuaries are generated if the wave action is limited and/or

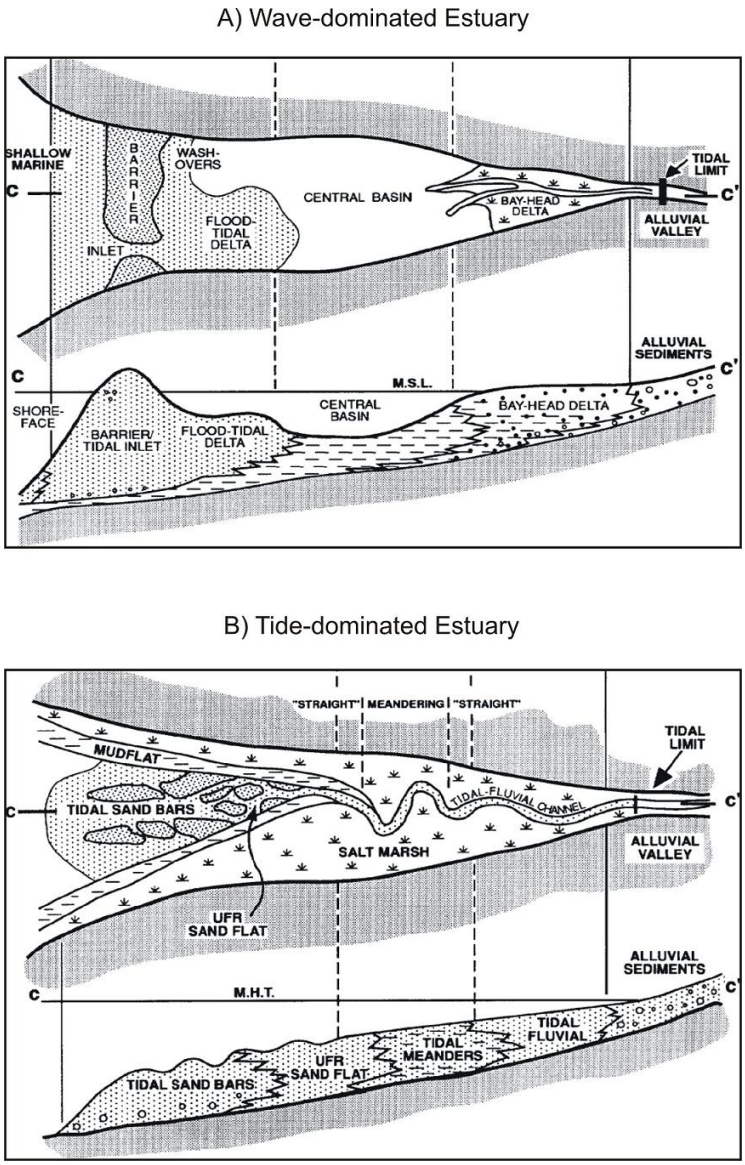

Figure 2.10: Distribution of morphological elements and sedimentary facies in plan view and cross sectional view for A) Wave-dominated estuary (top) and B) Tide-dominated estuary (bottom) (modified after Dalrymple et al. (1992)).

the tidal prism is large (Hayes, 1979). The tidal prism is the volume of water leaving the estuary inlet at the ebb tide. In this case the tidal current energy is dominated at the mouth of estuary and elongate sand bars are typically developed. Moving upstream from these sand bars, the main channel typically

narrows and a straight-meandering-straight progression of channel sinuosity is appeared. In the meandering part of tide-dominated estuaries, the finest channel sands are deposited. The muddy sediments are also accumulated in tidal flats and marshes along the sides of the estuary (Dalrymple et al., 1992).

Tide-dominated estuaries are usually funnel-shaped which means that the main channel typically narrows as moving from the sea to the land (Dalrymple et al., 1992). This change in the channel width relative to the intrinsic length of the channel is called the channel convergence. Channel convergence may appreciably affect the distribution of point bars within the tidal channel. Several authors have discussed the challenges that channel convergence may introduce into the tidal estuarine system (Lanzoni and Seminara, 1998; Marani et al., 2002).

The fluvial and tidal portion of a tide-dominated estuary is defined based on the tidal limit. The tidal limit is defined as a point where the energy of the tidal prism decreases and reaches zero (Dalrymple et al., 1992). Changes of tidal limit over time would result in the development of complex sedimentation and morphology.

The tide-dominated estuarine depositional environment was the dominant geological system during the deposition of the McMurray Formation. In the next section, a review of geology of the McMurray Formation is presented.

2.4 Geology of the McMurray Formation

A formation is a set of rock strata that has similar geological properties that are different from surrounding layers and related to a specific geological time or depositional environment. A set of two or more related formations is called a group.

In the Athabasca oil sands area, the majority of the heavy oil deposits are trapped within the McMurray Formation. McLean (1917) was the first who called the oil bearing sands overlying the limestone along the Athabasca River

as the McMurray Formation. The McMurray Formation is part of the early Cretaceous geological group that is called the Mannville Group of northern Alberta. The lower part of the Mannville Group contains the McMurray Formation and the upper part contains the Wabiskaw member, the Clearwater Formation and the Grand Rapids Formations. The McMurray Formation rests directly on top of the Devonian evaporates and carbonates with a sharp contact of an unconformity surface (see Figure 2.11).

The sub-Cretaceous unconformity played an important role in the sedimentation of the McMurray Formation. Before the deposition of the McMurray Formation, the Devonian carbonate was eroded and a broad north-westerly trending valley known as McMurray sub-basin was created. The Valley was surrounded by Precambrian Shield on the east and the carbonate of the Grosmont Formation on the west (Stewart et al., 1978). The deposition of the McMurray Formation in this valley was a response to the rise of the Cretaceous Boreal Sea to the north in very early Albian times (Flach et al., 1984; Ranger and Pemberton, 1997). Further transgression of the Boreal Sea deposited the shoreface sand and shale of the Wabiskaw member and the Clearwater Formation on the top of the McMurray Formation (Wightman et al., 1995).

Figure 2.12 shows as estimated Isopach map of the McMurray Formation and the north-westerly axis of the McMurray Valley system. The thickness of the McMurray Formation varies up to more than $110m$ (Ranger and Gingras, 2003). The overburden thickness on the McMurray Formation in the Athabasca deposits varies from $0m$ in outcrops along the Athabasca River (northeast of the deposit) to more than $450m$ at the southwest of the deposit.

2.4.1 Stratigraphy

Stratigraphy is related to the study of rock succession and the correlation of geological events and processes in time and space (Grabau, 1913; Dunbar and Rodgers, 1957). Several graphical, numerical and experimental methods and field observations are required to identify the stratigraphy of a study area.

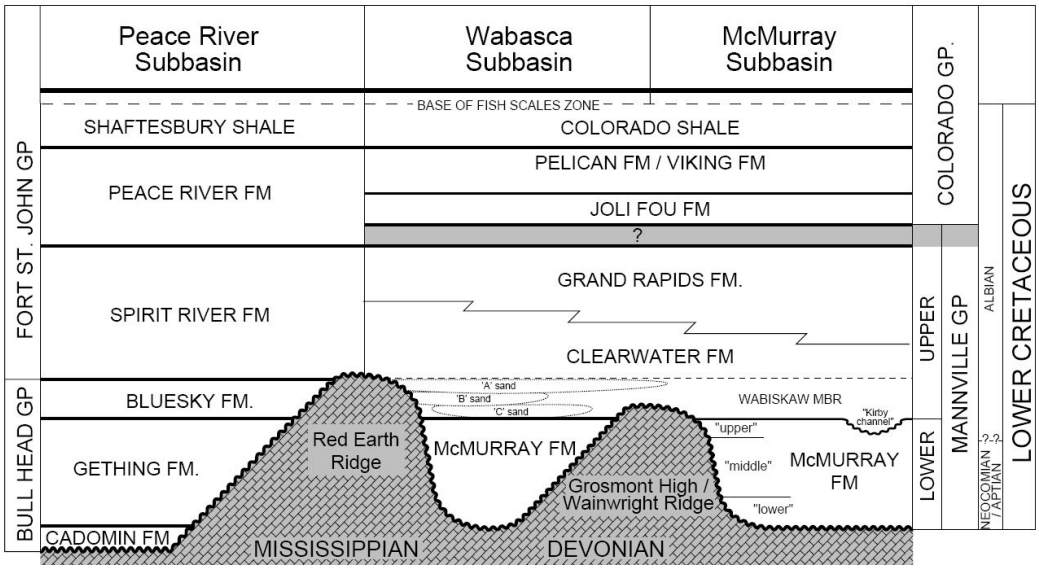

Figure 2.11: Lower Cretaceous sequence of Northern Alberta (Ranger and Gingras, 2003).

Many studies have been done to identify a reasonable stratigraphic subdivision for the complex depositional system of the McMurray Formation. In general, the McMurray Formation is bounded between a sequence boundary at the bottom separating it from the Devonian succession and a flooding surface at the top separating it from the Clearwater succession (Bagdan, 2005). Informally, Carrigy (1959) suggested three stratigraphy subdivisions consisting of lower fluvial succession, middle estuarine point bar succession and upper coastal plain units (see Figure 2.13). This idea has been supported more by other studies of outcrops and cores in the McMurray Formation (Stewart et al., 1978). In recent years, some authors (Flach et al., 1984; Hein et al., 2000; Hein and Cotterill, 2006) suggested to use a two-fold McMurray Formation description. They believe that the distinctions between the middle and upper McMurray are not possible on a regional scale. However, distinct lithofacies differences have been seen in the number of lease-wide studies (Ranger and Gingras, 2003; Crerar, 2003; Crerar and Arnott, 2007) that suggest the original tripartite subdivision. Throughout this thesis, this three-fold subdivision is adopted.

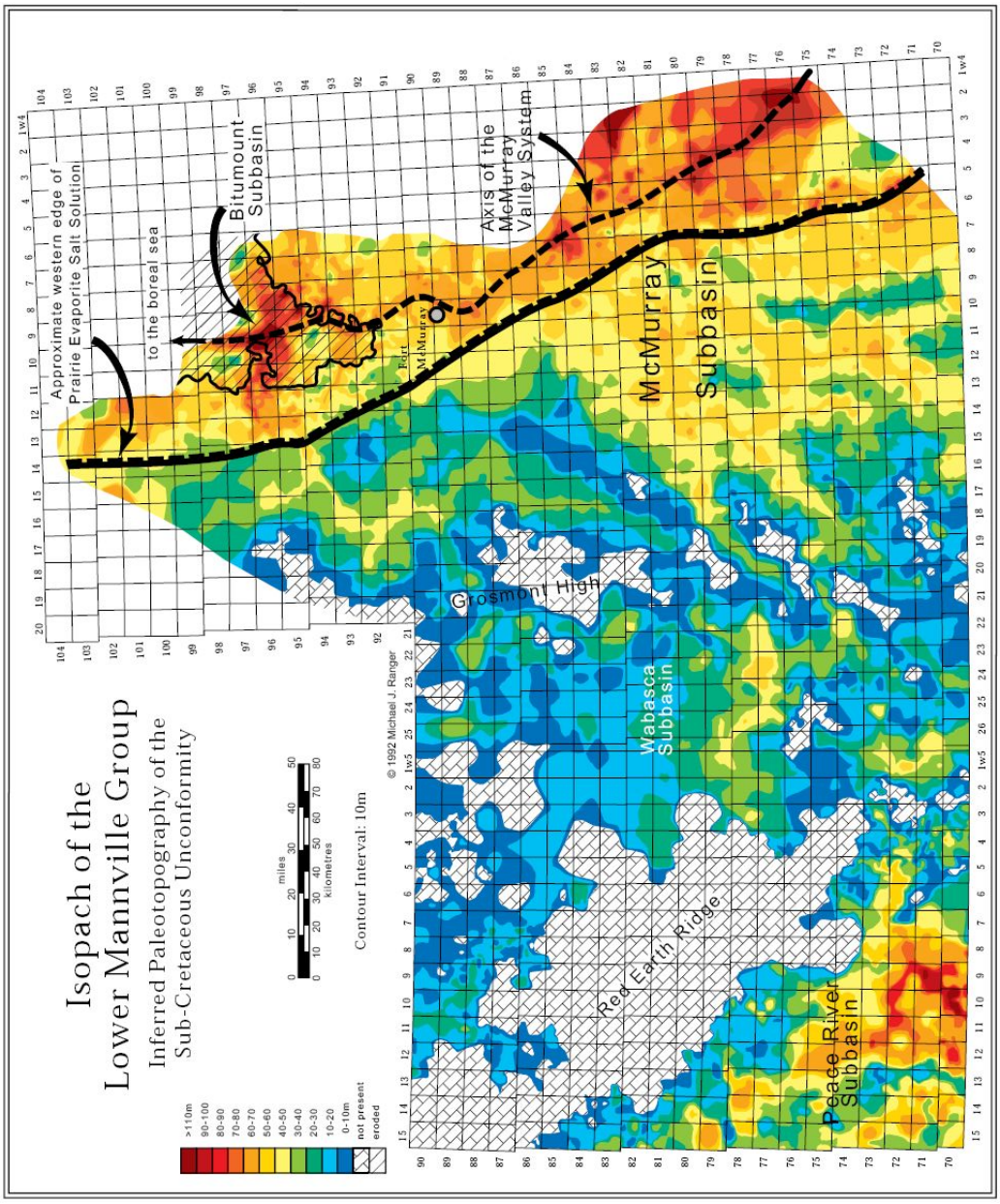

Figure 2.12: Isopach map of McMurray Formation. The dashline shows the axis of McMurray valley (Ranger and Gingras, 2003).

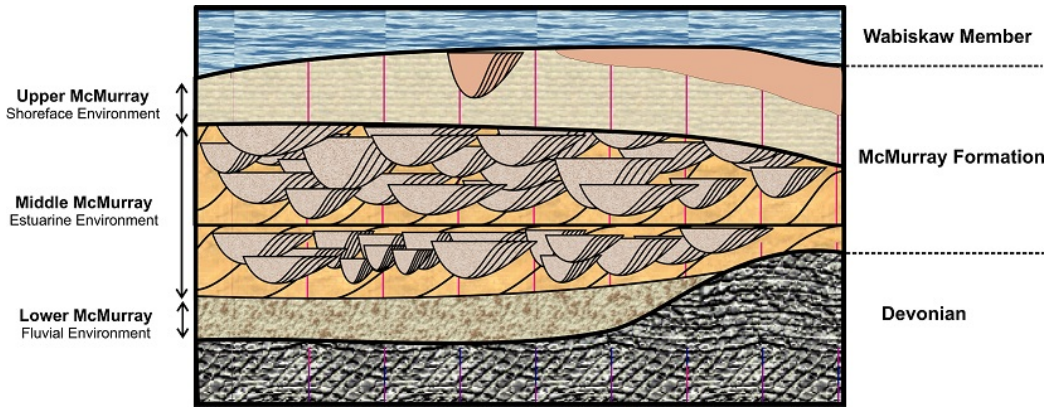

Figure 2.13: Stratigraphy subdivision of the McMurray Formation (modified after Mossop and Flach (1983).

Lower McMurray

The Lower McMurray unit mainly contains massive sandstone and pebbly conglomerates that was deposited within shallow meandering fluvial channels (Mossop and Flach, 1983; Ranger and Pemberton, 1997). This unit is mainly preserved along the topographical lows of the Devonian unconformity surface and mostly saturated with water (Hein and Cotterill, 2006). There are some indicators (rare bioturbation, presence of rooted and coal horizons) that the fluvial systems of the lower McMurray unit may have been the upper part of a greater estuarine system (Ranger and Gingras, 2003). The channel deposits are mainly point bars which are developed on the convex bank of fluvial river channels as a result of lateral migration (Fox, 1988).

Middle McMurray

The middle unit of the McMurray Formation is the thickest part and contains the best reservoir sands. This unit is dominated by inclined interstratified sand and mud and cross-stratified sands. The middle unit was originally interpreted to be fluvial lateral accretion deposits (Mossop and Flach, 1983). However, strong marine influences suggested that the middle McMurray member was deposited within a tidally influenced middle to outer estuarine system (Smith,

1987; Wightman and Pemberton, 1997; Ranger and Gingras, 2003). This unit either overlies the sediments of the lower unit or lies directly above the Devonian carbonates (Fox, 1988).

Upper McMurray

The Upper Unit of the McMurray Formation is characterized by horizontal strata which are often in sharp contrast to the large inclined sand beds of the middle McMurray and mainly contains interbedded sand and dark grey mud with low bitumen saturation (Ranger and Gingras, 2003). Flach and Mossop (1985) suggested an open marine depositional environment for this unit. However, Ranger and Gingras (2003) indicated two coarsening-upward cycles that rejects the idea of a fully marine depositional environment. They believed that the vertical arrangement of lithofacies within each coarsening-upward unit represents the characteristics of a shoreface environment.

2.4.2 Facies Description

Classification of facies in the McMurray Formation is not a trivial task because of the complex and heterogeneous geological features that vary laterally and vertically over very short distance. Many authors provided detailed faices description for the McMurray Formation based on studies carried out on outcrops, cores, and logs.

Mossop and Flach (1983) simply introduced three facies that are always present in the vertical order in the most outcrop and mine face exposures of the McMurray Formation. Hein et al. (2000) provided a very comprehensive and detailed classification and description of facies in the Athabasca deposit by introducing eighteen lithofacies. Crerar (2003) suggested eight facies that are organized into five depositional facies associations; braided fluvial, tidally-influenced meandering channel fills, associated overbank, open estuarine tidal flat, and shoreface to offshore. This facies associations have been defined based on the geometric stacking patterns and genetic relationships.

In this thesis, the most common and important reservoir and non-reservoir facies are described mostly based on the description provided in Ranger and Gingras (2003).

Clean Sand

One of the most important reservoir facies in the McMurray Formation is the large scale cross-stratified coarse sand that may be bedded or massive. This facies is characterized by excellent porosity and permeability and high bitumen saturation and is mostly presented in the middle McMurray unit. It consists of bedsets up to $0.5m$ or more in thickness that is normally truncated at the top by succeeding events or may be capped by a thin shale lamina. (Ranger and Gingras, 2003). The lateral extent of this facies may be 1 to $3m$ along the strike (Hein et al., 2000).

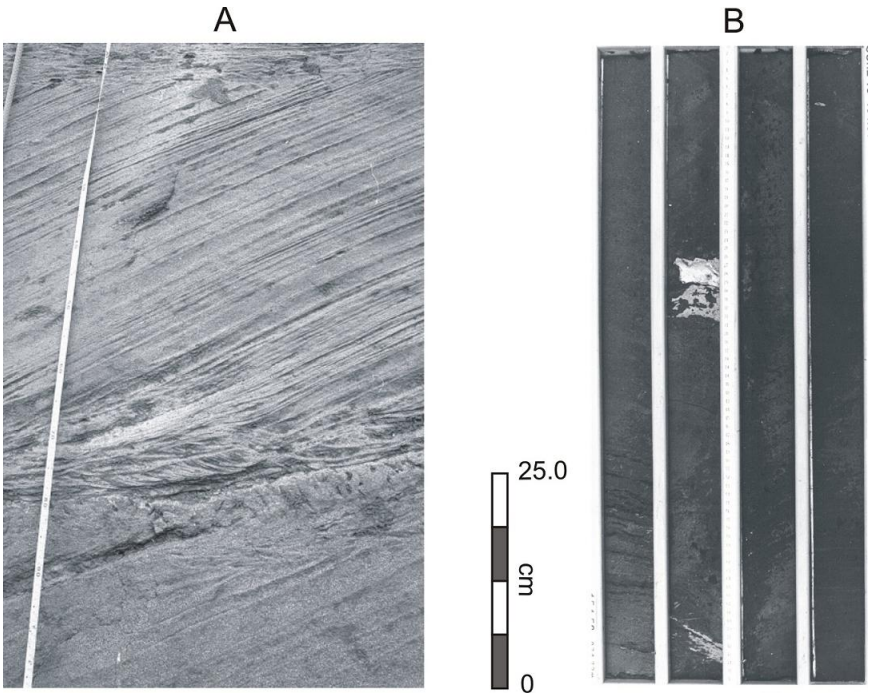

Figure 2.14: Clean Sand Facies of McMurray Formation in: A) outcrop (Ranger and Gingras, 2003) and B) core sample (Hein et al., 2000). Both figure are in the same scale.

This facies is often interpreted to be part of a high flow regime fluvial channel deposit; however, detail investigation of outcrops and cores shows strong tidal indicators (reverse flow ripples, reactivation surfaces, etc.) that are typical specifications of an estuarine system. Ranger and Gingras (2003) suggested considering this facies in the lower (outer) estuary proximal to the estuary mouth. Figure 2.14 shows an example of clean sand in outcrop and core sample for the McMurray Formation.

Inclined Heterolithic Stratification

Aside from the clean sand, Inclined Heterolithic Stratification (IHS) is another major facies association of the middle McMurray Formation. Thomas et al. (1987) was the first to call the heterogeneous deposits with notable primary dip by the term IHS. Previously, this facies was known as *epsilon cross-stratified sand* (Mossop and Flach, 1983; Allen, 1963).

IHS packages consist of inclined repetitive sets of decimeter to meter thick couplets of sand and mud. Based on the amount of mud in the IHS sets, they are often categorized into sandy IHS (dominated by clean sand) or muddy IHS (composed mostly of mud). Figure 2.15 shows IHS in outcrop and cores. Individual sand and shale/mud are known from outcrop to be laterally continuous from top of a facies unit to near the base (Thomas et al., 1987).

It was believed that IHS forms as a result of the lateral growth of active, large-scale bedsets such as point bars or Gilbert-type deltas (Carrigy, 1959) but according to the extensive study of several ancient and modern IHS deposits presented by Thomas et al. (1987), the majority of IHS deposits are products of point bar lateral accretion within meandering channel of freshwater rivers, tidally influenced rivers and creeks draining intertidal mudflats.

Stacking of two or more IHS sets is common in the McMurray Formation. Although, preservation of an entire channel deposit is rare in the Athabasca oil sand area due to reworking of sediments by meander rivers and tide currents, the general shape and geometry of channel deposit have been reported by some

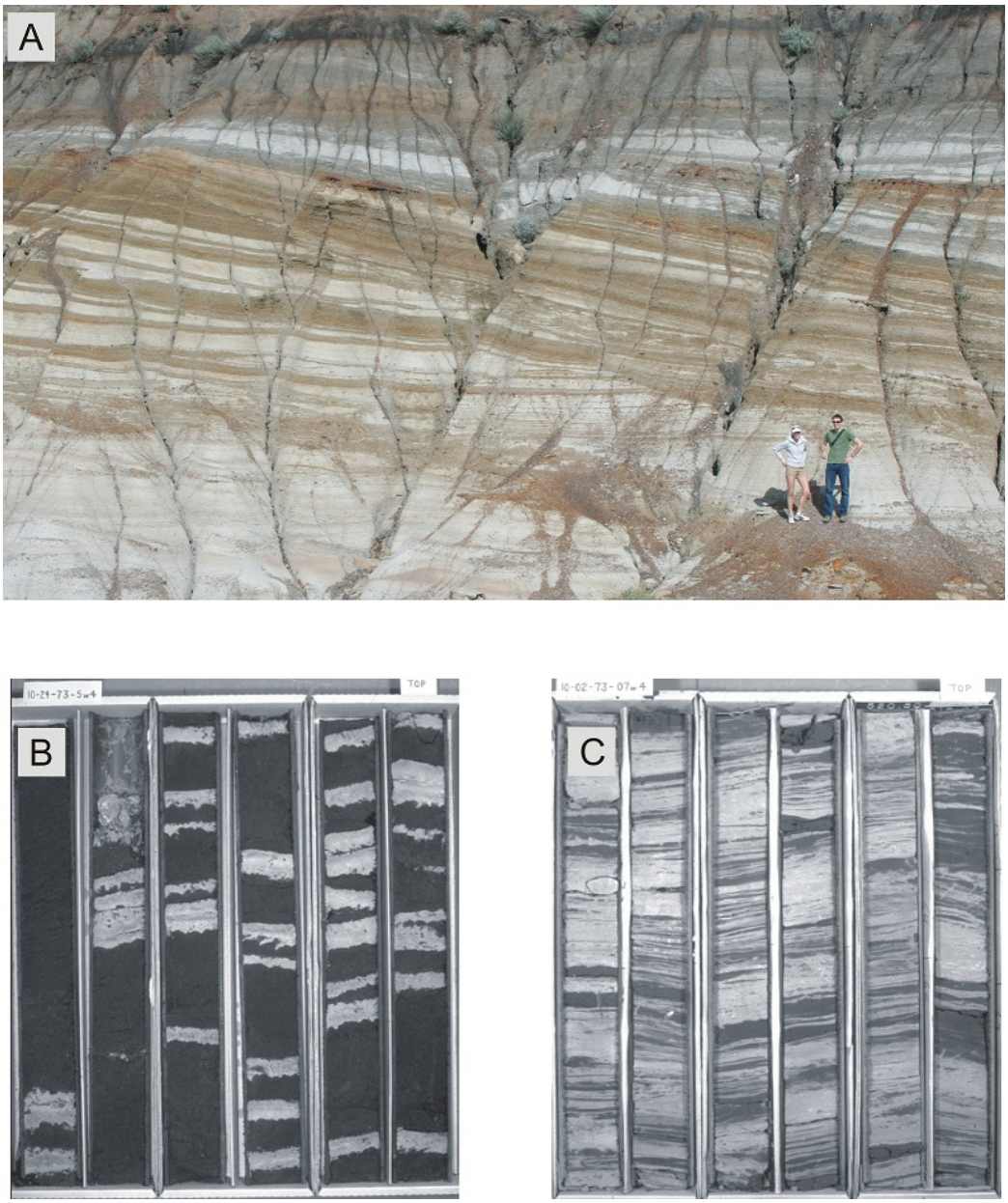

Figure 2.15: Inclined Heterolithic Stratification (IHS) in A) outcrop in Horseshoe Canyon Formation near Drumheller, Alberta B) sandy IHS cores (Ranger and Gingras, 2003), and C) muddy IHS cores (Ranger and Gingras, 2003).

authors. The normal thickness of a single IHS set in the McMurray Formation has been reported to vary between 8 to 25m within the channels that are 20

to $45m$ thick (Mossop and Flach, 1983). Brekke and Evoy (2004) and Fustic (2007) reported individual point bar deposits with lateral extents of more than $4km$ and $1.5km$ inferred from the time slice seismic images. The dip angle of IHS beds in McMurray Formation are seen to vary from 4° to 22° (Smith, 1988; Rahmani, 1988; Mossop and Flach, 1983).

The characteristics of IHS facies vary considerably within the estuarine system of the McMurray Formation. Lettley (2004) characterized and classified the IHS packages based on sedimentological and ichnological specifications. According to this study there are generally three different types of IHS deposits within the main estuarine channel system of the McMurray Formation; sand-dominated IHS in the upper reach, fine-grained muddy IHS in the middle reach, and sand-dominated IHS in the lower reach. These IHS deposits are different in terms of texture, structure, biogenic signature, and stratal organization (See Figure 2.16).

Breccia

Breccia is a common facies in the middle and lower McMurray Formation units. It consists of mud clasts that are distributed within a clean sand matrix (Figure 2.17). This facies is associated with the fluvial/estuarine channel deposits of McMurray Formation. As the channel migrates, the pre-existing bank collpases and generates mud clasts. Clasts may also be generated as a result of erosion of previously deposited muddy IHS. The mud clasts are later embedded in the sand sediments at the bottom of the channel.

Based on the mud clast content, the breccia facies is divided into two categories of matrix-supported (less clast) and clast-supported (mostly clast). The breccia facies in the McMurray Formation is mostly matrix-supported and varies in thickness from $10cm$ to more than $5m$ with limited lateral extent (Hein et al., 2000).

Despite the lower oil saturation compared to the clean sand, breccia is commonly categorized as net reservoir facies because of its relatively high porosity

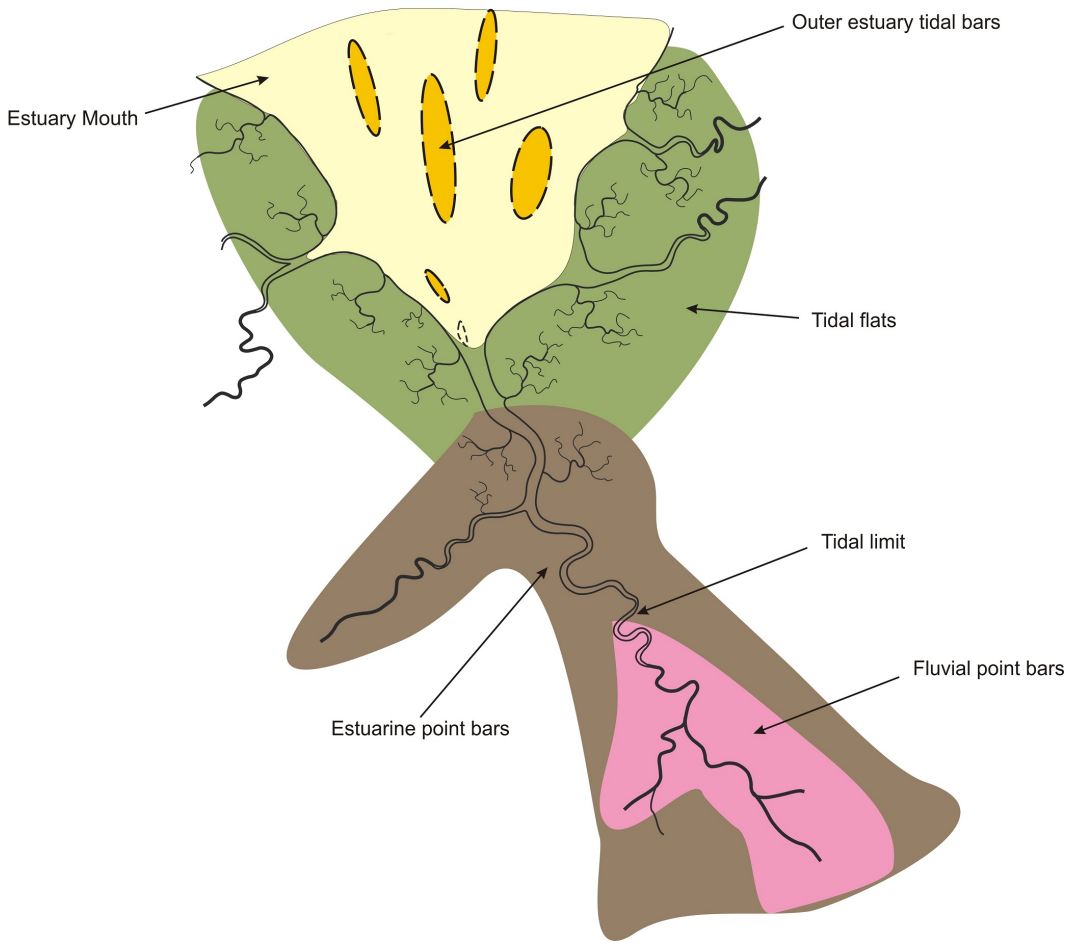

Figure 2.16: Distribution of point bars in Estuarine environment of middle McMurray Formation (modified after Lettley (2004)).

and permeability characteristics. Although, the mud clast content can be high, they are not all connected to each other and they do not act as a flow barrier.

In core, breccia is identified by prominent and well defined mud clasts in sandy matrix. It is quite difficult to distinguish this facies from the muddy IHS facies in the gamma ray log. In this case the dipmeter log can discriminate the breccia from muddy IHS by showing random dip directions over short interval (Hein et al., 2000).

Mudstone

Mudstone is the major non-reservoir facies in the McMurray Formation. Mud intervals that are commonly observed in the core are interpreted as the estuarine abandoned channel fill with several meters thickness (Ranger and Gingras, 2003). Another sedimentation source of mud in the estuarine deposit of the McMurray Formation is the tidal flat deposits however, because of several lateral migration of tidal channels this type of mud is poorly preserved (Crerar, 2003; Crerar and Arnott, 2007).

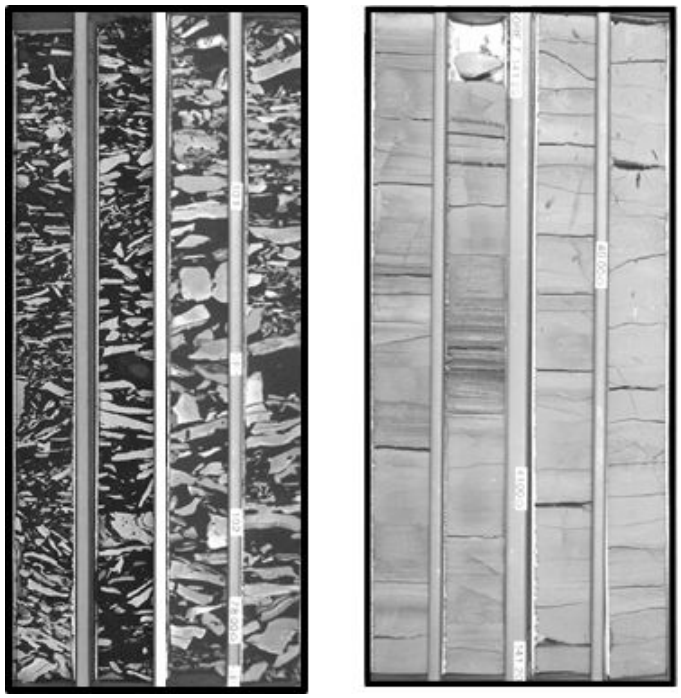

Figure 2.17: Breccia (left) and Mudstone (right) facies in core samples (Hein et al., 2000).

2.4.3 Depositional Model

As discussed above, the McMurray Formation is nominally composed of three informal units of lower fluvial, middle estuarine, and upper shoreface deposits.

At the early time of McMurray deposition, fluvial channels of the lower McMurray unit were developed and filled the topographical lows of the sub-Creataceous unconformity. Then, there was a much wider area available for the estuarine channel fill of the middle unit to accumulate and be preserved (Ranger and Gingras, 2003; Crerar and Arnott, 2007).

A detailed understanding of deposition of the middle McMurray unit has been of particular interest to many researchers. Carrigy (1971) interpreted IHS within the McMurray Formation as foreset deposits of small, Gilbert-type deltas prograding northward into a standing lacustrine or lagoonal body. Mossop and Flach (1983) proposed deposition of IHS under the deep meandering fluvial channels environment. Based on the study on the core and outcrops, they proposed the incised valley fills model for two facies associations of middle McMurray Formation (clean sand and IHS). They believed that both the massive cross-stratified sand and the IHS complex are sub-environment of the same system tract. The cross-stratified sands that typically underlie the IHS in outcrop have been interpreted as large scale bedforms that migrated on the channel bed. However, there are some indicators (fining-upward succession and indicators of brackish water conditions) that support the idea of deposition within a channelized central estuarine environment which was first introduced by Stewart et al. (1978). They believe that under the transgressive system, the sea level was repeatedly raised and fallen and changed the environment from fluvial to estuarine. This idea was later supported by work of Pemberton et al. (1982); Smith (1987); Ranger and Gingras (2003). Based on this idea, the large scale cross-stratified sand and the IHS bedsets are both depositional elements of a tide-dominated delta. The strong tidal indicators of cross-stratified sand suggests that it is part of the outer estuarine sediments, and IHS bedsets are part of the middle estuarine distributary channels (Figure 2.18).

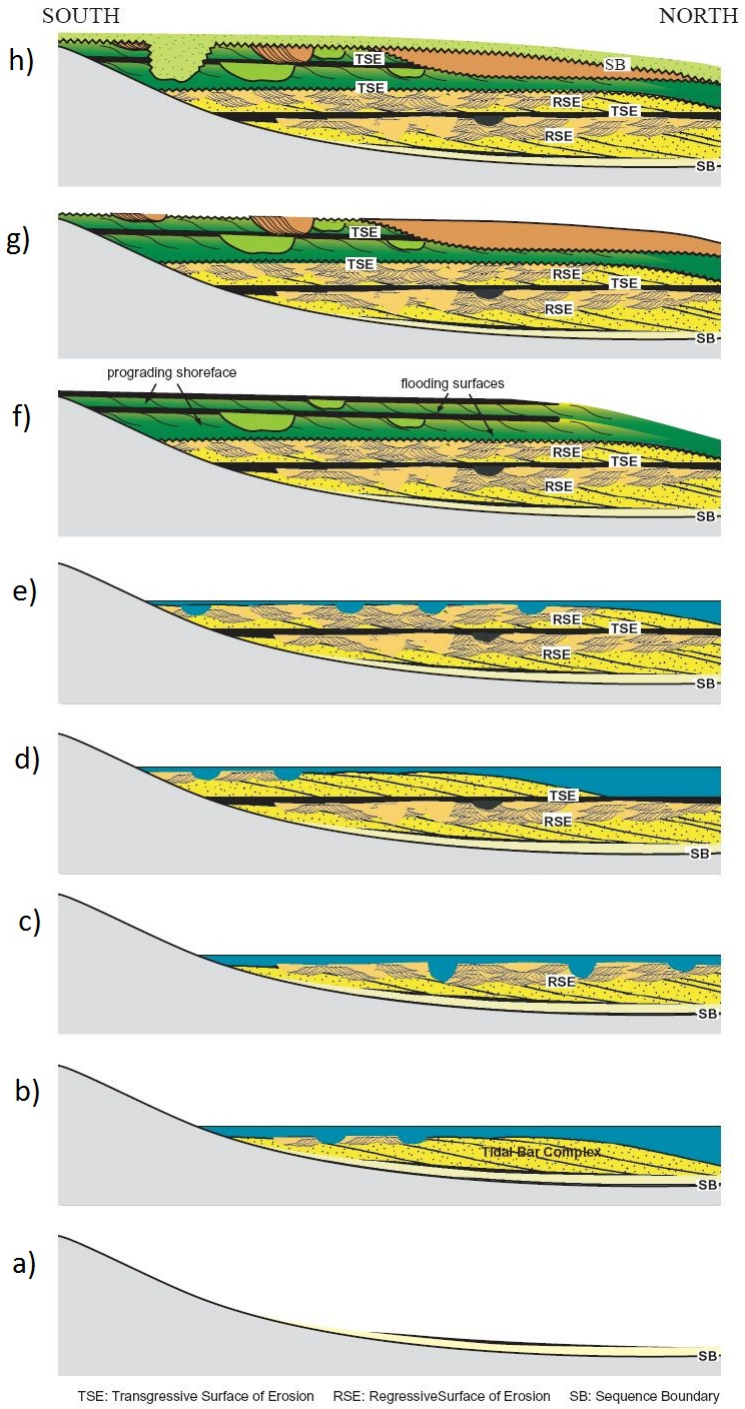

Figure 2.18: Depositional Model of the McMurray Formation suggested by Ranger and Gingras (2003). a) early fluvial of lower McMurray, b) early transgression and developement of tidal bar complex of middle unit, c) further development of middle estuary channel which truncate tidal bar complex, d) sea level rise and transgression, e) further development of tide-dominated estuary, f) sea level rise and transgression followed by development of shoreface parasequences g) sea level drop h) unconformity at top of McMurray Formation.

Chapter 3

Tidal Channel Modelling

The McMurray Formation was deposited within fluvial and estuarine environments. Channels play a key role in transportation and deposition of sediments in these systems. As explained in the previous chapter, the main facies of the middle McMurray Formation, IHS, was deposited on the banks of tidal channels. Therefore, their distribution, shale proportion, and the orientation of shale drapes (mesoscopic and macroscopic heterogeneity scales) are highly related to the geometry and distribution of the tidal channels in an estuarine system (megascopic scale). Many authors have studied tidal channel systems (Fagherazzi and Furbish, 2001; Marciano et al., 2005; Kirwan and Murray, 2007) . Most of the modelling approaches are based on the numerical equations of water and sediment transportation. However, less focus has been given to numerically modelling of the geomorphology of tidal channels.

The goal of this chapter is to provide a methodology to create numerical model that mimic the geometry of tidal channelized system. The method is an object/event based technique that enables generation of multiple realizations of tidal network channels based on the channel centreline simulation and mimicking the evolution process based on the pre-defined geological parameters.

Details of modelling are explained in the following sections. First, in Section 3.1, an analog modern tidal channel system is introduced as a conceptual model. Section 3.2 explains details of tidal meander parameterization with

mathematical functions. In Section 3.3, a stochastic modelling approach, called ESTUSIM, is explained followed by an example. Finally, in Section 3.4, some possible approaches to make dynamic tidal channel model are discussed.

3.1 Conceptual Model

Figure 3.1 shows conceptual model of an estuary with all associated channel systems provided in Lettley (2004). It also shows an aerial photo of a portion of a modern tidal channel networks in the lagoon of Venice that has similar tidal channel geometric features as tidal channels in the estuarine conceptual model. This snapshot shows a tree-shaped channel system that is equivalent to a tidal channel system of the McMurray Formation at the time of deposition at the ancient Cretaceous time. Although these multi-scale twisted channels are not completely preserved in the McMurray Formation deposits, the numerical modelling of such systems can provide a useful tool to understand and predict the behaviour and geometry of related channels.

The main geological architectural element in the tidal channel systems is meandering channel. The morphology and sedimentary of tidal channels are different from the fluvial channels. The deposits in tidal channels are finer grained than in a fluvial channel. The stability of tidal channels subject to tidal flow dynamics is more than the fluvial channels and occurrence of channel abandonment by chute cut-off and avulsion is lower in tidal channels because of higher water elevation and lower velocity. Channels in fluvial setting are much deeper than the tidal channels. Development of levee and crevasse elements in tidal channels are rare or absent (Barwis, 1978; Musial et al., 2012).

The conceptual model shown in Figure 3.1 is used as a reference for characterization and parameterization of tidal channels in the proposed methodology.

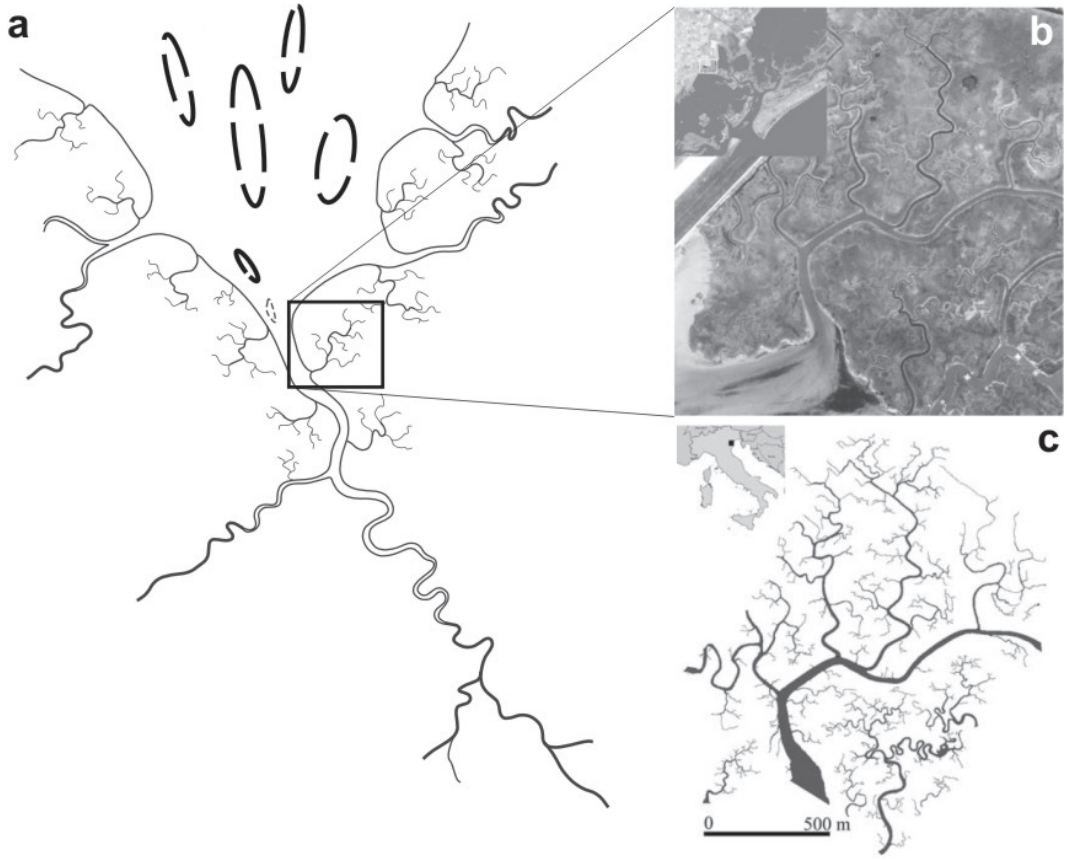

Figure 3.1: Tidal channels as part of a megascopic scale estuary. a) conceptual model of an estuary (modified after Lettley (2004)), b) aerial photo of a portion of lagoon of Venice, c) the digitized image which shows all the channels in the tidal network (Marani et al., 2002).

3.2 Parametrization

Parametrization of estuarine tidal channels is required for object/event based modelling of such a system. The most important characteristics of meandering channels in a tidal network include a channel convergence factor, width-to-depth ratio, channel branching, channel curvature, and channel profile, as described below.

3.2.1 Channel Centreline

There are many different methods available to model meandering channels geometry (Howard, 1992, 1996; Pyrcz, 2004; Cojan et al., 2005). An realistic and efficient method is to represent the central axis of the channel with a centreline. The disturbed periodic model that was introduced by Ferguson (1976) to provide a realistic centreline model. This model has been proposed for stochastic modelling of fluvial channel meandering by Pyrcz (2004). This method is utilized for tidal channel modelling.

The disturbed periodic model is defined by the following equation:

$$\theta + \frac{2h}{k}\frac{d\theta}{ds} + \frac{1}{k^2}\frac{d^2\theta}{ds^2} = \epsilon(s)$$

where θ is the tangent angle, k is related to the primary wavelength, h is the dampening factor and $\epsilon(s)$ is the disturbance value. The discrete approximation of the periodic model can be achieved by a second order autoregressive model of the following form:

$$\theta_i - b_1\theta_{i-1} - b_2\theta_{i-2} = \epsilon_i$$

where the coefficients are defined as:

$$b_1 = 2\exp(-kh)\cos(k\cos\phi)$$

$$b_2 = -\exp(-2kh)$$

This approximation can be applied to stochastically model the channel centreline. In this method the centreline is discretized into a number of points. Generation of a centreline is initiated by assuming a source and a target point. The source point is used to calculate the coordinates of the first two points. Then, the discrete approximation model is applied to calculate the coordinates of the following control nodes. As discussed in Pyrcz (2004), a spline interpolator can be applied to correct the location of the centreline control points to

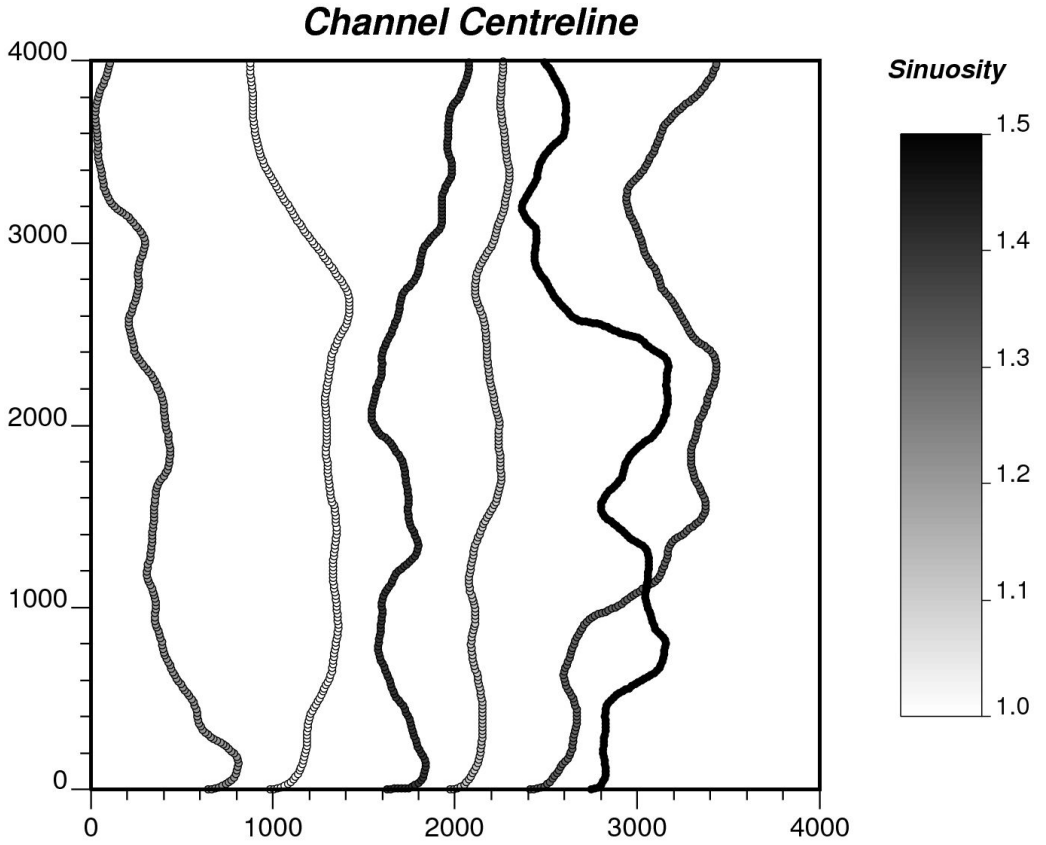

Figure 3.2: Example of six channel centreline generated with the disturbed periodic model using ALLUVSIM program (Pyrcz, 2004). The grayscale shows the channel sinuosity.

honour the target location. Figure 3.2 shows example of six channel centrelines generated with the disturbed periodic model.

One of the main advantages of this modelling technique is that all the properties and geometrical parameters of a channel that are assigned to the discretized centreline points can be stored with no connection to a rasterized grid system (see next chapter on grid-free modelling).

3.2.2 Channel Profile

The geometry of the vertical channel profile is utilized from the fluvial object-based modelling technique provided in Deutsch and Wang (1996) and Deutsch and Tran (1998). The asymmetric channel profile is parametrized by relative thalweg location (position of maximum thickness of a channel), width-to-depth ratio and depth. The thalweg location is closely related to the curvature of the channel. In the high curvature location, the maximum thickness is placed closer to the outside bank of the channel and in low curvature area it is placed at the centre of the channel. Figure 3.3 shows the channel profile variation along the channel line.

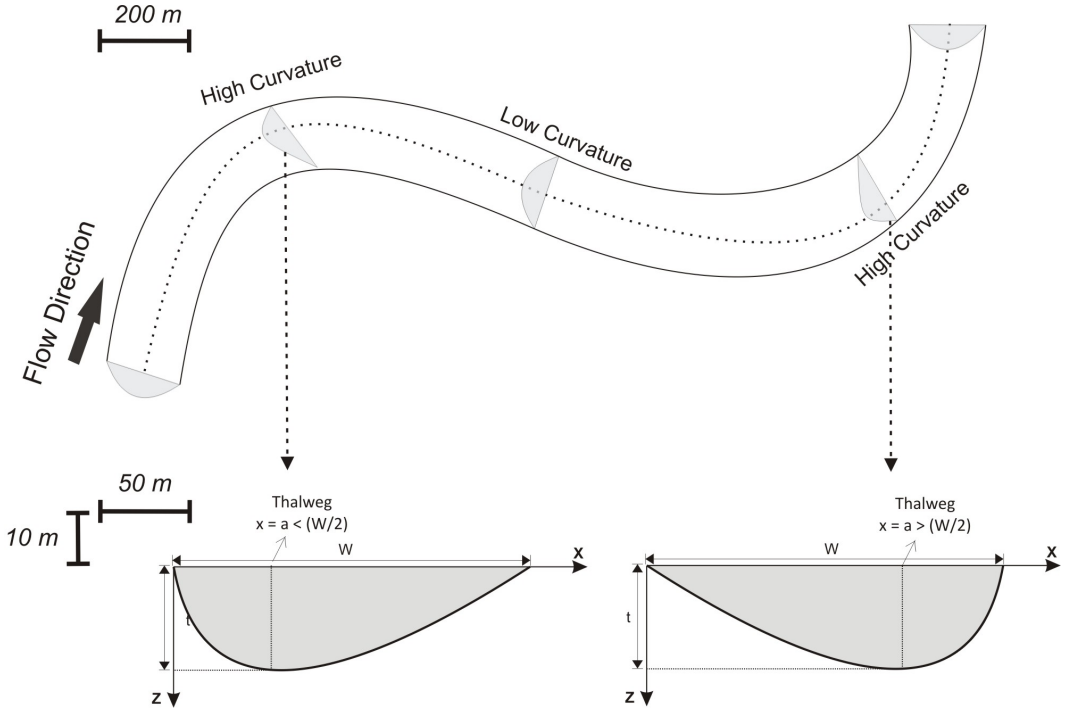

Figure 3.3: Change of channel profile respect to the local curvature of channel.

3.2.3 Width-to-Depth Ratio

The width-to-depth ratio (or aspect ratio) of tidal channels is an important parameter that has a strong effect on the erosional and migration mechanism of meander development. Studies on tidal channels reveal clear differences in the value of width to depth ratio. In salt marshes, the ratio is mostly in the range of 5 to 7 (Marani et al., 2002). This range is quite different from the value observed in the meandering rivers by Millar (2000) (8 to 48). The width to depth ratio for river-like tidal flats is almost the same as fluvial rivers (8 to 50).

3.2.4 Channel Convergence

Tide-dominated estuaries are usually funnel-shaped where the main channel typically narrows when moving upstream, that is, moving from the sea to the land (Dalrymple et al., 1992). This change in the channel width relative to the intrinsic length (distance to the starting discretization point of a channel) of the channel is called the channel convergence. Channel convergence may appreciably affect the distribution of point bars within the tidal channel. Several authors have discussed the challenges that channel convergence may introduce into the tidal estuarine system (Jay, 1991; Lanzoni and Seminara, 1998; Marani et al., 2002). Marani et al. (2002) investigated several tidal channels and noticed that there is an exponential relationship between the channel half width and the intrinsic length of tidal channels:

$$B(s) = exp(a * s + b)$$

where $B(s)$ is channel half width, $a < 0$, and b are constant coefficients, and s is the intrinsic lenght.

3.2.5 Channel Branching

Investigation of tidal environments such as estuarine and deltaic systems, reveal that during the evolution of the main channel, several channels may branch from

it (Fagherazzi et al., 1999; Marciano et al., 2005). The branching may take place at different scales. Considering the main channel as the first level channel, all the channels branching from the first level are called second level channels and all the channels branching from the second level are called third level channels, and so on. Depending on the scale of investigation, up to four channel levels may be expected. As shown in the digitized photo of Figure 3.1, most of the channel branching appears at locations with high channel curvature. This may be supported by the observation that the flow velocity is higher and there is higher chance of channel branching when the channel curvature is high (Ikeda et al., 1981).

3.2.6 Channel Curvature

Channel curvature is an important geometrical parameter of tidal channels for identifying the candidate branching locations. Curvature is generally defined as a parameter that shows the amount of deviation from the straight line. There are different mathematical definitions for curvature. The curvature at each location on the curve can be defined as the inverse of radius of the unique circle that touches the curve at that location:

$$C(s) = 1/r_s \tag{3.1}$$

where r_s is the radius of tangent circle. The curvature can also been defined as the gradient of tangent angle between two points on the curve:

$$C(s) = d\theta/ds \tag{3.2}$$

where θ is the tangent angle and s is an intrinsic distance on the curve.

Both methods are popular in the geometrical calculation of curvature. However, since they are not dimensionless, their range of variation is not pre-defined. For example, in the first method of calculation (Equation 3.1), curvature can take any value between zero to infinity. The defined range of variation for the

curvature is important in numerical calculation of local curvature maxima and minima for defining channel branching locations.

Here, for the application of tidal channel modelling, another definition for curvature is proposed. In this case, the calculated curvature is dimensionless and can take values between -1 to 1.

Considering a channel centreline and the associated discretization points on the channel curve with discretization distance of t. The curvature for each discretization point is defined as the ratio of the distance between the point and centre of the line passing the two adjacent points to the discretization distance (see Figure 3.4). Clockwise curvature is positive and counter-clockwise is a negative:

$$C_i = \frac{d_i}{t} = \frac{\sqrt{\left(x_i - \left(\frac{x_{i-1}+x_{i+1}}{2}\right)\right)^2 + \left(y_i - \left(\frac{y_{i-1}+y_{i+1}}{2}\right)\right)^2}}{t}$$

where d_i is the distance between the discretization point and the centre of line connecting two adjacent points, and x and y are the Cartesian coordinates of the discretization point. Figure 3.5 shows an example of channel centreline and the calculated curvature for all discretization points on the channel.

3.3 ESTUSIM Algorithm

An algorithm for stochastic modelling of an estuarine environment is developed and presented. The objective of this modelling is to stochastically generate a channel network that looks like the one in Figure 3.1. This algorithm is as follows:

1. Generate the main estuary channel centreline (first level)
   (a) Start from a random point at coastal line
   (b) Place a channel randomly

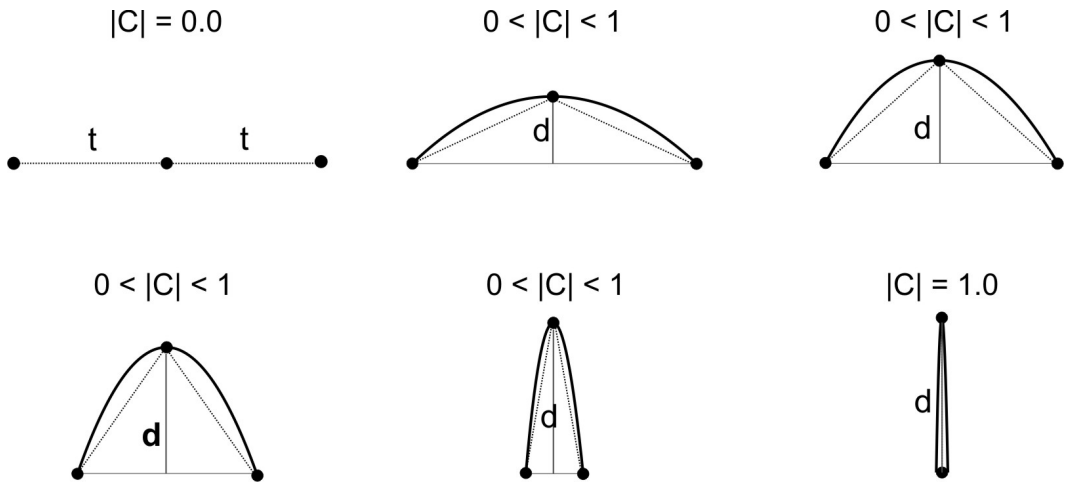

Figure 3.4: Dimensionless curvature definition for three discretization points on the channel centreline.

(c) Calculate channel width and curvature at each discretization points

(d) Rasterize the channel to the grid and assign a facies code to all grid inside channel

(e) Calculate the net-to-gross ratio (NTG), if NTG is less than the target got to the next level; else stop

2. Find the candidate locations for channel branching

   (a) Find local curvature maxima and minima

3. Pick candidate branching location

4. Generate a channel at each candidate points

5. Calculate the NTG, if NTG is less than the target got to step 2; else stop

The simulation is started by generating a channel centreline for the main estuary channel (level 1). A random point is selected as the source location from the user specified coastal line. The channel width is calculated for all discretization points on the main channel based on the initial channel width

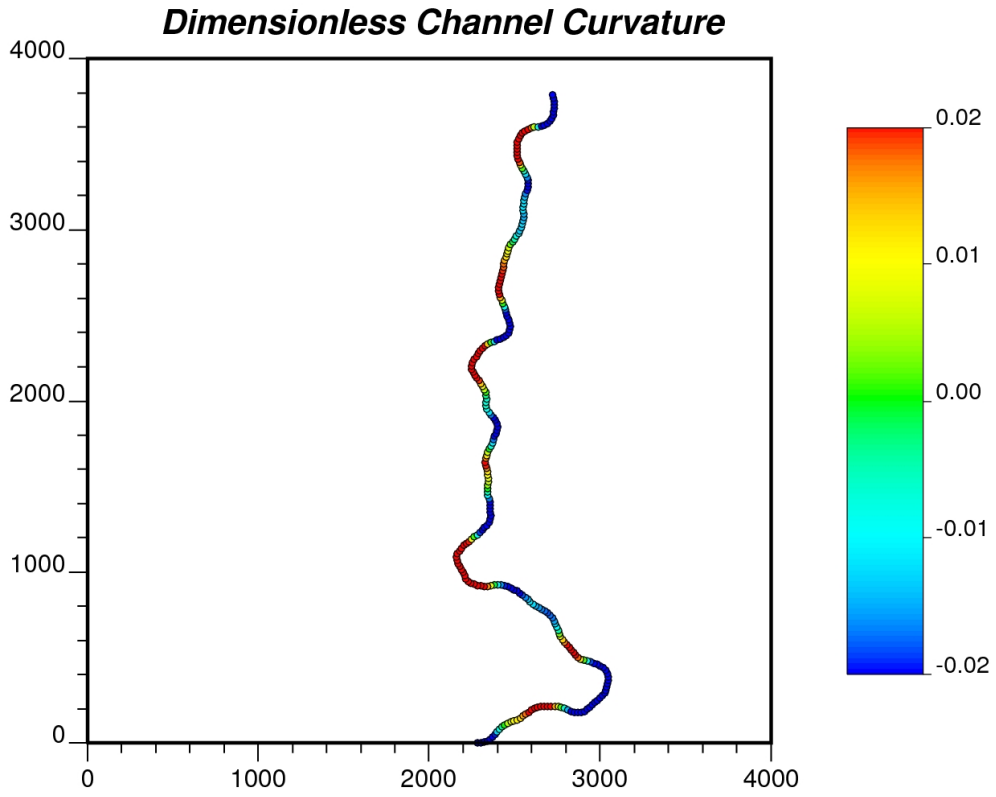

Figure 3.5: An example of channel centreline and the calculated dimensionless curvature.

value. The process of channel centreline generation is stopped when the channel width reaches the user-defined minimum channel width value. As a default, this value is set as the discretization grid size $((\delta x + \delta y)/2)$ however, a more realistic value can be acquired from the outcrops, analog modern tidal channel network, or general geological knowledge of the modelling area.

The next step is to find the candidate locations for channel branching. This requires calculation of the channel curvature at all discretization points and finding the local maximum and minimum channel curvature locations. The derivative of the channel curvature respect to the intrinsic length of the channel (dc/ds) are calculated at each discretization point. Locations where $dc/ds = 0$ is the local maxima and minia. When these locations are defined, branching prob-

abilities relative to their curvature values are assigned to them. Low probability values are also assigned to the other discretization points for a small possibility of branching at those locations. Then, candidate branching locations are picked from the generated probability distribution. For each channel level, a maximum number of channel branching is considered to avoid unrealistic branching geometry. These numbers are picked based on the expert knowledge and geological understanding of the modelling area.

Once the candidate branching locations are defined, the simulation proceeds by generating a new channel at second level that starts from the branching candidate locations. The orientation of a new channel is defined based on the azimuth angle calculated from the branching location and its adjacent discretization point on the upper level channel. This ensures that the new channel is appropriately placed in the model. The channel width and width-to-depth ratio for the new channel are considered to be equal to the upper level channel values at the branching location. This algorithm continues for all channel levels until the pre-specified net-to-gross ratio (channel to non-channel ratio) is reached.

3.3.1 Example

An area of $4\,km$ by $4\,km$ by $10\,m$ was considered for an introductory example. The shoreline was assumed to be at $y = 0$ line with the source location of $x = 2000\,m$. Three channel branching levels are considered. The general orientation of the first level channel was set from South to North.

A discretization grid cell size of $10\,m$ by $10\,m$ by $1\,m$ with the total of 1.6 million cells are considered. The maximum number of channels were specified for each channel level. The minimum channel width was considered to be equal to the cell size ($40\,m$). Figure 3.7 shows an example of the estuarine model generated with the ESTUSIM algorithm. Figure 3.8 shows three more realizations generated with the same specifications.

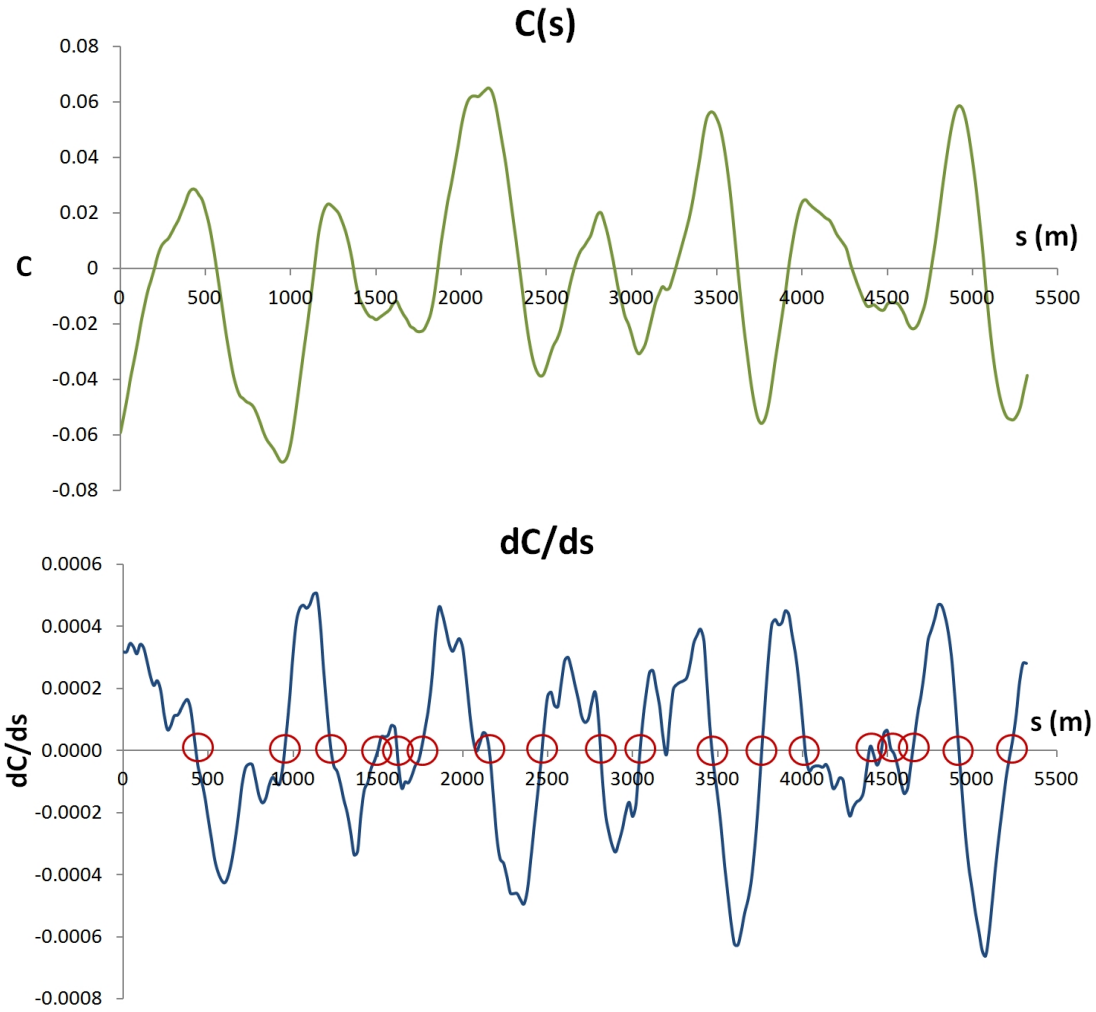

Figure 3.6: Plot of curvature versus intrinsic length and curvature derivative versus intrinsic length for a meander channel. Red circles shows candidate branching locations.

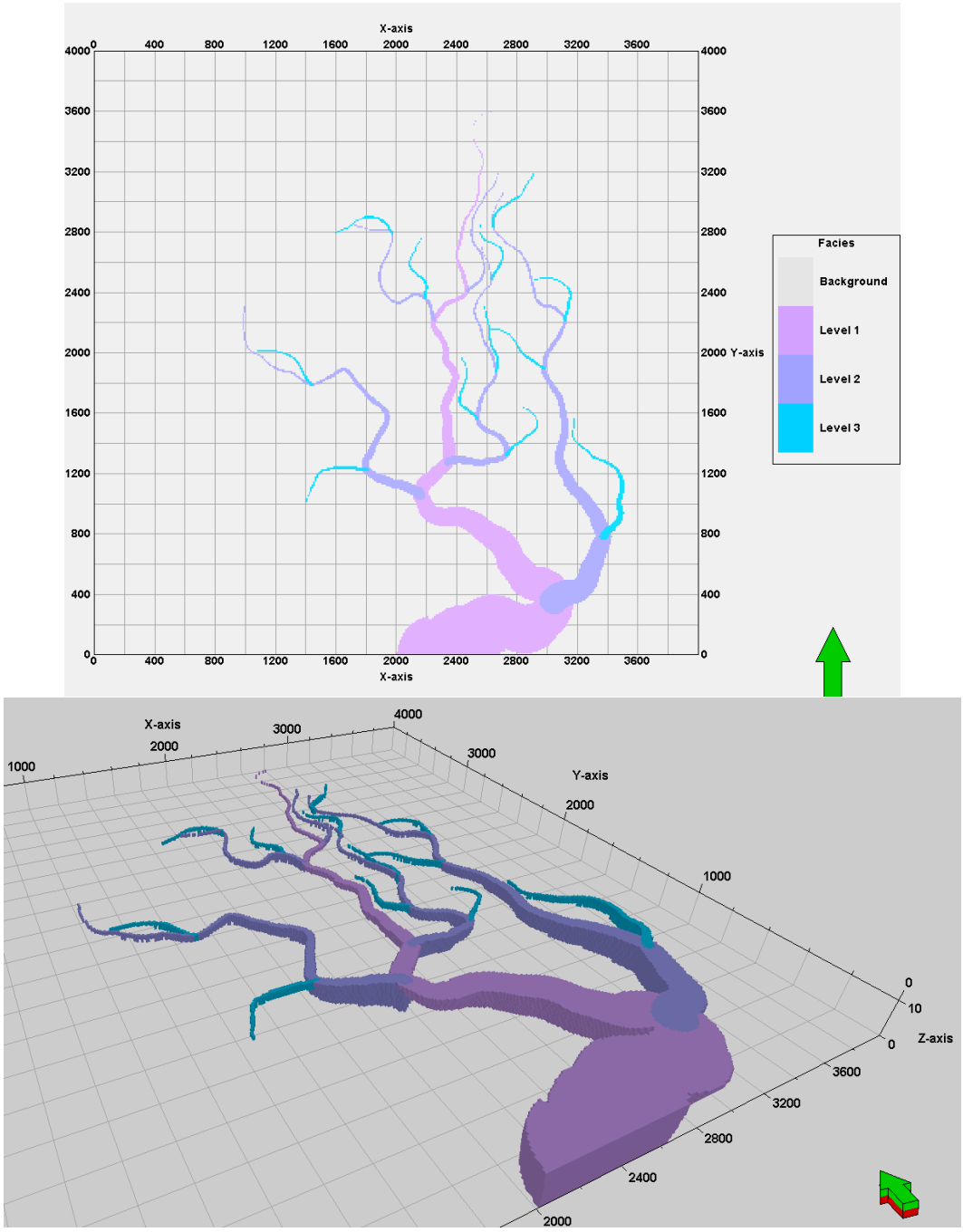

Figure 3.7: Plan view of tidal network model (top), and the 3D view (bottom). Colours show channels at different branching levels.

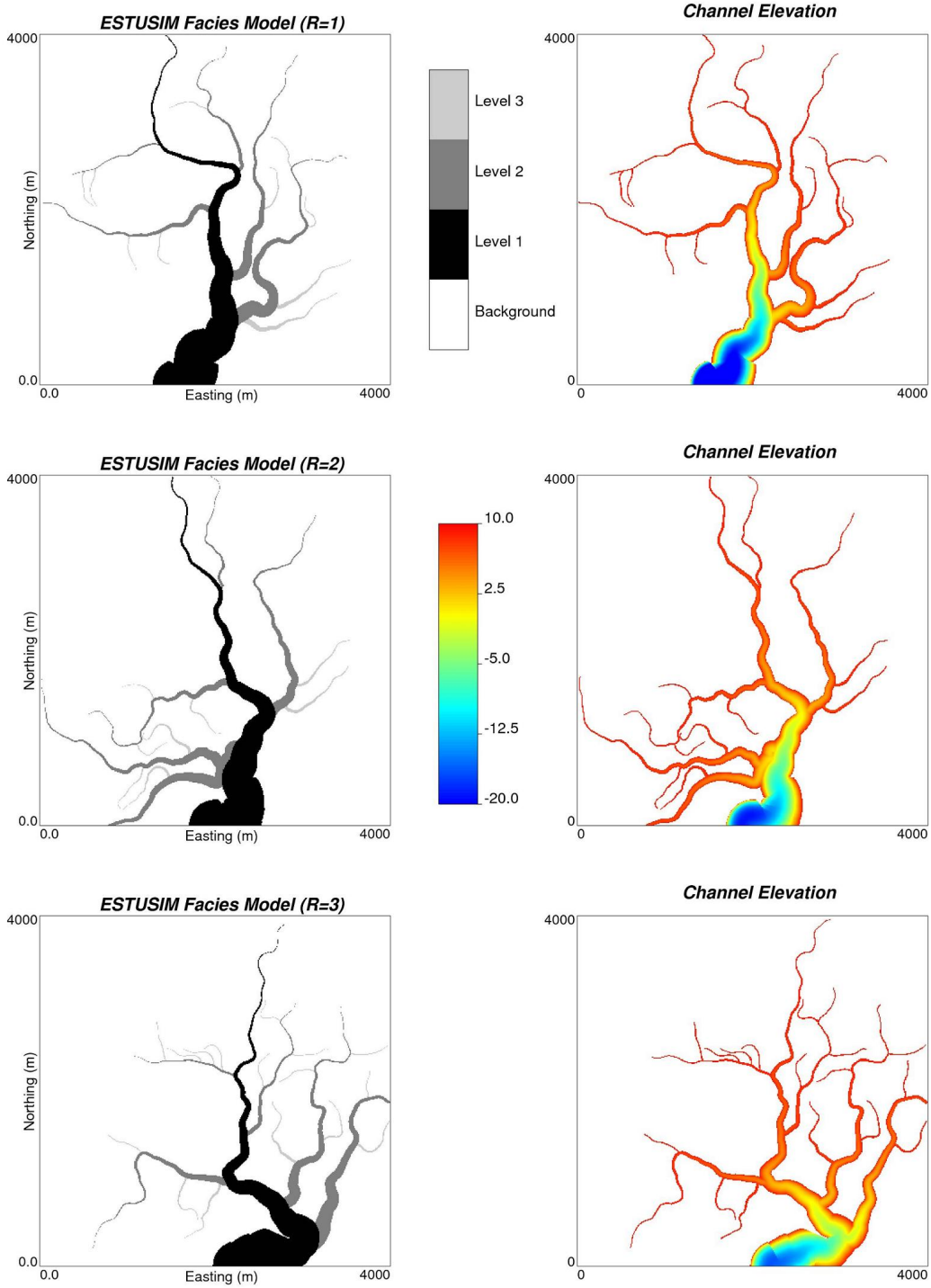

Figure 3.8: Three realizations of tidal channel system generated with ESTUSIM algorithm (left) and their associated channel elevation map (right).

3.4 Dynamic Channel Modelling

The ESTUSIM algorithm presented above is appropriate to generate a tidal channel network for a specific geological time step. The static model such as the one presented in the example may be suitable to be used as a training image in a multiple-point statistical method for cases where channel and non-channel facies are considered.

Preservation of clear long-scale channel geometry(such as the one shown in the above example) in an ancient tidal deposit is rare. Channels in a tidal environment may migrate laterally over time. This lateral migration of tidal channels leads to the development of inclined heterolithic stratification (IHS) bedsets over the channel accretionary bank (Thomas et al., 1987).

The scope of this chapter is not to investigate this in detail; however, some possible ideas are presented in this section to extend the model to include IHS facies in the model. One possible approach to make dynamic channels is to apply the bank retreat model of Howard (1992). This has been implemented for the fluvial channels by Pyrcz and Deutsch (2004). The bank retreat model may not be appropriate because the evolution and migration of tidal channels are different from the fluvial channels (Barwis, 1978). In a tide-dominated estuary, the direction of water flow and sediment flow is occasionally changed. This bi-directional flow is a unique characteristic of tidal channels and leads to a morphology of channels different from fluvial rivers (Fagherazzi et al., 2004).

One idea is to apply the bank retreat model in both flow direction to make realistic channel migration. This is investigated in an example. A single channel centreline was considered. The bank retreat model is applied to migrate the channel for five time steps. Two cases of bi-directional and uni-directional flow were investigated. In the bi-directional case, direction of flow was reversed at each time step by solving the bank retreat model starting from the end of channel. Figure 3.9 and 3.10 show the results of both cases. Results show the differences in these two cases. In the uni-directional flow case, channels are

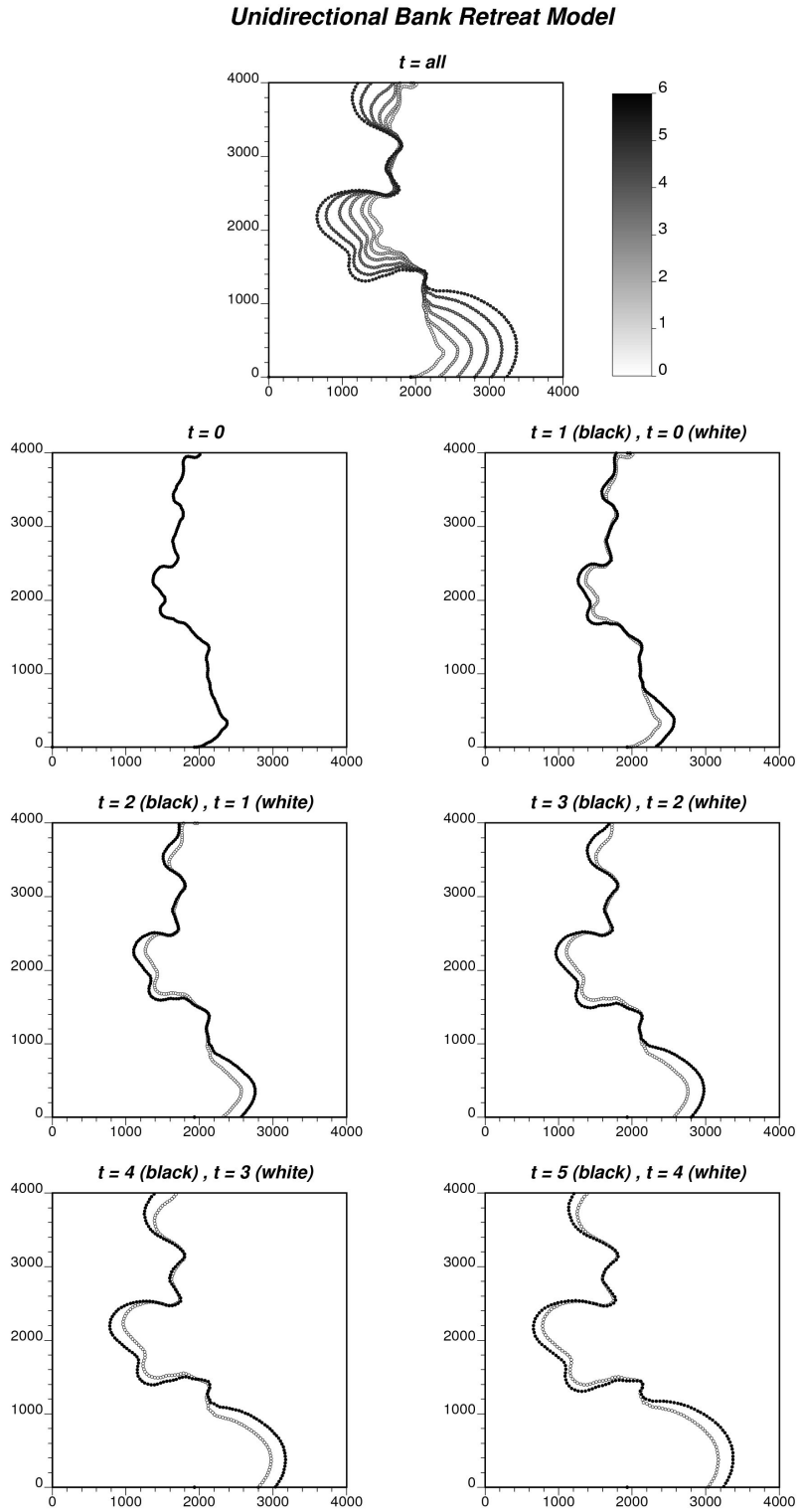

Figure 3.9: Channel migration as result of uni-directional flow. Top shows channel centrelines at the starting step and five lateral migration time steps. The rest show channel at a specific time step and its previous time step for comparison.

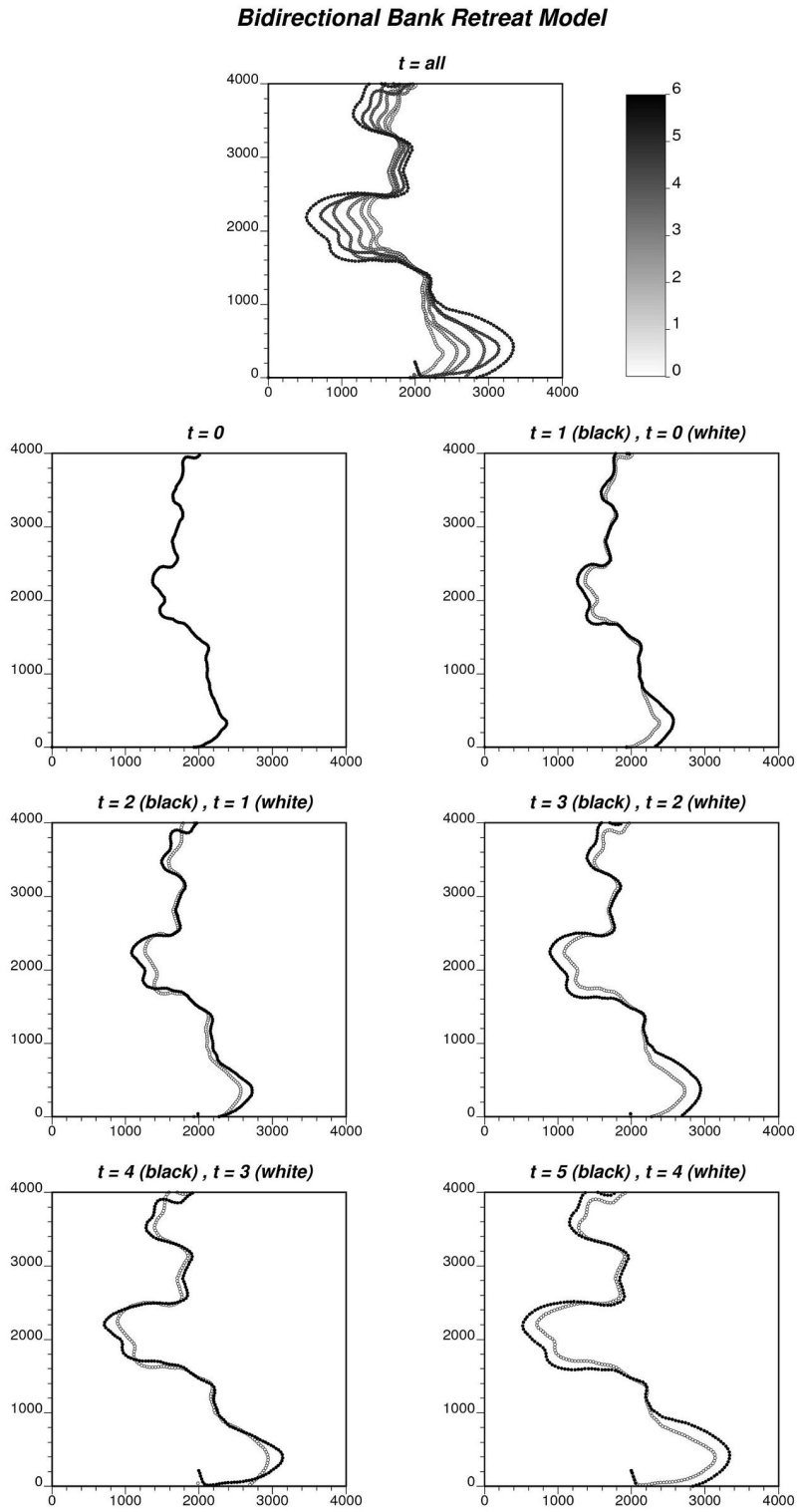

Figure 3.10: Channel migration as result of bi-directional flow. Top shows channel centrelines at the starting step and five lateral migration time steps. The rest show channel at a specific time step and its previous time step for comparison.

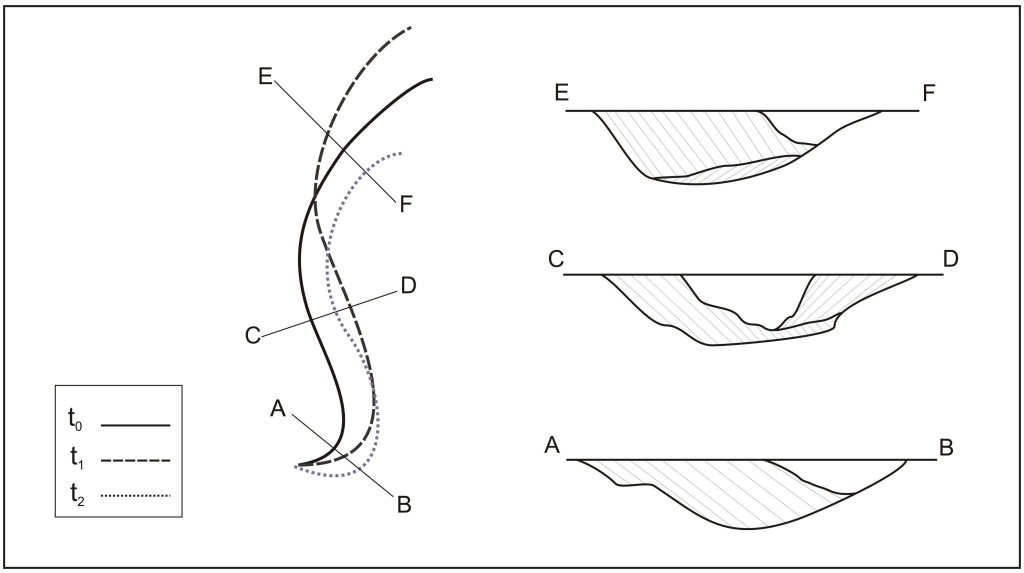

Figure 3.11: Geometric operations can mimic the evolution of tidal channel in an estuarine system. Plan view of channel centreline at three time steps (left) and the associated cross-sections (right).

migrated uniformly with less migration at the low curvature locations (lower flow velocity). However, in the bi-directional flow case, channels are migrated even at the lower curvature location and this leads to asymmetric channel migration.

Another possible approach for mimicking the evolution of tidal channels is to apply some geometric operations such as rotation, translation, stretch, and compression. These method mimics the real processes happening in the estuarine system to some extent. Figure 3.11 shows how this simple geometric operations can generate realistic point bar sets.

3.5 Summary

The ESTUSIM algorithm presented in this chapter is useful for reproducing the geometry of tidal channels in a tidal network. This method is applicable in the modelling of tidal channels in the McMurray Formation. The required input parameters for modelling can be borrowed from the outcrops, modern analogs,

and sequence stratigraphy interpretations.

The static model can be used as a training image in the multipoint geostatistical methods (MPS). Conditioning of the model to well data can also be achieved with the MPS techniques.

Implementation of the ESTUSIM algorithm in dynamic mode would result in generation of inclined heterolithic strata as a result of lateral channel migration. Two possible algorithms for this purpose are suggested.

Chapter 4

Grid-free Modelling of IHS Facies

This Chapter develops a grid-free facies modelling technique that is applicable to the geological architectures present in the McMurray Formation. Both small scale and large scale architectural elements of a typical estuarine system, especially the IHS facies, are defined and then represented with mathematical functions and parameters. An object-based simulation algorithm is designed to mimic the geological evolution of IHS facies in the McMurray Formation. The final grid-free model generated with the simulation engine can be rasterized at different scales for different purposes.

Section 4.1 explains a general framework for grid-free facies modelling. In Section 4.2, the architectural elements of the McMurray Formation estuarine system are explained. Parametrization of the main architectural elements are discussed in Section 4.3. Both unconditional and conditional simulation algorithms are explained in detail in Sections 4.4 and 4.5. Rasterization of grid-free estuarine models are discussed in Section 4.6. Section 4.7 provides some examples of the proposed methodology.

4.1 Grid-free Modelling Framework

The main idea of grid-free modelling is to generate stochastic reservoir models in which all geological objects and sequences are represented without mapping them to a discretized grid system. This is similar to the concept of vector graphics in which the visual objects are represented with mathematical functions and not as sets of pixels as in raster graphics (Figure 1.4).

The general framework of the grid-free OBM is shown in Figure 4.1. In general, implementation of the grid-free modelling framework involves setting up the following components:

1. Geological Object Database
2. Simulation Engine
3. Rasterization Engine

These three components are linked together in different steps of modelling. General specifications and parameters of geo-objects are specified in the geological object database. The simulation engine uses the information from the database and generates grid-free models. The rasterization engine takes the grid-free model and transforms it to rasterized models as necessary for further geostatistical modelling.

4.1.1 Geological Object Database

The geological object database is a library that contains the specification for all possible geological objects and the associated architectural elements. Note that the geological object database is not a necessary component in the grid-free workflow. However, having such a library enables the practitioner to generate multiple geological object databases that can be applied to different depositional environments. Also, it allows the practitioner to easily include or exclude certain geo-objects in the modelling workflow.

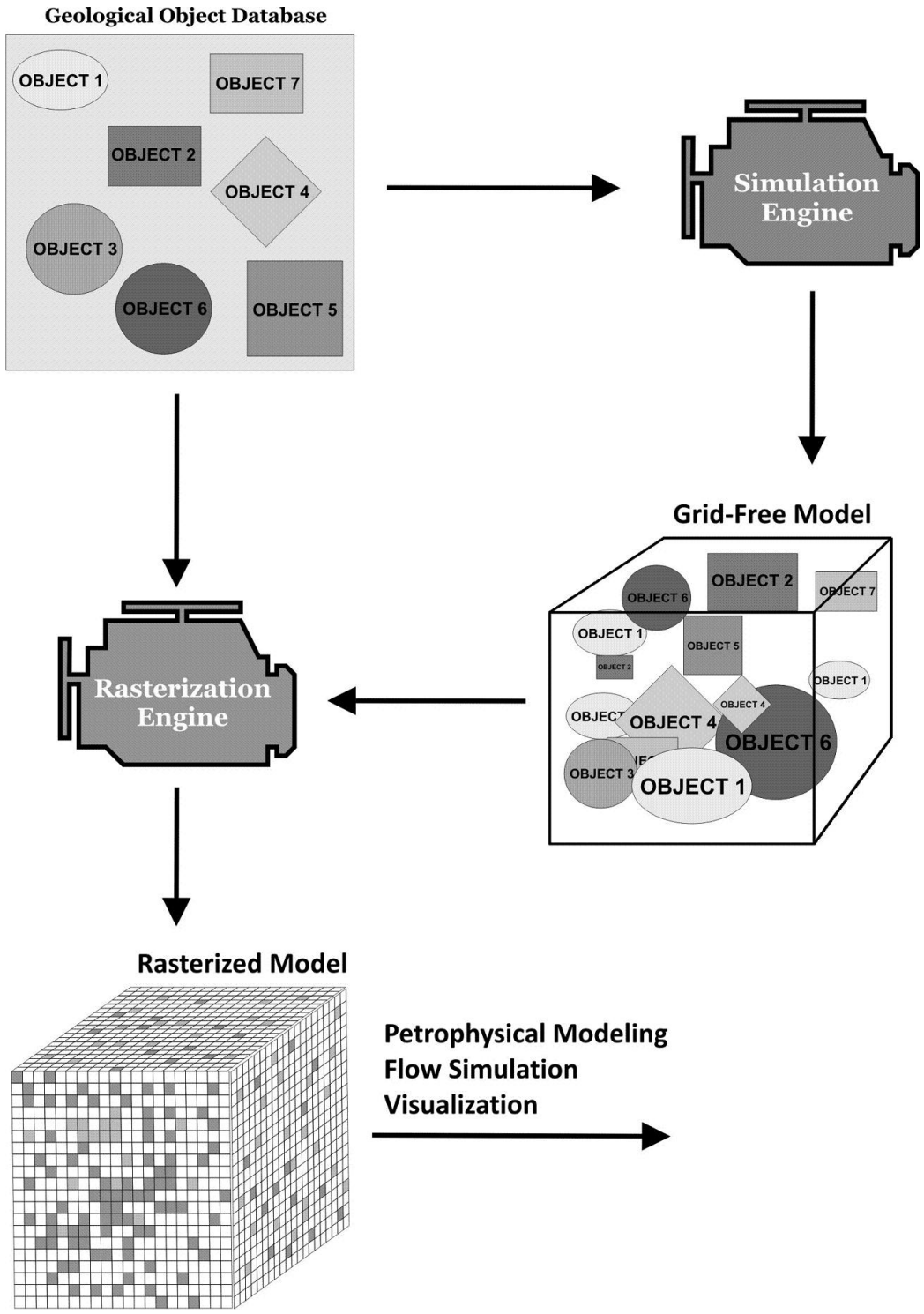

Figure 4.1: Framework of grid-free object-based modelling.

In this thesis, this database is an ASCII file where each geo-object is specified with an object ID number, name, number of parameters, and list of parameter keywords. The object ID number makes it possible to easily access the defined object in other components of the grid-free modelling workflow. For example, Figure 4.2 shows a possible format to describe an ellipsoid in the geological object database. Here the ellipsoid is simply parametrized by the centre location coordinates, three ranges and three angles.

```
object 001
ELLIPSOID
9
{
x0 y0 z0
rx ry rz
ax ay az
}
```

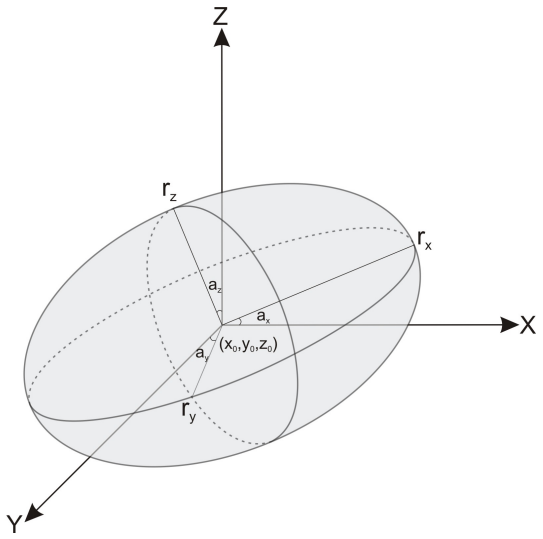

Figure 4.2: Example of a geological object (ellipsoid) represented with parameters in a geological object database.

4.1.2 Simulation Engine

The simulation engine is an important component of the grid-free modelling workflow. Generally, it is a stochastic object or event based modelling algorithm that generates the grid-free geological model by following specified geological rules using objects from the geological object database.

In the stochastic OBM framework the distribution of the geo-objects parameters are predefined by the user. The first step is to decide which object/event is required for the current stage of modelling. Then, the specification of the selected object is gathered from the geological object database. The simulation proceeds by randomly choosing the parameter values from the pre-defined distribution. Then, the object is placed in the model randomly or by following geological rules and processes (erosion, aggradation, lateral migration,...).

The algorithm of object placement in the grid-free modelling is different from the conventional techniques. In conventional methods an object is placed in the model by rasterizing it to the grid system. In the grid-free mode, an object is placed in the model by assigning coordinates, size and orientation to it.

The output of a grid-free simulation engine contains various information about all the objects in the model. Key geometric parameters such as size, orientation and location are required. Geological time is another important parameters that is included in the grid-free output file; this specifies the vertical position in the model and precedence with respect to other objects.

4.1.3 Rasterization Engine

The output of the grid-free simulator is a model that contains information about the location, orientation, time of appearance and geometric parameters of each object. Since the available geostatistical property simulators such as SGS are not compatible with the grid-free model, the grid-free model should be reformatted (gridded) before it can be used for further continuous petrophysical property modelling. The rasterization engine is a tool to transform the grid-

free geological model to the gridded model for purpose of further petrophysical properties modelling, flow simulation, or visualization.

Rasterization is the process of finding all grid cells inside each object and assigning a code to those cells. The rasterization algorithm involves several steps. First the rasterization engine loops over the geological time steps and begins with the oldest time step or object placed. Then, for each time step, all the objects are considered. For each object the smallest bounding box, aligned with the desired grid, is defined. The bounding box makes rasterization faster by considering only those cells inside the bounding box. In the last step, the centre points of all cells that are inside the bounding box are checked against the object's boundary. If the centre point is inside,then the cell is coded as the facies associated to the occupying object (Figure 4.3).

It is possible that a grid cell is occupied by multiple objects. Rasterization of a grid-free model allows calculation of facies proportions within each cell. Each cell can be refined by sets of points and the proportion of all facies can be calculated within the cell volume. Discretizing the grid cell with several points results in a better approximation of the distribution of the facies. The level of refinement depends on the size of the cells in the grid, level of accuracy and the scale of the objects desired by the user. The calculated facies proportions can then be used in future facies upscaling process or facies and property modelling (Derakhshan et al., 2010; Babak et al., 2013).

Since the parameters and specifications of all objects are stored in the grid-free model, it is possible to calculate many other properties such as the anisotropy direction, within-object trend, and permeability tensor during the rasterization process.

4.1.4 Visualization

Visualization of the grid-free model is not as straightforward as the conventional cell-based model. As mentioned earlier, the concept of grid-free modelling is similar to the vector graphic. There are many software packages available for

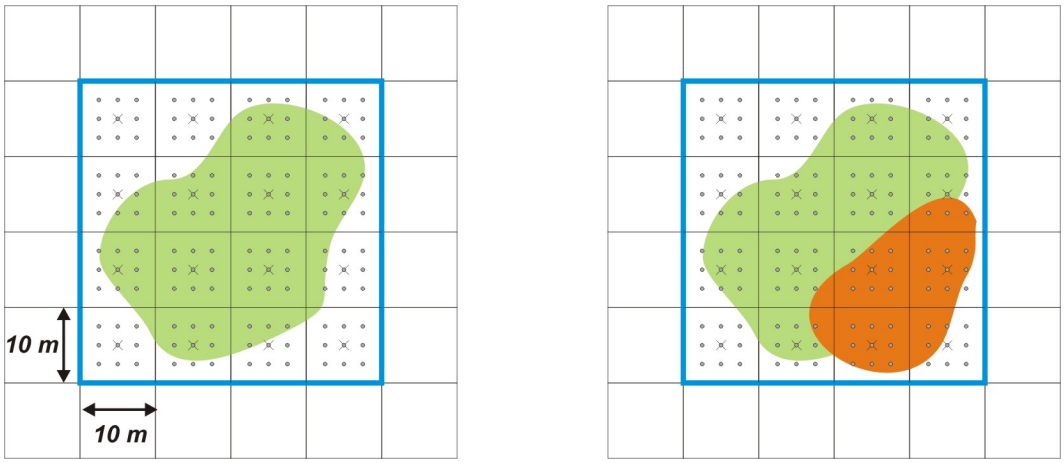

Figure 4.3: Grid refinement, object and the bounding box. New object (orange) takes over the refined grids that were occupied before with the old object (green). The blue square is a bounding box used for the rasterization process. The dots show the discretization points inside each cell.

visualization of vector graphics. To utilize these, the output file of the grid-free simulator has to be reformatted. One example of 2D vector image visualization file format is SVG (Scalable Vector Graphic). It is an XML-based file format that has been developed for applications in World Wide Web (Quint, 2003). The X3D file format is the extension of SVG for 3D computer graphic visualization (Daly and Brutzman, 2008).

In addition to XML-based visualization packages, the visualization toolkit (VTK) is another widely used visualization package that can be used for visualization of grid-free models Schroeder et al. (1998). It is an open source C++ class library and interface that can be used for 3D visualization.

4.2 Architectural Elements

Thomas et al. (1987) provided an extensive review of the architectural elements and geometry of IHS deposits in the estuarine system. The description provided here is mostly based on their work. Figure 4.4 shows the architectural elements of a single IHS set. Five architectural elements are considered; (1) cross stratified

sand (CSS), (2) point bar sand (PBS), (3) shale drapes (SH), (4) breccia (BR), and (5) channel fill (CHF). Specifications and the general geometry of each are described as follows.

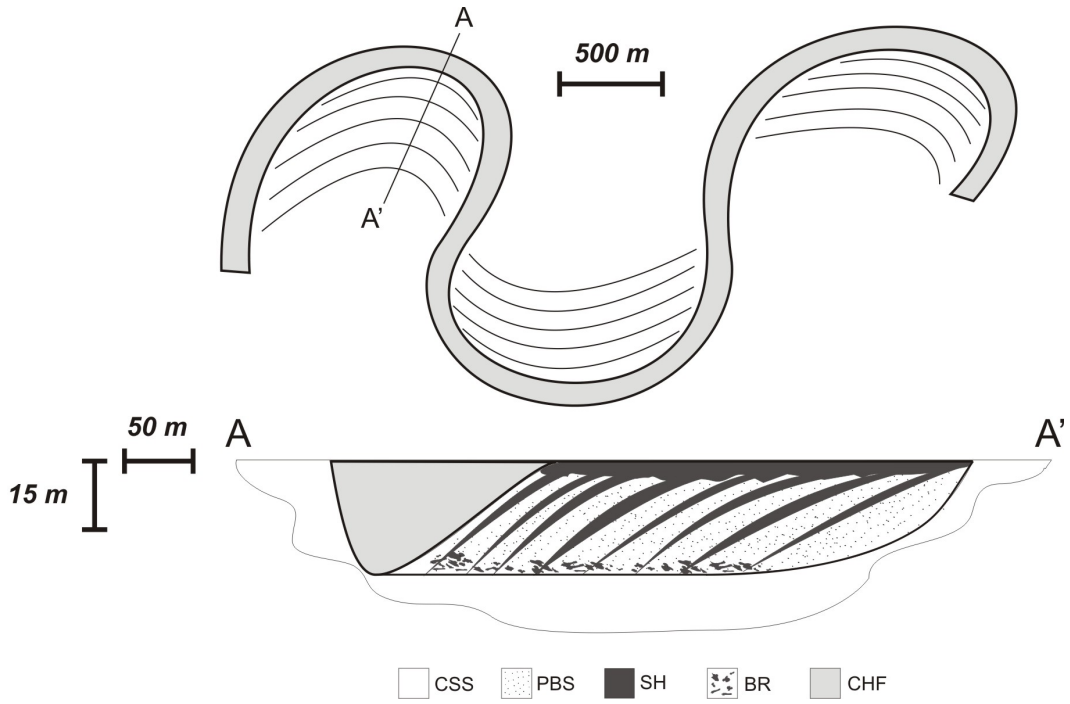

Figure 4.4: Architectural Elements of point bar deposits in the McMurray Formation. Top: a plan view of a meandering channel (gray) and approximate extension of point bar deposits (shaded area). Bottom: a cross section through the point bar deposit and the abandoned channel.

Cross Stratified Sand (CSS)

As discussed earlier in Chapter 2, the cross-stratified sands facies (CSS) is the best reservoir sand. This facies has as strong tidal indicators and suggested to be part of outer estuarine system (Pemberton et al., 1982; Ranger and Gingras, 2003). The main estuarine and the associated tributary channels are incised into this facies. Multiple incisions may remove or re-arrange this facies. The geometry of cross stratified sand in a fluvial setting, as described in Bridge (1993), is generally interpreted as curved-crested ripples and dunes. Here, for

the application to the McMurray Formation, this element is considered as the background facies and no specific geometry is assumed.

Point Bar Sand (PBS)

The basic lithological building blocks of the IHS set are inclined units that comprises of alternating sand and mud. The point bar sands (PBS) sand member of this unit has been observed to be homolithic (Thomas et al., 1987).

Point bar sands are deposited on the inner bank of meander channels as a result of channel migration. Lateral accretion generates lobe-shaped areas (shaded areas in the top of Figure 4.4). This area is referred to as the IHS volume that encompasses both inclined sand and shale units. Here, the assumption is that the PBS element fills the inside of each single IHS set volume. Shale drapes and breccia elements are represented as separate elements placed inside an IHS volume.

Shale Drapes (SH)

The shale members of the inclined unit are called shale or mud drapes (SH). Individual shale drapes are known from outcrops to be laterally continuous from the top of a facies unit to near the base with decreasing thickness. There is a general fining-upward trend inside this facies that make it heterolithic; however, in this dissertation, the variations of properties within the shale facies are not considered important because shale will act as a barrier for fluid flow in virtually all cases.

IHS sets are usually capped by a sheet layer of shale that has the same facies characteristic (top shale). Here, the top shale is modeled as a separate element that contains the same facies type as the shale drapes.

Breccia (BR)

The mud clast breccias (BR) can be found at the bottom of a channel succession as a result of erosion of previously deposited muddy point bars and overbank collapse. Although this element consists of many muddy clasts randomly distributed in a background sand matrix, here for simplicity, this element is assumed to be a thin layer positioned at the bottom of the IHS volume. For very detailed modelling, each centimetre scale clasts can be considered as an object and placed at the bottom of IHS volume. The breccia layer is characterized with a thickness (as a percentage of the IHS volume thickness) and placed at the bottom of IHS volume.

Channel Fill (CHF)

The channel fill element (CHF) is the channel geometry that bounds the IHS set and is filled with mud and sand but usually acts as a permeability barrier. If channel abandonment occurred, the channel is filled mostly by mud in a fining-upward trend. The channel element is very similar to the one used in the tidal channel modelling in the previous chapter. Here, the depth of the channel is assumed to be equal to the thickness of overbank IHS deposit.

4.3 Parameterization

Parameterization of geological objects is one of the first steps in any object/event based techniques. It involves reproducing the shape of the geological features by representing them as geometrical shapes. To apply the grid-free modelling framework to the estuarine deposit of the McMurray Formation the architectural elements presented in previous section should be parameterized. Parameterization of a single IHS set involves 3D representation of the volume, top shale, bottom breccias, shale drapes, and channel fill.

IHS Volume

The IHS volume is the key component that all the facies associations are placed inside or attached to. A simple IHS set volume geometry can be characterized by two lobe-shape planes for the top and bottom that are connected together with two inclined sigmoidal surfaces in the front and back (Figure 4.5). In plan view it is clear that the bottom lobe-shape plane has similar geometry as the top , but with a larger surface area . This difference in the surface area of the top and bottom planes is closely related to the dipping of strata from top to the bottom. A larger dip angles results in less difference between top and bottom plane size.

Any $x-y$ cross section of the IHS volume is a lobe-shape geometry that has greater surface area than the top plane and lesser than the bottom plane. This geometric feature simplifies the parameterization of IHS volumes. Assuming a uniform vertical profile for the front and back surfaces would further simplify the parameterization; the 3D geometry of the IHS volume is simply represented by the two lobe-shape planes at the top and bottom and a vertical profile.

As shown in Figure 4.5, the top plane can be parameterized with five parameters. W_o is the opening width of the IHS set which can be related to the meandering wavelength of initial channel meanders. W_m is the width of the IHS set in the middle and can vary arbitrarily. L is the length of IHS set which is related to the channel migration distance. The b_i coefficient identifies the relative location of maximum IHS width as fraction of length (L), and c_i relates to the curvature of initial channel.

Using these five parameters, the coordinates of six key points can be calculated relative to the point p_0 in the figure that is called the anchor points of IHS set. In the grid-free simulation mode, the IHS volume is represented with these key points. The coordinates of the six key points can be calculated relative to the anchor point as follow:

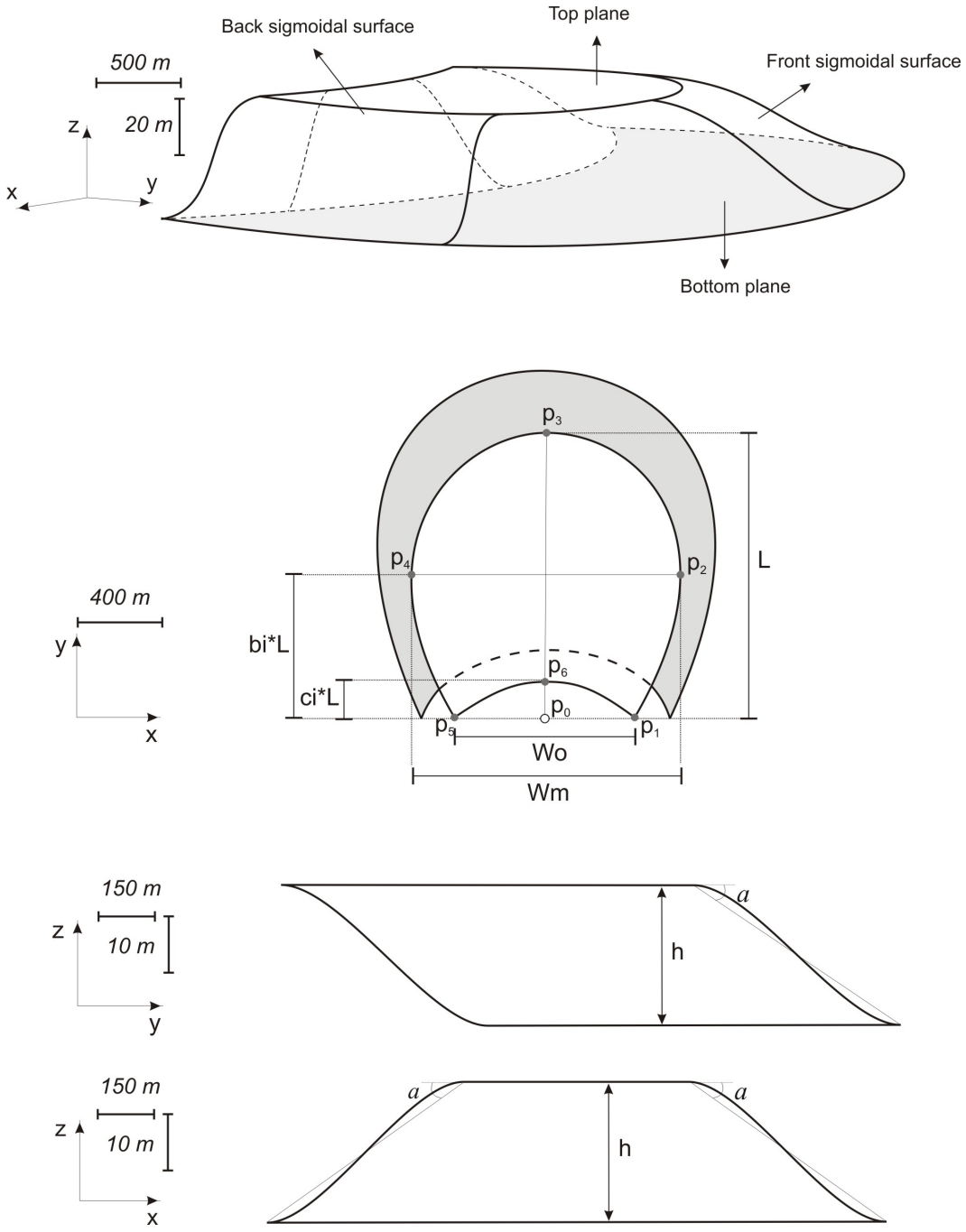

Figure 4.5: Geometric parameterization of IHS volume. 3D view of one IHS volume (top), plan view of IHS volume with associated parameters (middle), and cross sections (bottom).

.

$$P_1 : \begin{cases} x_1 = x_0 + 0.5 * W_{min} \\ y_1 = y_0 \end{cases} , \quad P_2 : \begin{cases} x_2 = x_0 + 0.5 * W_{max} \\ y_2 = y_0 + b_i * L \end{cases}$$

$$P_3 : \begin{cases} x_3 = x_0 \\ y_3 = y_0 + L \end{cases} , \quad P_4 : \begin{cases} x_4 = x_0 - 0.5 * W_{max} \\ y_4 = y_0 + b_i * L \end{cases}$$

$$P_5 : \begin{cases} x_5 = x_0 - 0.5 * W_{min} \\ y_5 = y_0 \end{cases} , \quad P_6 : \begin{cases} x_6 = x_0 \\ y_6 = y_0 + c_i * L \end{cases}$$

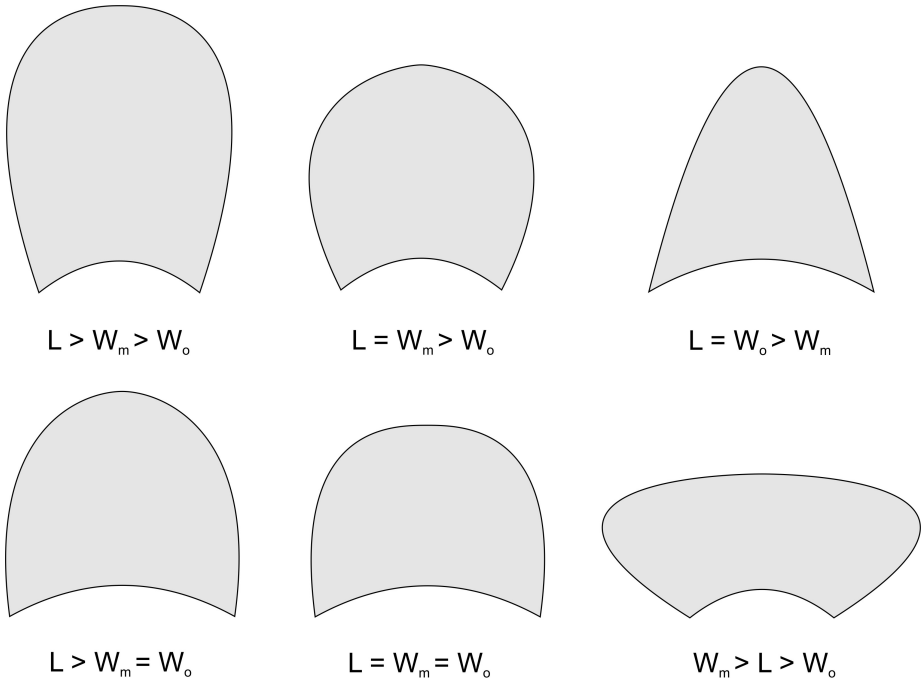

Figure 4.6: Examples of top and bottom surface geometry for different size parameters.

The anchor point is not only important in positioning of the IHS set but it will be used in the parameterization of shale drapes and the rasterization of IHS sets. This is discussed in more detail in the shale drape parameterization.

To generate a lobe-shape geometry with the key points, a smooth interpolator such as a cubic spline can be utilized to connect the key points and generate the boundaries of the top plane. One spline connects points p_1 to p_6 generating the front boundary and another one is used to connect points p_1-p_6-p_5 for

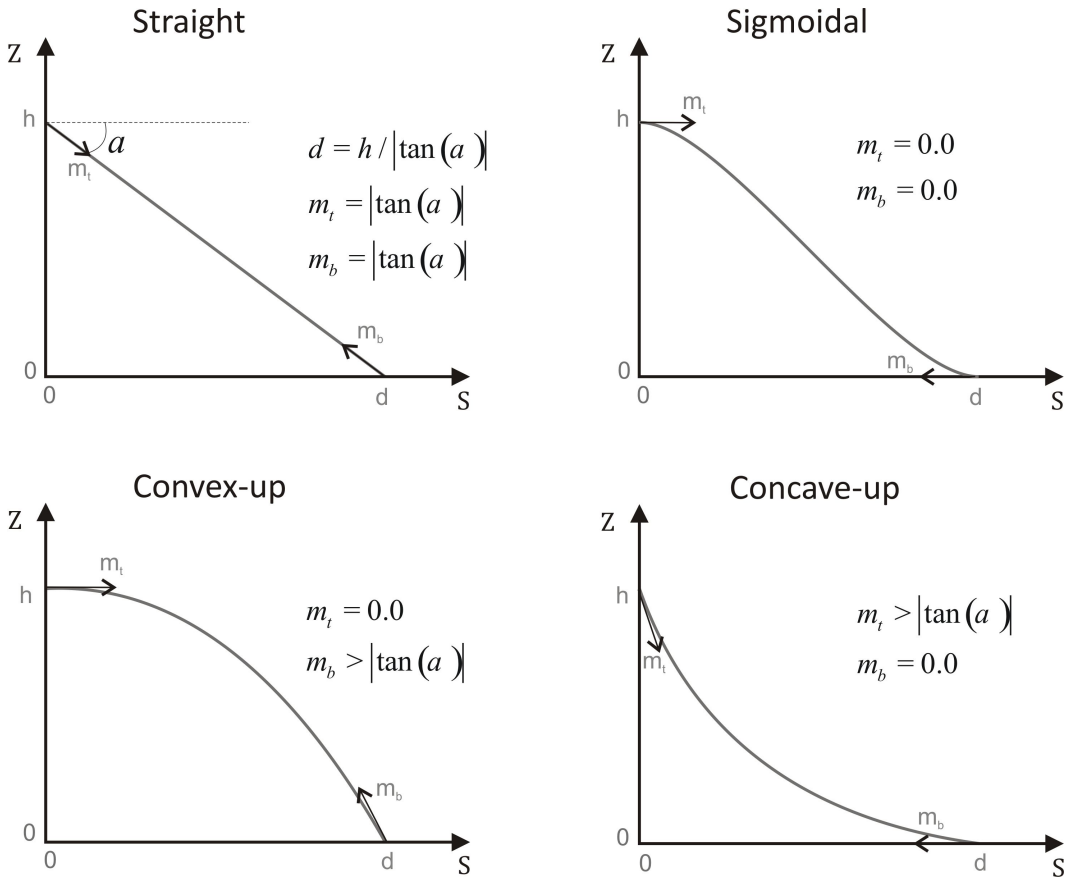

Figure 4.7: Vertical profile parameterization.

the back boundary. Figure 4.6 shows some examples of IHS sets with different parameters in plan view.

According to Thomas et al. (1987), the vertical profile of inclined strata can be characterized as straight, sigmoidal, concave-upward, or convex-upward curves. This mostly applies to the shale drapes because preservation of single non-eroded IHS set in the estuarine system is rare and detection of its profile is not possible. Here, the same vertical profile shape is assumed for both the IHS volume and the shale drapes. A cubic polynomial shown below is utilized to generate different IHS vertical profiles.

$$Z(s) = a_1 s^3 + a_2 s^2 + a_3 s + a_4$$

where the a_i values are coefficients and s is the distance in any channel migration direction. The coefficients of the cubic equation are calculated from the other IHS set parameters including thickness (h), dip angle (α), profile slope on top (m_t), and profile slope in bottom (m_b). Different vertical profiles can be generated by changing the top and bottom slopes. Figure 4.7 shows different possible profiles that can be generated with this parameterization. Note that the vertical profile is assumed to be constant in all directions. The IHS volume is fully characterized by the top six points and the vertical profile parameters.

Shale Drape

Shale drapes are important elements of the IHS facies association that impose heterogeneity in the IHS sets and effect thermal production performance. Variation of size (millimetre to meter) and the huge scale difference with respect to the IHS volume requires vary the detailed parameterization of the shale drapes. Figure 4.8 shows details of the shale drape parameterization.

As shown in Figure 4.8, shale drapes are lense-shaped objects with different thicknesses that are either completely or partially extended over the accretionary surfaces. In the vertical direction, they follow the same profile as the IHS volume with decreasing thickness from top to bottom. The top horizontal thickness (t_{drape}) and the vertical extension of shale drapes (h_{drape}) are the parameters that are used for shale drape modelling.

In the grid-free simulation, shale drapes are characterized with four key points on the top plane and the vertical profile. Coordinates of the key points are calculated with the relative location of the accretionary surface and top horizontal channel thickness. These four key points are used to generate boundaries of each drape. A cubic spline is used to connect p_1 to p_2 to p_3 generating the front boundary and another one is used to connect p_1 to p_4 to p_3 generating the back boundary. The vertical thickness variation is assumed to be linear from the top to the bottom; however, another pattern of variation could be considered.

To place the shale drapes in the IHS volume, the location of the accretionary

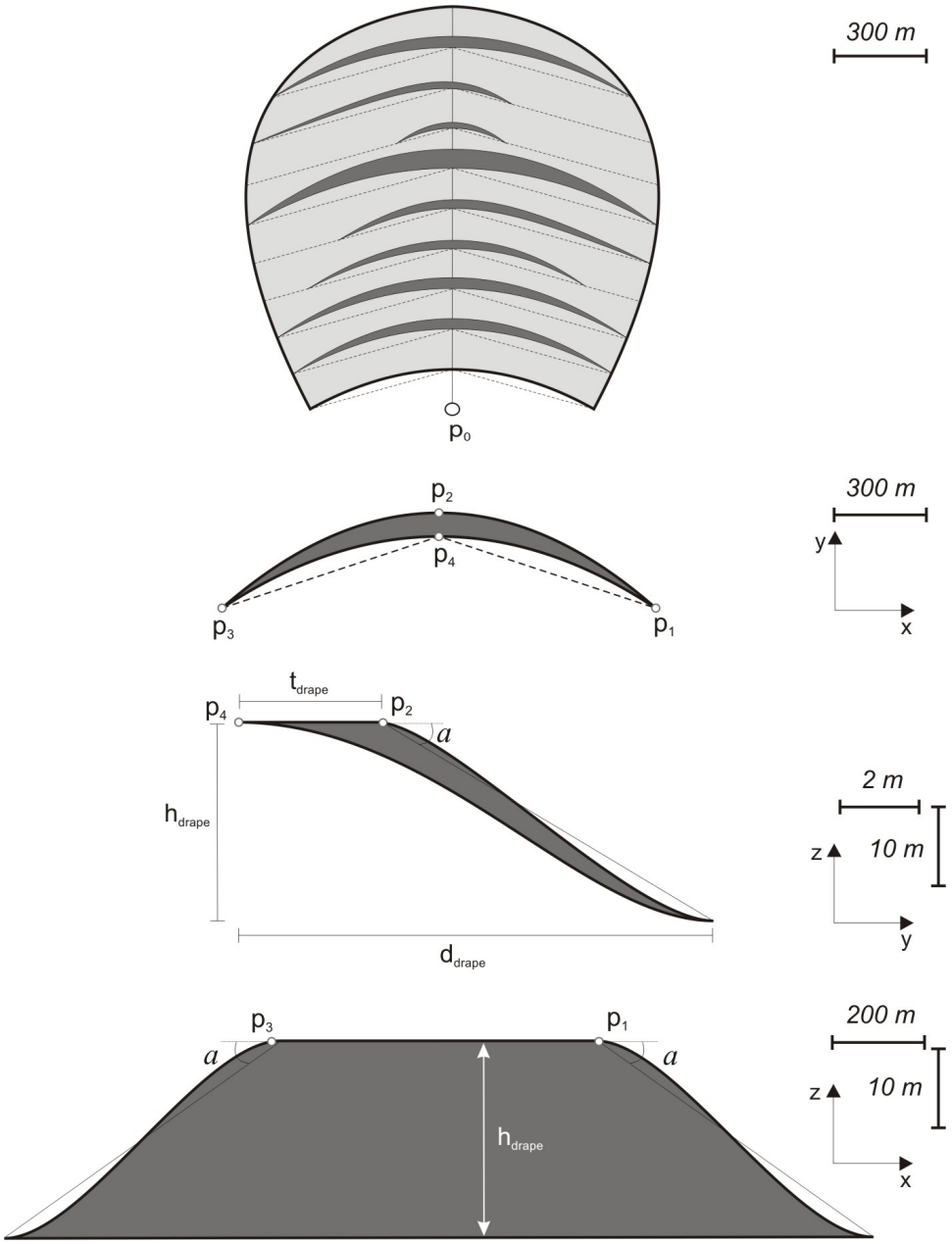

Figure 4.8: Parameterization of shale drape (SH) element. Plan view of PBS with shale drapes (top), plan view of single shale drape (second from the top), cross sections of a single shale drape with associated parameters (second from the bottom and bottom). The light gray shows sand member of the IHS and the dark gray shows shale drapes.

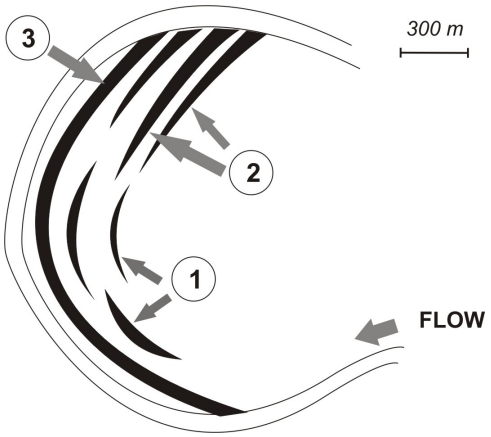

Figure 4.9: Plan view of a single IHS set showing possible shale drape configurations: 1) irregular discontinuous, 2) distal attached discontinuous and 3) continuous (modified after Thomas et al. (1987).

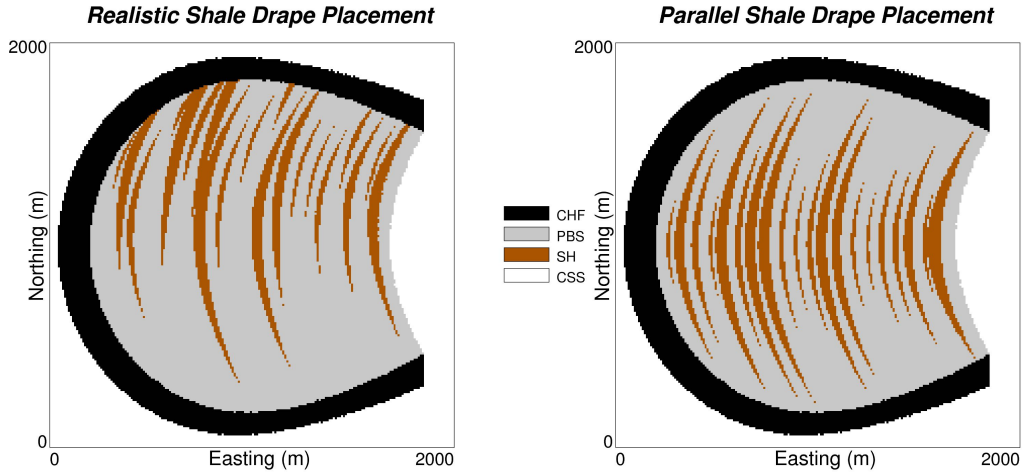

Figure 4.10: Realistic shale drape placement (left) and the parallel shale drape placement (right). The flow direction is similar to the one shown in Figure 4.9.

surfaces must be determined first. Then the shale drapes are placed on top of the accretionary surfaces. The accretionary surfaces are assumed to be parallel to each other with a constant offset following the same curvature as the initial channel curvature. The only parameter required to determine the location of accretionary surfaces is the number of accretionary surfaces (n_{acs}). The accre-

tionary distance $((1 - b_i) * L)$ is then divided into sections and the coordinates of accretionary surfaces are calculated relative to the anchor point. Note that the accretionary surfaces are not generated as separate objects in the modelling but they are used to indicate the relative location of shale drapes.

The shale drapes can be placed in the IHS volume in different ways. According the Thomas et al. (1987), three different configuration of shale drapes are expected to exist in the IHS sets: 1) irregular discontinuous, 2) distal attached discontinuous and 3) continuous (Figure 4.9). Random placement of shale drapes on the accretionary surfaces reproduces the type 1 and the type 2 however, to model the distal shale drapes, a direction for the river current flow should be considered (Figure 4.9). In this dissertation, this shale drape placement is referred to as realistic shale drape model. The shale drapes may also be modeled parallel to each other. In this case, shale drapes are placed on the center point of the accretionary lines. Figure 4.10 shows the realistic and the parallel placement models.

Channel

Each single IHS set is surrounded by an abandoned channel. Figure 4.11 shows the bounding channel parameterization. Since the inner bank of the channel has already been generated by the IHS volume, the vertical geometry of the channel can be easily generated with the vertical channel width function. A quadratic function is used to model the channel width in the vertical direction.

$$W(z) = a_1 z^2 + a_2 z + a_3$$

where the a_i's are coefficients of the quadratic approximation and are defined using the following assumptions:

$$\begin{cases} W = (1 + t) * (h / \tan \alpha) & , \quad z = h \\ W = 0 & , \quad z = 0 \\ W' = 0 & , \quad z = 0 \end{cases}$$

where t is the thalweg ratio, h is the bankfull channel thickness and α is the dip angle of IHS set (see Figure 4.11).

Top Shale and Breccia

The top shale and the breccia facies at the bottom of the IHS set are considered as sheet layers and can be parameterized as a fraction of the total thickness of the IHS set. These two elements of the IHS set are optional and can be excluded by setting the thickness to zero. Figure 4.12 shows an example of a single IHS set with the associated architectural elements.

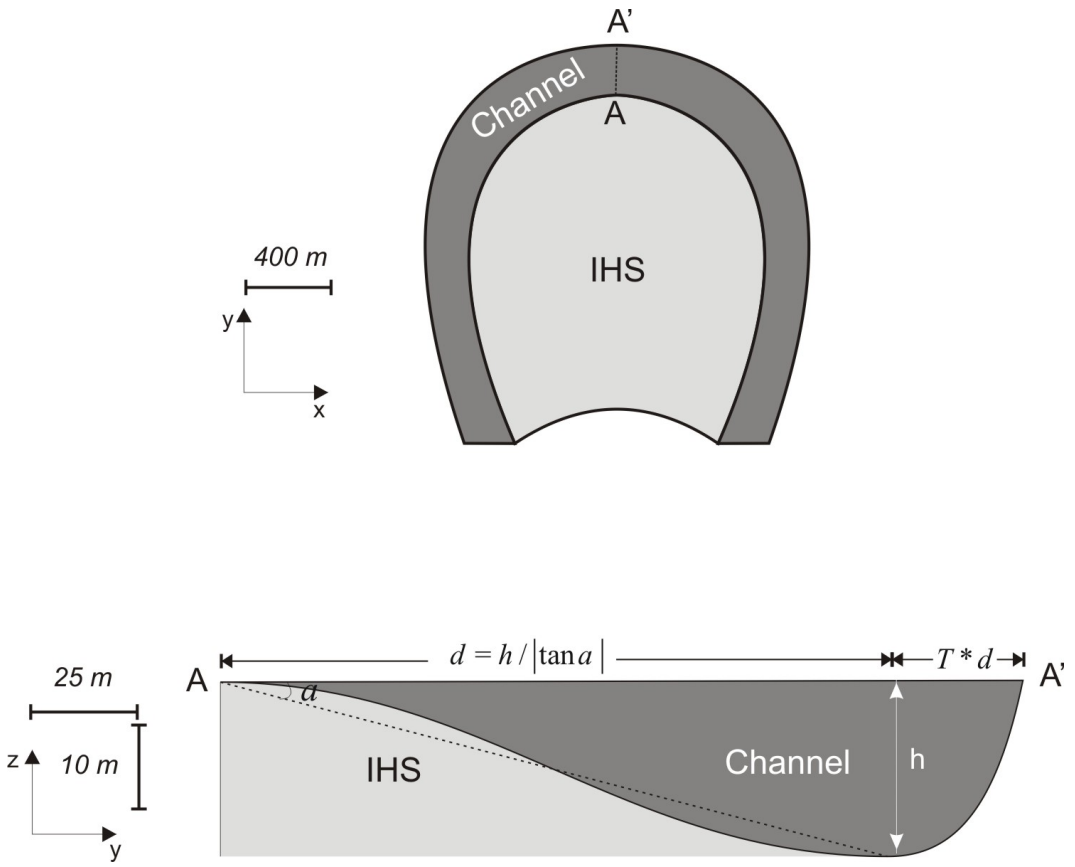

Figure 4.11: Parameterization of abandoned channel fill (CHF) element. Plan view of IHS and abandoned channel fill (top), and cross section of IHS and CHF elements with associated parameters (bottom).

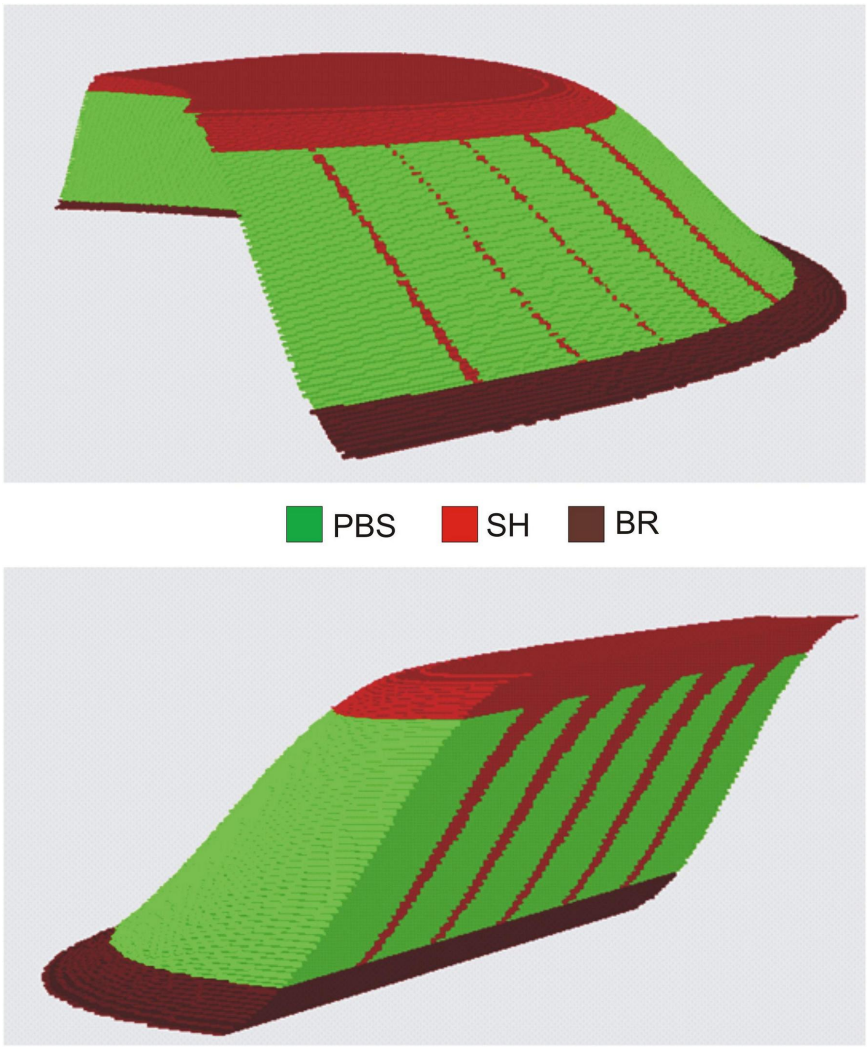

Figure 4.12: Example of IHS Set and the associated architectural elements, 3D view from east (top) and the cross section from west (bottom). The vertical section is exaggerated.

4.4 Unconditional Simulation Algorithm

The simulation engine is a stochastic object/event based technique. Objects are generated based on some geological rules and stored in a grid-free format. Vertical and lateral channel stacking are the two main geological rules implemented. Only the location, orientation, and the geometric parameters of objects are stored in the output file. Objects are recorded based on their geological time (oldest to youngest).

Vertical stacking starts from the base of the model. The number of aggradation levels is provided to the simulator to control the vertical stacking. This information may be inferred from the well logs, outcrops or other analogue data. More aggradation level leads to generation of complex cosets that are superimposed and overlap. Few layers will result in highly laterally imbricated IHS with significant hiatal breaks, while many layers will result in less lateral imbrication and more vertical imbrication for the same overall proportion of IHS.

Within each vertical stacking level, several lateral stacking IHS sets are placed. The lateral stacking of IHS sets are controlled with the number of meandering channels in each aggradation level. More channels leads to generation of more amalgamated IHS sets.

Meandering channels are not generated, instead, a channel line which represents the general orientation of the meandering channel is considered. The channel line is located by a source location and an azimuth angle; IHS sets are attached to the line in such a way as to generate a realistic meandering channel pattern. Figure 4.13 shows how several IHS sets are attached to the channel line. Channel meandering wavelength, amplitude to wavelength ratio, and IHS width to the wavelength ratio are required for IHS generation. These variables are used to calculate the top key points of the IHS body discussed previously and the location of IHS's anchor point. Other required geometric parameters for the IHS set are drawn from the user-supplied probability distributions. Once the IHS volume is generated, other associated architectural elements are placed.

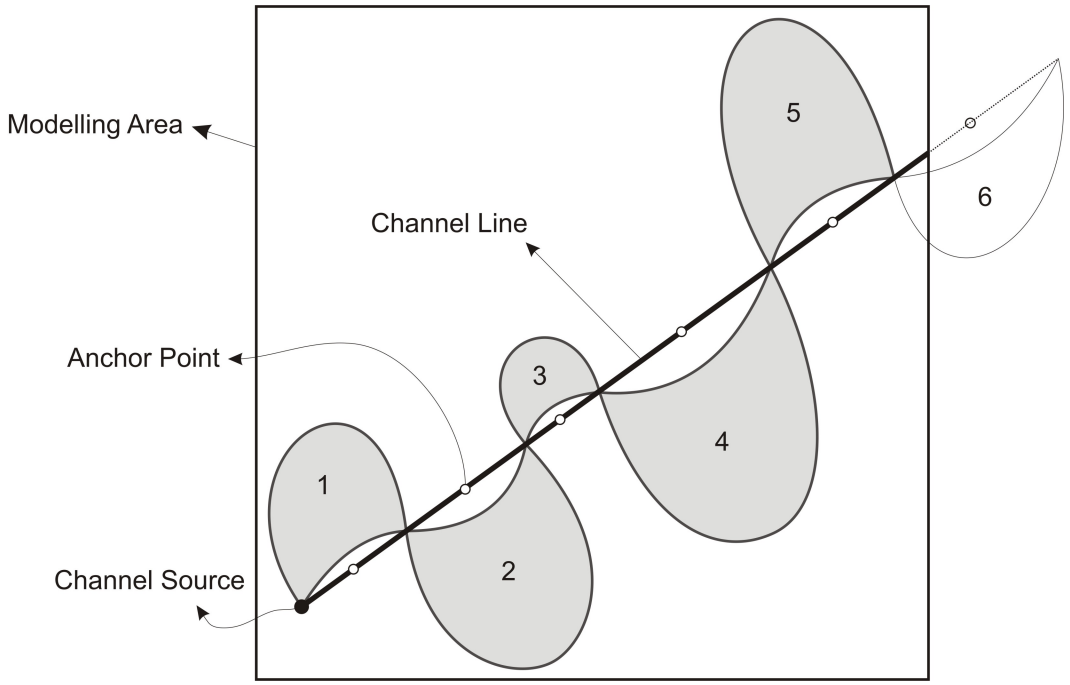

Figure 4.13: Process of attaching IHS sets to the channel line. The order of attachment is shown with numbers . IHS set number 6 is not included because its anchor point falls outside of the modelling area.

The number of shale drapes in each aggradation level is controlled with the shale frequency parameter. Higher shale frequency results in muddier IHS packages. Generation of IHS sets along the channel line halts when the new IHS set anchor point falls outside the modelling area.

Object Hierarchy

There are multi-level links between the geological objects defined in this methodology. In order to keep consistency between the parametrization of objects at multiple-scale, an object hierarchy is introduced. Figure 4.14 shows the object hierarchy chart. Each element is this hierarchy chart carries properties that are consistent in all the lower level elements.

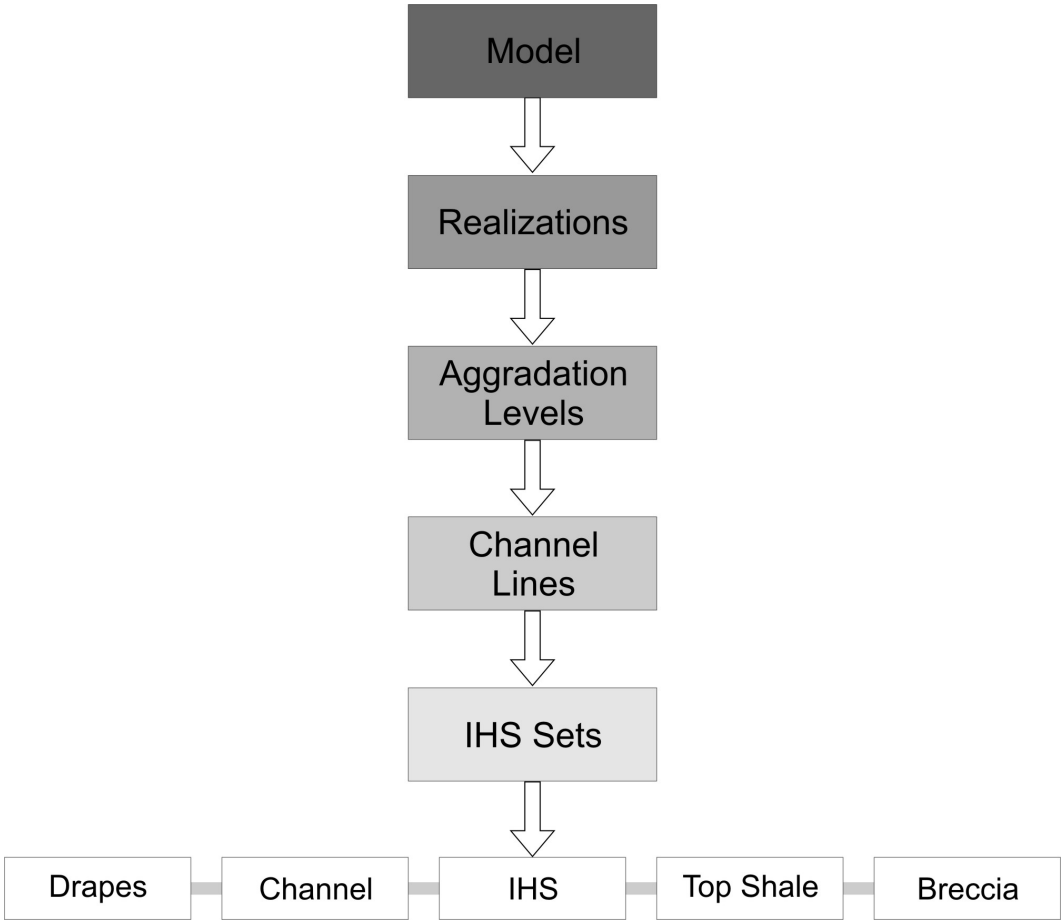

Figure 4.14: Object Hierarchy used in grid-free IHS modelling programs.

In this hierarchy chart, *Model* which contains all the information is at the top hierarchy level. Each model may contain several *Realizations*. Within each realization there are several *Aggradation Levels*. *Channel line* is the next hier-

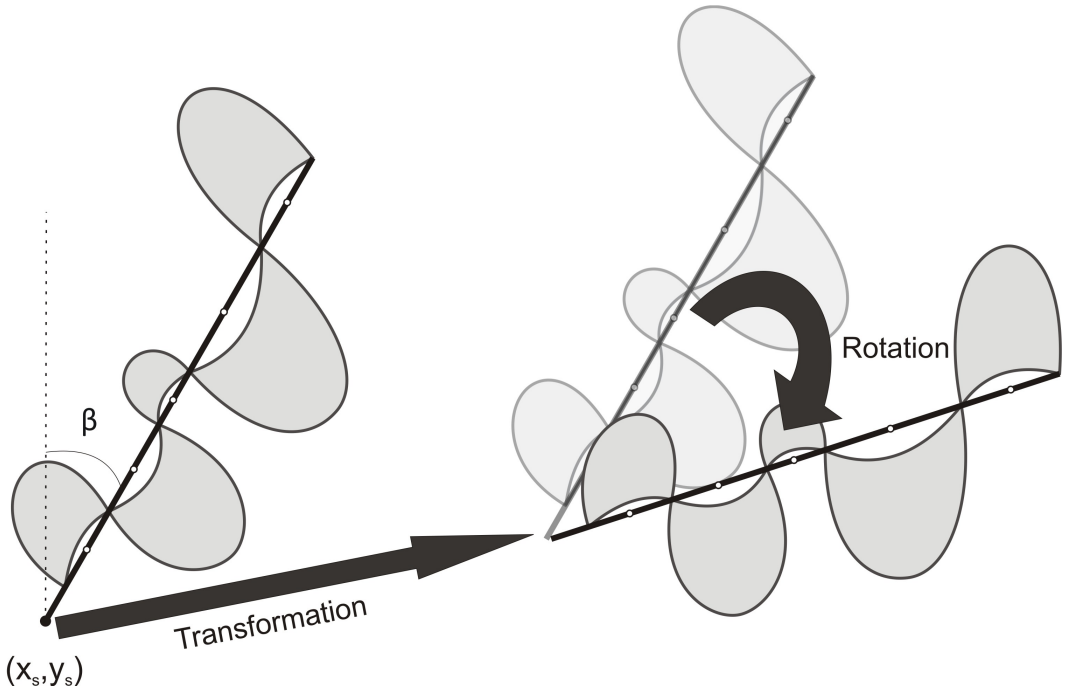

Figure 4.15: Transformation and Rotation of IHS sets by changing the channel line parameters.

archy level. Several channel lines may present at each aggradation level. Each channel line consists of several *IHS Sets* and each IHS sets composed of five architectural elements.

All the object coordinates are represented relative to the object just higher up in the hierarchy. This hierarchical scheme makes it easier to manipulate objects by simple changing the properties of the higher level element. For example, each channel line is parametrized by its start location coordinates and azimuth angle of its main direction. By changing these two parameters, all the channel lines and associated IHS sets can easily be transformed or rotated. This is illustrated in Figure 3. Transformation and rotation of objects can be used for fast well conditioning.

4.5 Conditional Simulation Algorithm

Some algorithms have been developed for conditioning of an object-based model (see Chapter 2). The algorithm used here is a combination of the rejection algorithm and modification algorithm with improvements to the previous method by Pyrcz et al. (2009).

Only three main facies are considered for conditioning; cross-stratified sand as the background, IHS set, and mud-filled channel. Conditioning the grid-free model to the small scale shale drapes is difficult due to the complexity and lack of input data. Once three facies of CSS, IHS, and mud-filled channel are appropriately placed in the model, shale drapes and breccia can then be simulated inside the IHS facies.

The first step is to prepare the data for conditioning. The thickness of each interval is checked first. If the thickness is more than the possible IHS thickness provided by the user, then the interval is divided into several smaller intervals. Then all data (facies intervals) are sorted based on their top elevation. Simulation starts from the bottom of the model so the lower elevation data gets priority for simulation. The main reason for this is to follow the sedimentation process. All data are assigned to the appropriate aggradational level based on their top elevations. Data are also sorted based on the proximity to the source line. Data points that are farthest from the source line gets higher priority. This is because the closer data to the source will have better chance to intercept a random channel line.

Simulation starts by generating a random channel line using the user-defined parameters. If the thickness of the generated channel line is less than the well data, another channel is generated. This process is very fast, because only the basic geometric of the architectural elements are generated and interpreted only at well locations.

The next step is to check if the well data matches the generated channel line. In this step the data point is checked against the box containing the IHS

set to see if it is inside. If the well data falls inside any of the IHS boxes of the generated channel line, then the next step is to check previously conditioned data with this channel line and count the number of good and bad intercepts. When the generated channel line matches previously conditioned data, it is counted as a good intercept, and if not, it is counted as a bad intercept. If there are no bad intercepts then the channel line is accepted and the algorithm proceeds to simulate the next available data. If there is a bad intercept, the parameters of the channel line and its associated good and bad intercepts are stored and another channel line is generated. This process is repeated until either a channel line with no intercepts is found or a user-specified maximum number of attempts are made.

When simulation reaches the maximum number of attempts and cannot find a channel line without a bad intercept, the best case with the lowest number of bad intercepts is selected. Then, two geometric operations of rotation and transformation are randomly applied to the selected channel line with the goal to reduce the number of bad intercepts. Since the IHS sets are parametrized based on the hierarchy levels to the channel line, rotation or transformation of a channel line can efficiently and simply be done by changing the starting point coordinates of channel or changing the channel line angle(see Figure 4.15). This step is repeated several times and the number of bad intercepts is counted after each try. Then the best case with the lowest number of bad intercepts is considered.

When all the data in the current aggradation level is honoured, the simulation proceeds by generating new channel lines until the user-specified maximum number of channels is reached at the current level. Note that, after each channel generation or modification, the previously honoured data are checked for violation (interception with a non-desired object).

4.6 Rasterization

Geo-objects are rasterized in the order of their geological time (older objects first). IHS volume is rasterized first, slice by slice in the z direction from the bottom. For each slice in the z direction, the transformation distance is calculated using the cubic equation of the vertical profile, the top six points of IHS body are then transformed by that distance. A cubic spline interpolator is used to smooth the boundary of the IHS at the current z slice. All grid cells in the $x-y$ plane that fall inside the IHS boundary are coded as point bar sands (PBS). Top shale (SH), breccia (BR), channel fill (CHF) and the shale drapes (SH) are rasterized with the same procedure. The linear thickness variation (thicker at the top) should also be considered in the rasterization of shale drapes.

4.7 Examples

To demonstrate the proposed methodology, one unconditional and two conditional facies model for the middle McMurray Formation are presented. For the unconditional example, a modelling area of $5\,km$ by $5\,km$ by $50\,m$ was considered. A general South-North direction was assumed for the channel lines. Four aggradation levels were considered with 5, 7, 5, and 10 channels in each level respectively. Shale drape frequencies were selected in a way to reproduce a vertical trend in the shale contents of the model; the IHS sets in the upper levels are muddier. To visualize the grid-free model it has been rasterized with $10\,m$ by $10\,m$ by $0.5\,m$ grid cells for the whole area, a total of 5 million cells. Figure 4.16 shows multiple cross sections of the generated facies model. Small scale features are well reproduced, because of the small grid size in the vertical direction.

One of the advantages of the grid-free modelling is the ability to rasterize the model at different resolution or local rasterization of a large grid-free model. To illustrate this feature, an area of $1\,km$ by $1\,km$ was selected at the centre

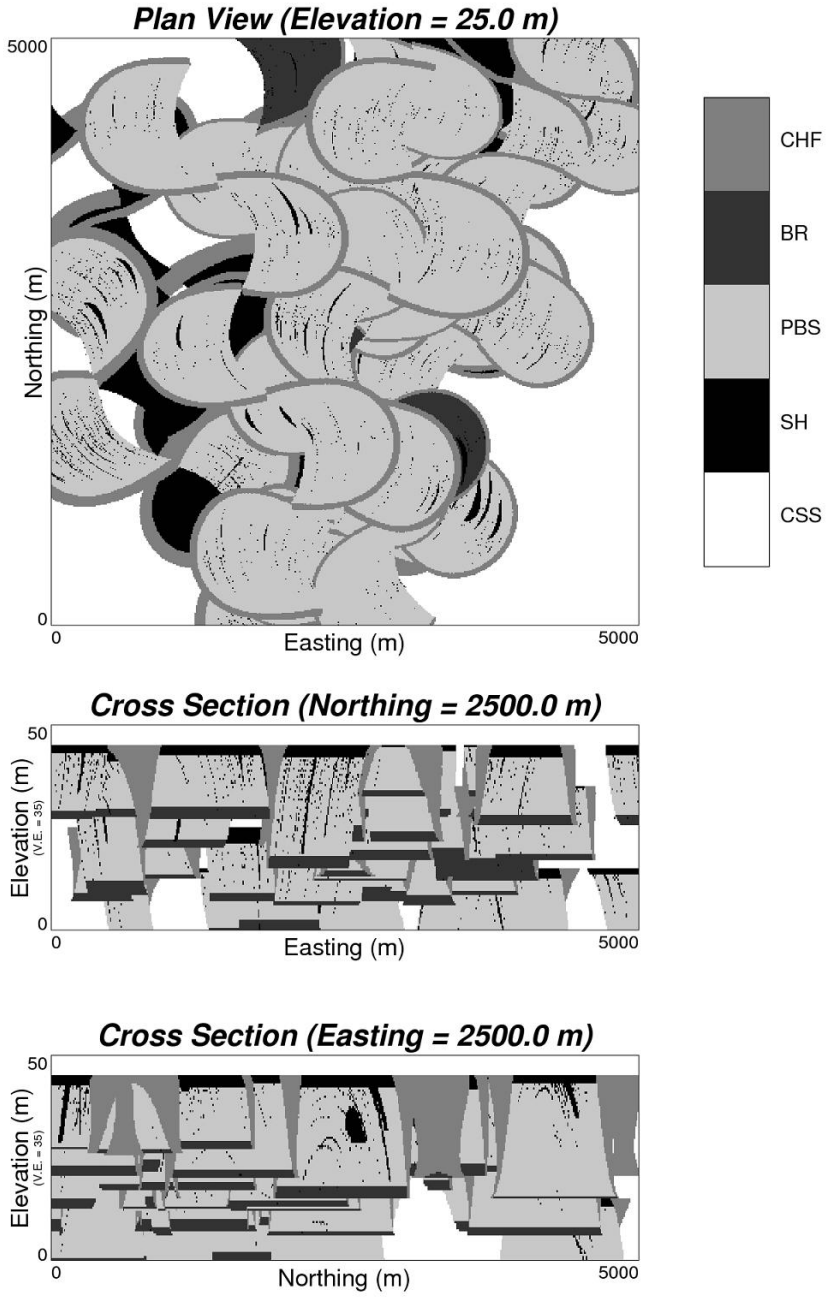

Figure 4.16: Example of unconditional IHS Facies Model for the McMurray Formation generated with the grid-free modelling technique. The vertical sections are exaggerated 35 times.

of the grid-free model presented above. Figure 4.17 shows an example of local rasterization with smaller grid size.

Two examples of conditional simulation are presented to show the proposed conditioning algorithm. In the first example, nine data points related to nine different vertical wells were considered with a single aggradation level. A modelling area of $5\,km$ by $5\,km$ by $20\,m$ was considered. Models were rasterized with $10\,m$ by $10\,m$ by $0.5\,m$ grid cells. Figure 4.18 shows the location of well data and the model in plan and cross section view.

In the second example, four well data with four aggradation levels were considered. The number of aggradation levels and also the number of channels in each level are picked based on the conditioning data density; the more vertical data density, the more aggradation levels to consider and the more data in the aggradation level, the more the number of channels to simulate. Figure 4.19 shows the results of conditional model. As shown in well sections for both cases, most of the conditioning data are honoured in the models.

4.8 Comments on the Well Conditioning

The conditioning methodology presented above is not guaranteed to condition completely nor to be free of artifacts, especially if data density relative to the size of the architectural elements is high.

Selecting the appropriate input parameters for simulation is also important for the quality of the data conditioning. More discussions on the required input parameters are provided in the next chapter. In general, increasing the standard deviation of input parameters (for example the azimuth angle of the channel lines) will help the algorithm to find a better match to the conditioning data, but this may also introduce some artefacts such as unrealistic geometries.

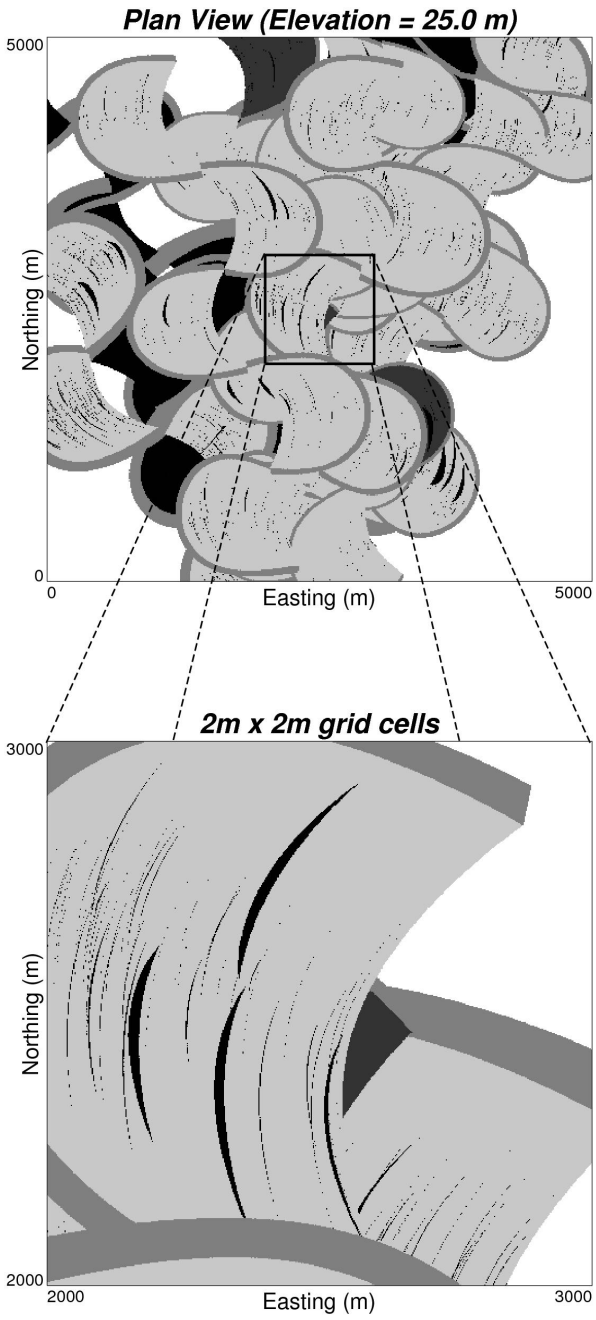

Figure 4.17: Local rasterization of the grid-free facies model. Top model is rasterizaed with $10\,m$ by $10\,m$ grid and the bottom model is rasterized with $2\,m$ by $2\,m$ grid.

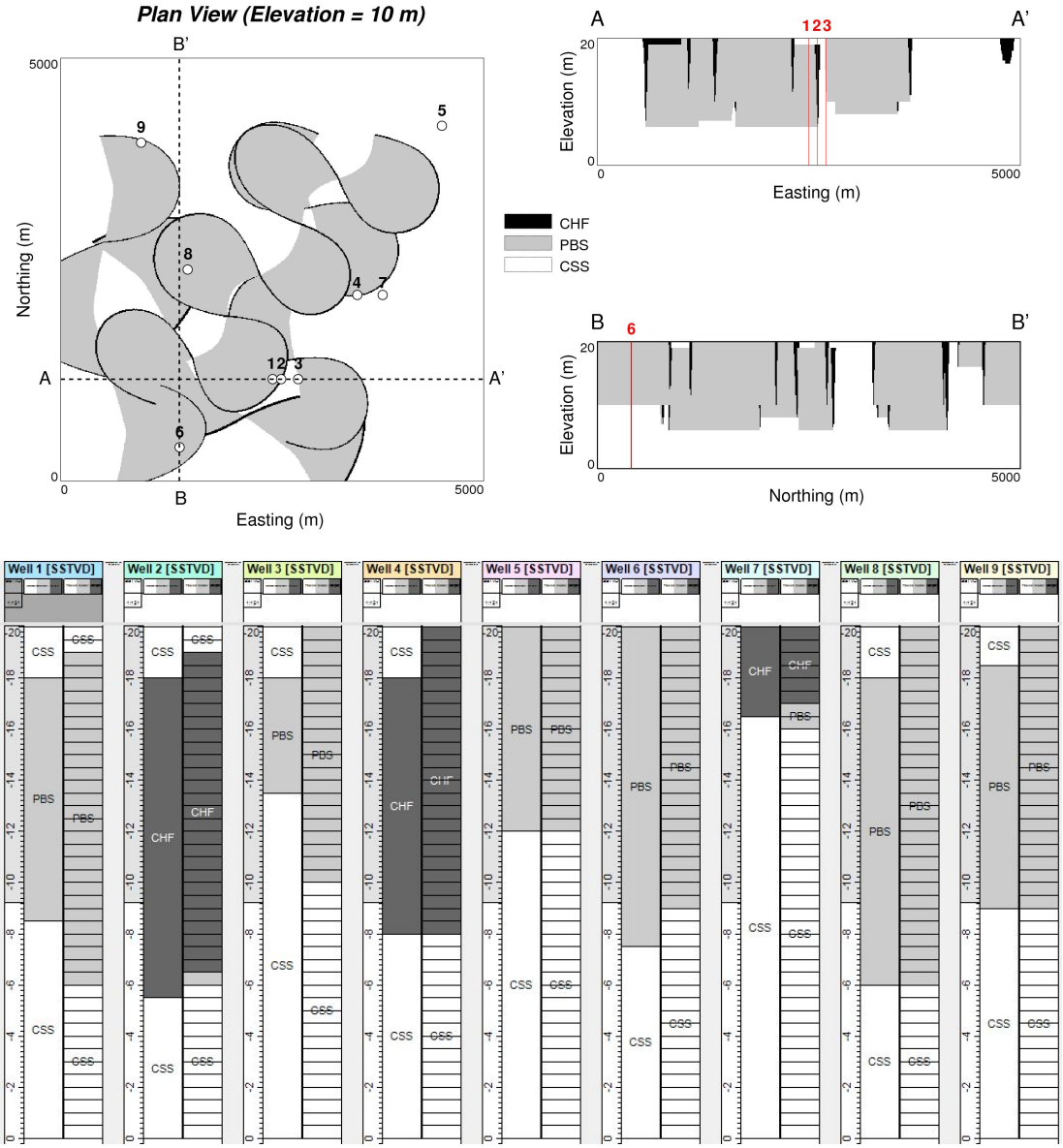

Figure 4.18: Top: example of conditional Facies Model for the McMurray Formation generated with grid-free modelling technique. The vertical sections are exaggerated 70 times. Location of conditioning wells are shown with circles in the plan view and vertical lines in cross sections. Bottom: well section showing nine conditioning wells; left tracks show the original data, and right tracks show the model at each well locations.

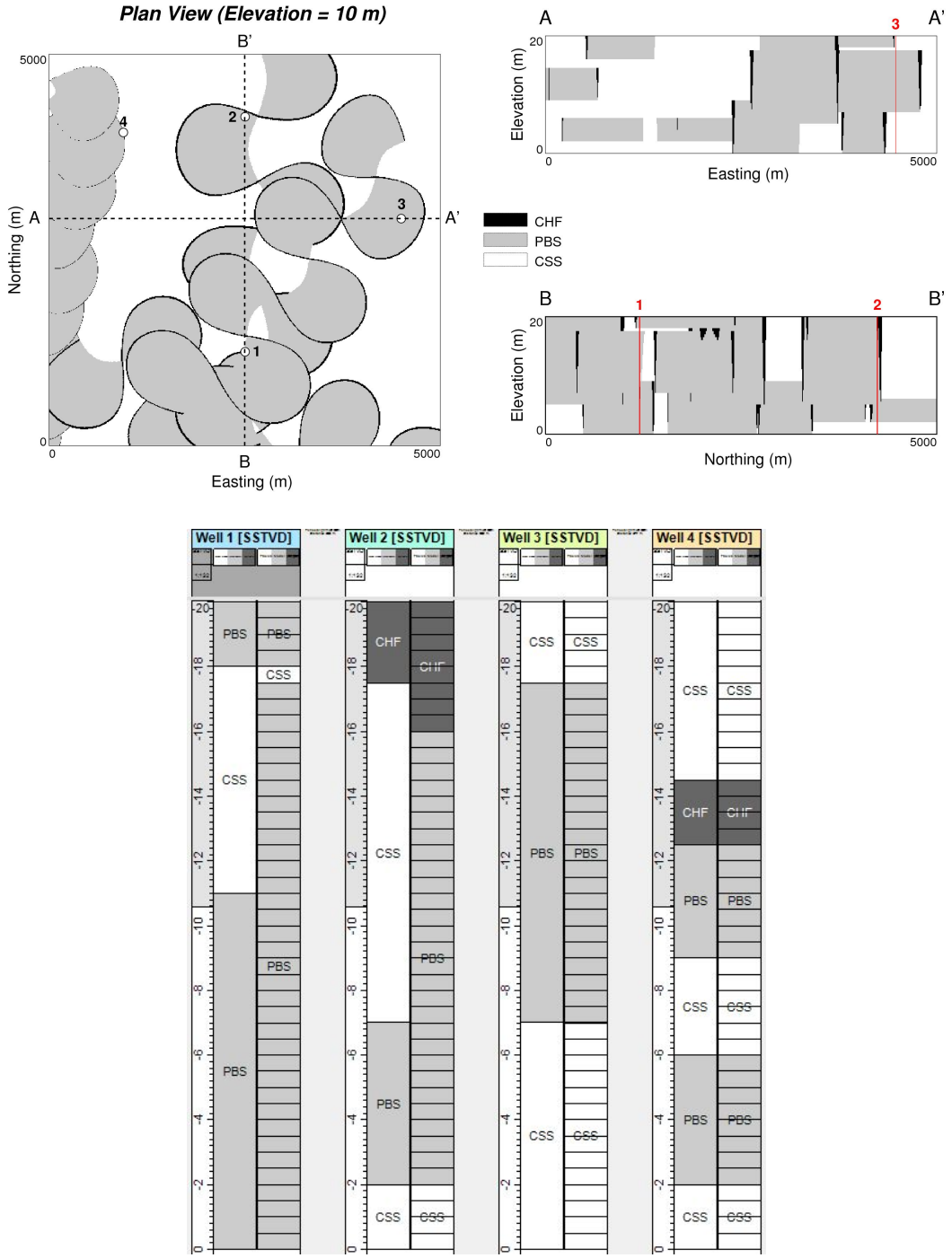

Figure 4.19: Top: example of conditional Facies Model for the McMurray Formation generated with grid-free modelling technique. The vertical sections are exaggerated 70 times. Location of conditioning wells are shown with circles in the plan view and vertical lines in cross sections. Bottom: well section showing four conditioning wells; left tracks show the original data, and right tracks show the model at each well locations.

Chapter 5

Applications

This chapter presents two applications of the grid-free facies modelling algorithm presented in previous chapter.

Section 5.1 introduces two `FORTRAN` programs that are developed based on the proposed grid-free methodology. The `IHSSIM` programs is developed to generate grid-free estuarine facies models of the McMurray Formation. The `IHSRAST` program is developed to generate rasterized models of estuarine facies by using the results of the `IHSSIM` program.

Section 5.2 presents the application of grid-free facies modelling in development of an estuarine training image library. This library contains training images that have been created by the two developed programs explained in Section 5.1. Different possible scenarios and reservoir types are explained and details of generating the estuarine training image library are provided.

5.1 Programs

In order to implement the proposed methodology of grid-free IHS facies modelling, two GSLIB type FORTRAN codes called IHSSIM and IHSRAST are developed. Details of these programs are provided in this section.

5.1.1 IHSSIM Program

IHSSIM program is a GSLIB style (Deutsch and Journel, 1998) program that is developed to generate both unconditional and conditional IHS facies realizations. The program starts with reading the parameter file. If the parameter file does not exist, then a default parameter file is generated automatically.

The default parameter file for IHSSIM is shown in Figure 5.1. The well conditioning data file is specified in line 1. Facies data should be provided as intervals. In line 2, the column numbers for the well ID, x, y, top and bottom elevation of each data interval and the facies code are specified. The output grid-free model is written out to the file that is specified on line 3 of the parameter file. Lines 4 to 6 ask for the size of the model in x, y, and z coordinates. The channel source is specified with the mean and standard deviation of x and y coordinates in line 7. the mean and standard deviation of channel azimuth is specified in line 8. In line 9, the relative value of the channel sinuosity should be specified. The meander wavelength is closely related to the channel bankfull width. According to the study by Leeder (1973), the point bar width is almost eleven times of the channel bankfull width in the meander fluvial channels. A sinuosity value of -1 refers to the lowest possible sinuosity and 1 shows highest possible sinuosity. Zero sinuosity in this program relates to the case where the meander wavelength of channel is exactly eleven times of the channel width. This ratio changes linearly between 7 to 15 for the highest and the lowest sinuosity cases, respectively.

Lines 10 and 11 specify the mean and the standard deviation of the IHS length and IHS width. The mean and standard deviation of Gaussian distribu-

tions for the IHS thickness and dip angle of shale drapes are specified in line 12 and 13. The maximum number of accreationary surfaces is specified in line 14. This is required for allocation of arrays for drapes. The number and elevation of the aggradation levels are specified in line 15. Line 16 asks for the number of channels in each aggradation level. The shale drape frequencies in each level are specified in line 17. Shale drape placement options can be specified in line 18. The options of distal attached and the parallel shale drapes can be selected by specifying code 1 or 2. The top shale thickness and the bottom breccias are specified in terms of percentage of total IHS thickness in lines 19 and 20. The probabilities of appearance for each profile type should be specified in line 21. The random number seed and the number of realizations to be generate are specified in line 22 and 23.

The general program workflow is shown in Figures 5.2 and 5.3. The simulation starts with picking a random location and angle for the channel source and channel azimuth, respectively. Then the geometric parameters of IHS set is randomly picked from the user specified distributions and the object is located on the channel line. More IHS sets will be generated for this channel if the anchor point of a new IHS set falls inside the modelling area. In order to maintain the continuity of the channel along the channel line, the channel width, IHS thickness, and IHS dip are assumed to be constant along the channel stream. The number of shale drapes in the IHS sets are controlled by the shale frequencies. A larger frequency value leads to generation of more shale drapes. Although, the program does not use any vertical trend, the facies proportions can be partially controlled by the number of levels, number of channels and the shale frequencies in each level. The simulation terminates when enough realizations are generated.

The output file of the `IHSSIM` program is an ASCII file format. Figure 5.4 shows example of an `IHSSIM` output file. The output file is consistent with the object hierarchy level. There are different keywords that are used in the output file. Table 5.1 describes the keywords.

Figure 5.1: An Example parameter file for IHSSIM.

```
                          Parameters for IHSSIM
                          *********************
Line  START OF PARAMETERS:
1     well.dat              -file for well data
2     1 2 3 4 5 6           - column for well ID,x,y,ztop,zbot,facies code
3     ihssim.gfm            -file for output grid-free model
4     0.0 5000.0            -xmn, xmx
5     0.0 5000.0            -ymn, ymx
6     0.0 50.0              -zmn, zmx
7     2500 100 0 10         -CH source:  mx, stdevx, my, stdevy
8     0 30                  -CH azimuth angle:  m, stdev
9     0                     -CH sinuosity:  1=highest, -1=lowest
10    500 50                -IHS Length:  m, stdev
11    500 50                -IHS width:  m,stdev
12    20 5                  -IHS thickness:  m, stdev
13    10 2                  -IHS dip:  m, stdev
14    2000                  -max.  number of accretion surfaces
15    4 15 25 35 45         -number of levels, level elevations
16    5 7 5 10              -number of channel in each level
17    0.1 0.2 0.3 0.4       -shale drape frequency in each level
18    1                     -shale drape option:  1=realistic, 2=,parallel
19    10 5                  -top shale thickness(% of IHS thickness):m,stdev
20    10 5                  -breccia thickness(% of IHS thickness):m,stdev
21    0.6 0.3 0.1           -profile probability:sigmoidal,convex-up,concave-up
22    75079                 -random number seed
23    1                     -number of realization to generate
```

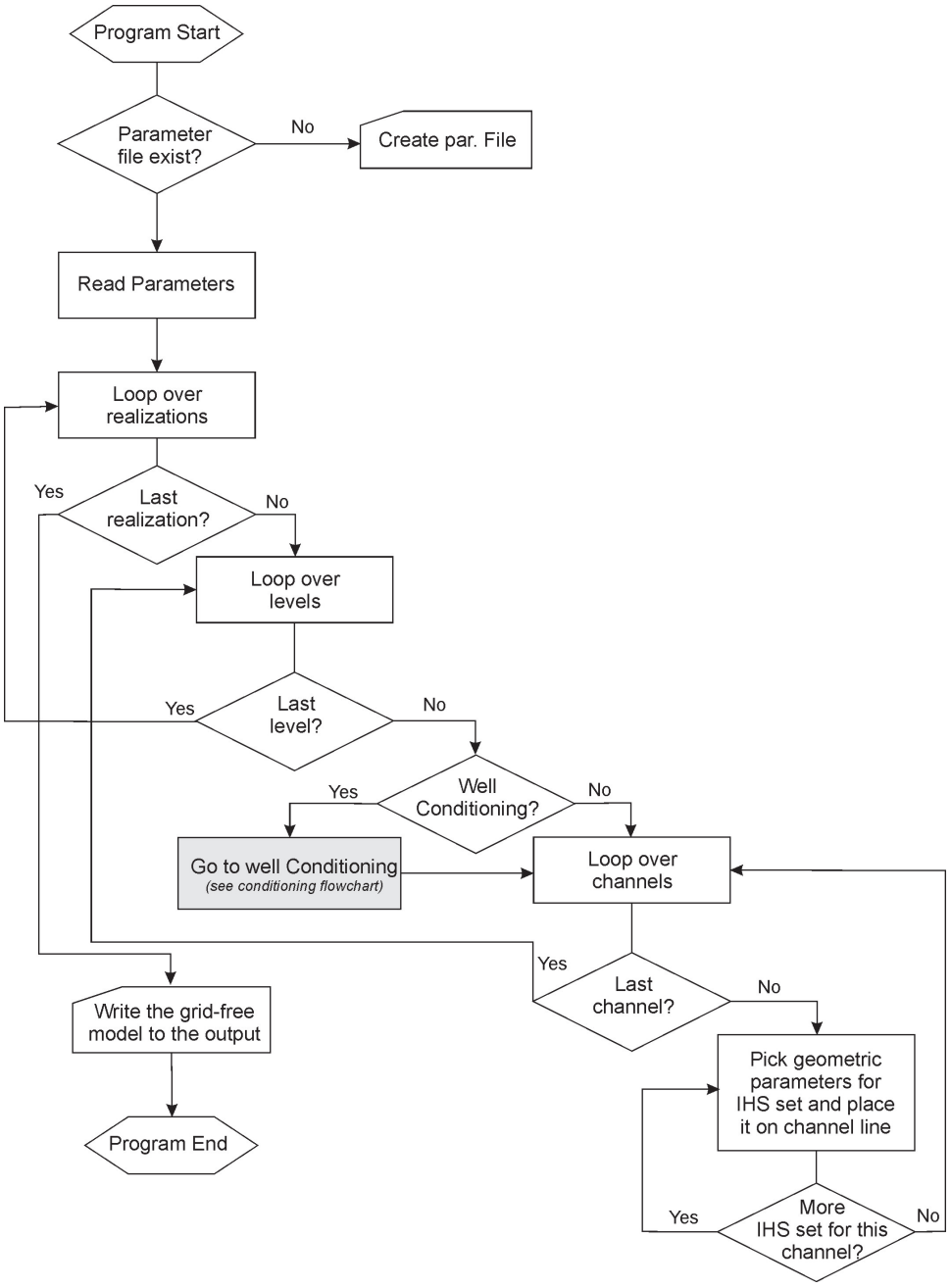

Figure 5.2: Workflow of the `IHSSIM` program for grid-free IHS facies modelling.

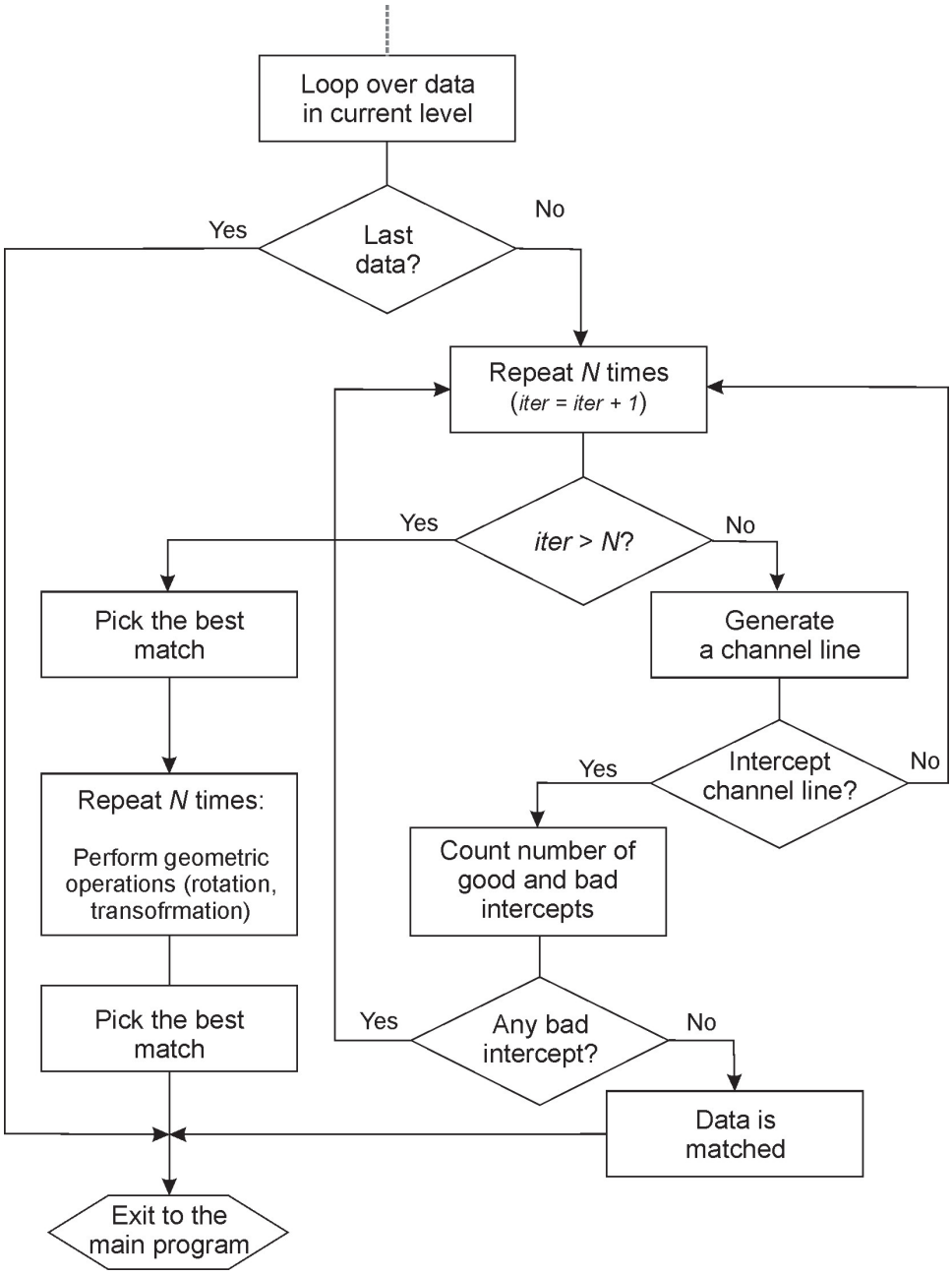

Figure 5.3: Flowchart of the well conditioning in the `IHSSIM` program.

```
Grid Free IHS Facies Model version 2.00

MODEL       1       0.00    5000.00       0.00    5000.00       0.00      20.00

REALIZATION        1       4       4      30       3
 LEVEL             1       5.00       1
  CHANNEL          1    3163.48     603.62     350.46      93.42       0.00      16.11      15.61       2
   IHS_SET         1       3
   {
    BODY        1043.54  0.00 1036.38  556.44  502.08 1052.77   30.71  496.33  86.46  0.00  558.71   105.28
    BOX          -41.98    1140.62       0.00    1139.78
    ANCHOR       565.00       0.00
    PROFILE     0.00000    0.00000
    TOP_SHALE      0.02
    BRECCIA        0.01
    DRAPE       1056.44  359.90  551.51  500.20   34.88  359.21  552.27  472.04  28.17720  14.82560
    DRAPE        908.17  530.95  548.11  610.14  181.55  536.72  548.55  594.20  15.93714   8.38542
    DRAPE        842.45  895.40  545.04  982.80  227.39  904.22  545.49  960.67  22.13113  11.64443
   }

   IHS_SET         2       3
   {
    BODY      1130.00  0.00 1103.47 -538.81 1647.43 -1016.23  2130.65  -477.42  2043.38  0.00 1592.76 -101.62
    BOX         1017.91    2198.68   -1103.38       0.00
    ANCHOR      1586.69       0.00
    PROFILE     0.00000    0.00000
    TOP_SHALE      0.02
    BRECCIA        0.02
    DRAPE      1333.36  -155.42  1586.08  -201.03  1841.53  -158.86  1586.11  -190.09  10.94768  5.96733
    DRAPE      1130.00  -642.00  1607.12  -779.99  2103.22  -643.54  1606.35  -750.61  29.38935  16.01945
    DRAPE      1178.05  -739.30  1604.50  -865.37  2053.64  -745.94  1603.96  -838.94  26.44006  14.41186
   }


 LEVEL             2      16.00       1
  CHANNEL          1    2396.80      14.51       8.00      90.74       0.00      12.47      19.39       1
   IHS_SET         1       3
   {
    BODY   53.14  0.00  -187.25  -460.19  342.76 -906.86  861.07 -446.67 608.99 0.00 332.24  -90.69
    BOX         -229.07     905.25    -960.06       0.00
    ANCHOR       331.07       0.00
    PROFILE     0.00000    0.00000
    TOP_SHALE      0.00
    BRECCIA        0.02
    DRAPE         29.53 -552.36  333.64 -628.12  639.42 -555.79  333.59 -617.22  10.89498  5.16066
    DRAPE       -113.28 -542.50  333.20 -687.33  784.13 -545.27  333.15 -669.88  17.44419  8.26284
    DRAPE         32.58 -735.38  328.97 -812.76  629.06 -742.04  329.00 -801.45  11.31435  5.35930
   }
```

Figure 5.4: Example output of IHSSIM grid-free model.

Table 5.1: Keyword used in `IHSSIM` program.

Keyword	no. of Variables	Description
`MODEL`	7	Identifies the number of realizations in the model and the model size in the format of *xmin, xmax, ymin, ymax, zmin, zmax*
`REALIZATION`	5	Realization number, total number of Levels, total number of channels, total number of IHS sets, maximum number of shale drapes
`LEVEL`	3	Level number, level elevation, number of channel lines in this level
`CHANNEL`	9	Channel number, x coordinates, y coordinates, azimuth angle, irregularity angle, relative top elevation, thickness, dip angle of IHS sets, number of IHS sets
`IHS_SET`	2	IHS number, number of shale drapes
{	0	Indicates the start of IHS parameters block
}	0	Indicates the end of IHS parameters block
`BODY`	12	Shows (x, y) coordinates of top six control points of IHS body
`BOX`	4	Indicates the IHS bounding box corner relative coordinated in the format of *xmn xmx ymn ymx*
`ANCHOR`	2	Relative anchor points coordinates in the format of *xm ym*
`PROFILE`	2	Profile top slope, and bottom slope
`TOP_SHALE`	1	Top shale thickness
`BRECCIA`	1	Breccias thickness
`DRAPE`	10	Indicates (x, y) relative coordinates of top four points of shale drape, and thickness at top, and the vertical length

5.1.2 IHSRAST Program

IHSRAST is the rasterization engine that has been developed to generate the gridded facies model of IHS sets.

Figure 5.5 shows the default parameter file for IHSRAST. The grid-free model file that was generated with the IHSSIM program should be specified in line 1. Line 2 asks for the output gridded facies model file name. The grid specifications are specified in lines 3 to 5. The architectural elements facies code can be specified in line 6. If a negative value is specified for an element, then that element is not rasterized and therefore not included in the final gridded model. This option enables the user to generate models that have selected architectural elements. For example, if one is interested to generate a model including only channel fill, then this would be possible by specifying all the architectural elements facies code other than the CHF by a negative values. Figure 5.6 shows some examples of this rasterization option in the IHSRAST program.

Line 7 in the parameter file asks for the realization number to be rasterized. The program allows users to choose from four different rasterization on line 8. If the rasterization option in line 8 is set to cross section rasterization, then the slice number should also be specified in line 8. If the facies proportions at each grid are required then the refinement grid numbers in each coordinate direction have to be specified in line 9.

Figure 5.5: An Example parameter file for IHSRAST.

```
                          Parameters for IHSRAST
                          **********************
Line  START OF PARAMETERS:
1     ihssim.gfm          -file for grid-free model
2     ihsrast.out         -file for output gridded model/cross sections
3     500 5 10            -nx,xmn,xsiz
4     500 5 10            -ny,ymn,ysiz
5     50 0.5 1            -nz,zmn,zsiz
6     0 1 2 3 4           -facies code for CSS,SH,PBS,BR, and CHF
7     1                   -realization number
8     2 40                -rasterization option(1=3D model,2=xy slice,3=xz
                          slice,4=yz slice) , slice number if > 1
9     5 5 1               -discretization in x,y,and z if rasterization
                          option >1
```

Figure 5.7 shows the general workflow of the IHSRAST program. The grid-free model generated with the IHSSIM program is the input to the rasterization program. Rasterization starts by finding and indexing the objects that must be rasterized. if a cross section is selected as a rasterization option, the section plane is compared to all objects boxes and the objects that crosses the plane are indexed. For faster rasterization, the program loops over the objects first and then loops over the grid cells inside the object's box.

The IHS volume is rasterized first. This is implemented slice by slice in the z direction. For each slice in the z direction the transformation distance is calculated using the cubic equation of vertical profile and then the top six points of the IHS body is transformed by that distance. A cubic spline interpolator is used to make a smooth boundary of the IHS at the current z slice. Then, all grid cells in the $x - y$ plane that falls inside the IHS boundary are coded as point bar sands (PBS). Top shale (SH), breccia (BR), channel fill (CHF) and the shale drapes (SH) are all rasterized with the same procedure. The linear thickness variation (thicker at the top) is also considered in the rasterization of shale drapes.

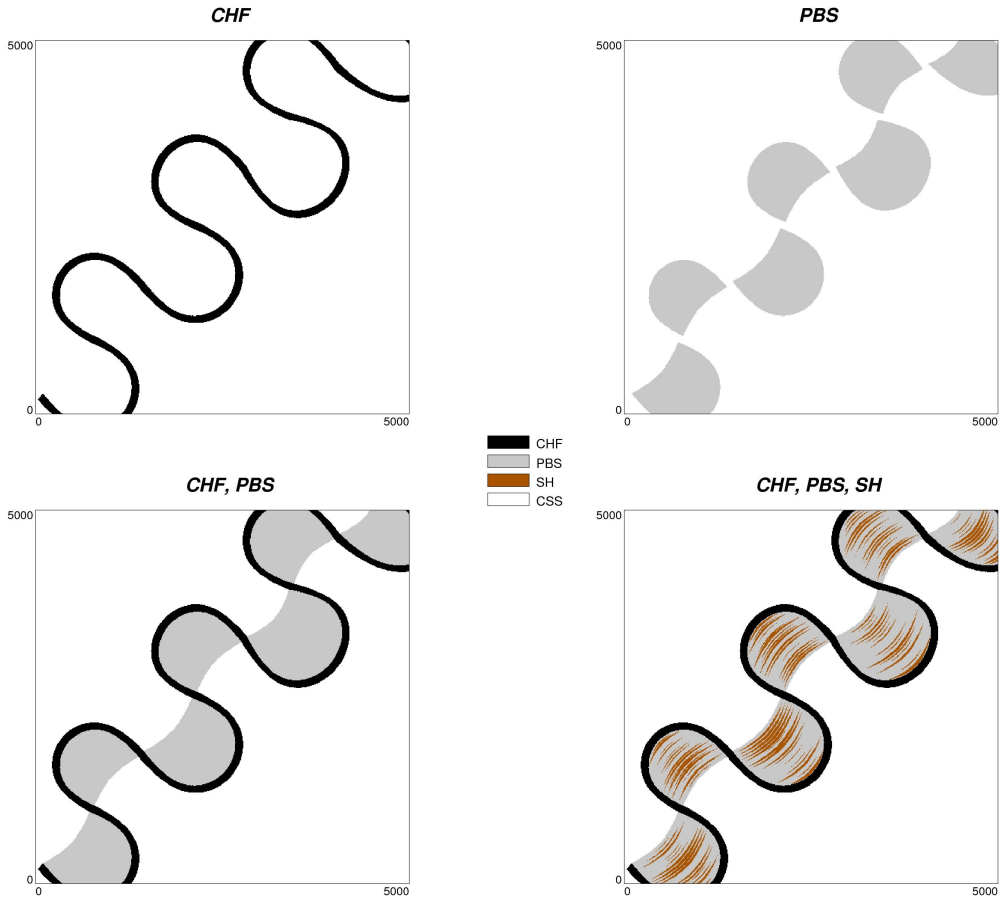

Figure 5.6: Rasterization of specific architectural elements from a grid-free model.

5.2 Estuarine Training Image Library

Variogram-based geostatistical facies modelling techniques such as sequential indicator simulation generate facies models that do not capture the realistic non-linear complexity present in most reservoir geology. They only account for two-points statistics between data and ignore non-linear relationships. Multiple point statistics (MPS) have received much attention recently and rely on higher order statistics. In this method, higher order statistics are extracted from training images.

The training image (TI) is an important input for multiple point simulation

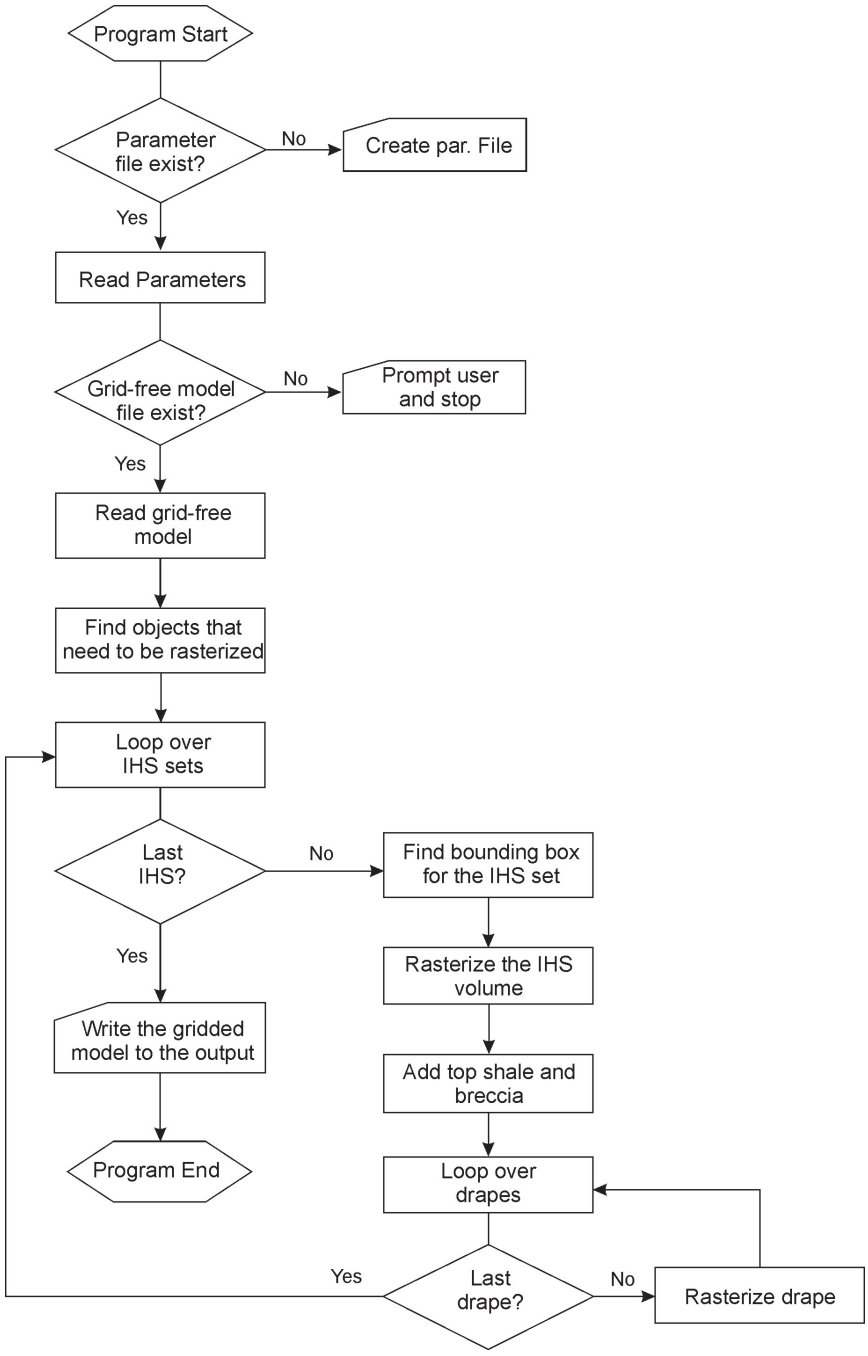

Figure 5.7: Workflow of the `IHSRAST` program for grid-free IHS facies modelling.

algorithms. A training image is a conceptual geological model that provides information about the facies structures and geometry of geological features. Information that can be used to understand the facies structure of a study area is generally provided from well data, outcrop images or geological interpretations. A digitized outcrop photo or a conceptual geological map can be used directly as a training image but they only provide information in two dimensions. It is difficult to integrate available information to construct 3D conceptual models. Process-based forward simulation (Tetzlaff and Harbaugh, 1989; Boisvert, 2007) event-based modelling (Pyrcz, 2004), and unconditional object-based simulations (Pyrcz, 2004; Maharaja, 2008) have been used to generate 3D training images.

Since all the critical information that are used in MPS is extracted from a TI, using an appropriate TI that represents the geology of the area of interest has a large impact on the result of facies modelling. A training image library (TIL) provides sets of categorized training images that can be used for MPS. A training image library for fluvial and deepwater reservoirs has been developed before (Pyrcz, 2004). The training images represent a range of net-to-gross ratios and a variety of depositional styles.

The fluvial training image library includes 498 TIs that are generated based on the marked point processes, FLUVSIM (Deutsch and Tran, 1999), surface based models and bank retreat fluvial models. Each TI in this library represents a volume of about $4000\,m$ by $4000\,m$ by $20\,m$ that are discretized by 256 by 256 by 128 grids.

An unconditional grid-free object-based facies modelling technique is presented in previous chapters of this dissertation with the application in the estuarine environment of McMurray Formation. Two `GSLIB` type programs were developed to generated unconditional grid-free facies model and to rasterize the grid free model. These tools can be used to generate multiple training images of estuarine systems for the McMurray Formation and other relevant formations. This training image library can be used in different applications. Training im-

ages can be used directly as an input to MPS simulation or they can be directly used as a facies model. Different scenarios of IHS deposits are considered and grid free training images are generated and rasterized in cross sections.

5.2.1 Methodology

The `IHSSIM` program was used to generate training images of the estuarine system. TIs generated with `IHSSIM` are grid-free models and represent the large scale geometry of IHS sets as well as the small scale shale drapes inside the IHS volume. In general, generating an estuarine training image involves the following steps:

1. Defining the scenarios, that is, the parameter set to use
2. Generating a grid-free TI
3. Rasterizing the TI

A detailed explanation of each step is presented in the following sections.

5.2.2 Scenarios for Training Image Generation

Different scenarios must be defined to generate a library of TIs that realistically represent the estuarine system of the McMurray Formation. Figure 5.8 shows six different IHS sets morphotypes for different depositional environment. Among those, numbers 2 and 5 represent possible IHS scenarios for the McMurray Formation. Number 2 illustrates a low to moderate energy meandering river of the Athabasca upper delta plain (Calverley, 1984). Number 5 shows rhythmic IHS couplets of moderate energy mesotidally influenced meandering river of McMurray Formation (Smith, 1985). Both cases can be generated by selecting appropriate parameters in `IHSISM` program.

Five important factors are selected; IHS set size, similarity of IHS sets, channel stacking pattern, shale content of IHS, and the amount of breccias. Each factor is represented by a letter ranging from a to e. Since there is no

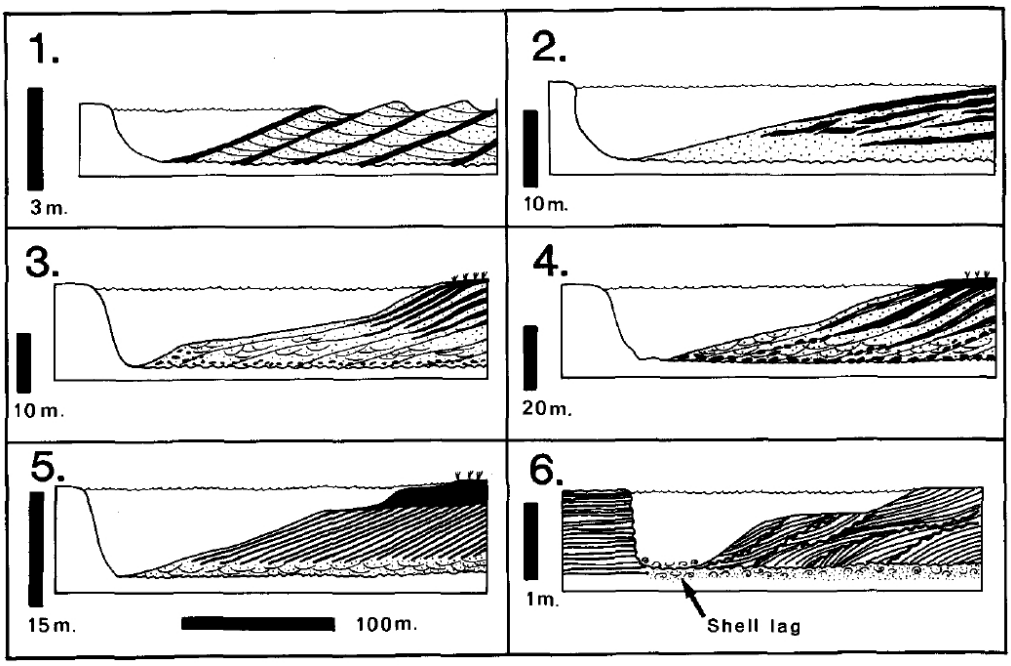

Figure 5.8: Schematic illustration of six idealized IHS set for different depositional environments (Thomas et al., 1987). Case number 2 and number 5 show possible IHS sets types for McMurray Formation.

control on the net-to-gross ratio (NTG) of the training images in the grid-free mode, the factors are selected so that the resulting TIs represent a variety of NTG ratios. This was mostly controlled by shale content in the training image. All five selected factors are related to the parameters of the `IHSSIM` program.

The IHS size can be fully controlled with the IHS length, width, sinuosity, thickness, and dip angle in the `IHSSIM`. Amount of shale in the TI is related to the maximum number of accreationary surfaces, shale drape frequency and top shale thickness.

The channel stacking pattern is related to the number of aggradation levels and number of channels in each level. Several studies have been done on the geology of the middle McMurray Formation and different IHS deposit parameters are reported. Mossop and Flach (1983) reported a meander wavelength of $2750\,m$ in their study area. This number was $1600\,m$ for the study area of Cr-

erar and Arnott (2007). The average range of dip of heterolithic strata forming McMurray Formation is reported to vary between 8° to 15° (Mossop and Flach, 1983; Langenberg et al., 2002; Ranger and Gingras, 2003; Crerar and Arnott, 2007).

Three levels are considered to capture the range of variation of each factor. For IHS size, level 1 refers to the small, level 2 refers to medium, and level 3 refers to large. Level 1 of similarity means IHS sets are more similar in shape. For channel stacking pattern, level 1 is related to loosely amalgamated, level 2 refers to moderately amalgamated, and level 3 refers to highly amalgamated channels. For Shale content and breccias, level 1, 2, and 3 refers to low, medium, and high amounts respectively. Table 5.2 shows all factors and their associated parameters and levels.

Table 5.2: Factors and the associated parameters considered for generation of estuarine training image library.

	Factors	Associated IHSSIM Parameters	Level 1	Level 2	Level 3
a	IHS Size	Length (mean)	320	850	1750
		Width (mean)	320	850	1750
		Sinuosity (mean)	-1	0	1
		Thickness (mean)	15	20	25
		Dip (mean)	15	12	8
b	Similarity	Length (stdev)	100	200	300
		Width (stdev)	100	200	300
c	Channel Stacking	# of levels	3	5	7
		Elevation	48-32-15	48-40-35-28-15	48-35-30-28-20-15-10
		# of channels in each level	3-3-3	3-3-5-5-7	5-5-7-7-7-10-10
d	Shale Content	Max. no. of accreationary surfaces	50	55	60
		Shale drape frequency	0.1-0.2-0.3	0.4-0.5-0.6-0.7-0.8	0.5-0.6-0.7-0.7-0.7-0.8-0.9
		Top shale thickness	0	5	10
e	Breccia	Breccia thickness	0	5	10

5.2.3 Grid-free Training Image Generation

Considering five factors and three levels, there are $3^5 = 243$ training images to be generated. Each grid-free TI represents a volume of $5000\,m$ by $5000\,m$ by $50\,m$. This is a reasonable size for a typical reservoir study. The total number of objects involved in each training image varies from hundreds to thousands of objects. A training image with thousands of objects occupies 2-5 MB of memory and can be compressed to tens of KB. Generating grid-free training images with `IHSSIM` is very fast and construction of the TI library took only 10 minutes. Grid-free TIs are named in the format of "TI-a-b-c-d-e.gfm" where a-e represent different factor levels. For example, TI-1-2-2-3-1 refers to the training image generated for level 1 of factor a, level 2 of factor b, level 2 of factor c, level 3 of factor d, and level 1 of factor e. Main advantage of grid-free training images is that they can be rasterized to any desired grid resolution.

5.2.4 Training Image Rasterization

Grid-free TIs cannot be used or visualized unless they are rasterized with the `IHSRAST` program. Parameters and tips to use `IHSRAST` program is presented in Chapter 5. Training images in the estuarine TI library can be rasterized to any grid resolution. However, the resolution should be selected so that the small scale features are adequately characterized with the selected grid size. Rasterization of a TI with large grid cells result in missing important small scale features of the IHS sets, however rasterizing with very small grid cells may not be possible because of long computational time and memory requirements. There is also a possibility to rasterize only a specific part or a cross section of a grid-free training image.

Since full rasterization of all the training images with small grids is not possible all of the 243 training images in the estuarine library are rasterized in plan, long and cross sections. Plan section of TI is rasterized with 1024 by 1024 grids with size of $4.88\,m$ by $4.88\,m$. Long sections and cross section are

rasterized with 1024 by 128 grids with size of $4.88\,m$ by $0.39\,m$. Figure 5.9 shows training image size and specifications. Figure 5.10 to 5.12 show some examples of training images in the training image library.

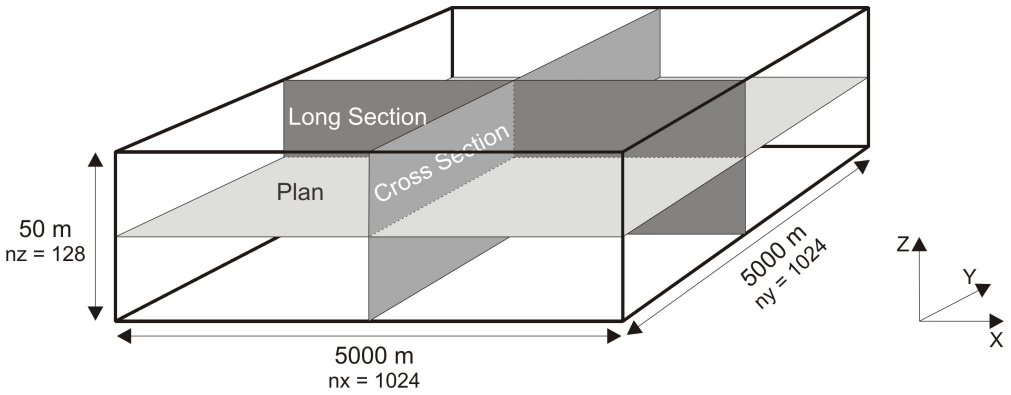

Figure 5.9: Training image size, rasterized sections, and specifications considered for estuarine training image library.

5.2.5 Selecting an Appropriate Training Image

Training images in the library have different statistical and spatial properties such as facies proportions, variograms, and multiple point statistics. Choosing an appropriate training image from the grid-free training image library may be challenging. Based on the application that the training image will be used for, different options are recommended to select from the estuarine training image library.

Training images may be used qualitatively as a conceptual geological model. In this case, the appropriate training image may be chosen from visualized cross sections provided as a part of the training image library. If enough information about the geology of the reservoir is available, data provided in Table 5.2 can be used to select the most relevant training image.

Training images may be used directly as facies model in geostatistical modelling of petrophysical properties such as porosity and permeability. If the resource estimation is the goal of property modelling, an appropriate TI should

be chosen based on the net-to-gross ratio. In this case, the NTG ratios of all training images in the library are calculated to help select the appropriate TI. Since fully rasterized training images are not available in high resolution, the cross sections can be used to calculate NTGs.

If the training image is going to be used as an input to MPS simulation, some statistical measures of the training image could be considered. Using an inappropriate TI that does not represent the geology of the area of interest could have a large impact on the result of MPS simulation. Multiple point histograms, transition probabilities, distribution of runs, and connectivity functions can be considered as a measure to rank training images (Pyrcz, 2004; Boisvert, 2007).

5.3 Summary

This chapter developed two tools based on the algorithms presented in the previous chapters; two fortran programs to implement conditional and unconditional facies modelling, and a training image library for the estuarine reservoir of the McMurray Formation. For the application of the McMurray Formation modelling, two different approaches are recommended:

- using the `IHSSIM` and the `IHSRAST` programs to build object-based facies model of the IHS facies association. In this approach, the geometry of the architectural elements are well reproduced however, conditioning of model to dense data will be problematic.

- picking a training image, that resembles the geology of the modelling area, from the generated training image library and using it as an input to the MPS facies modelling techniques.

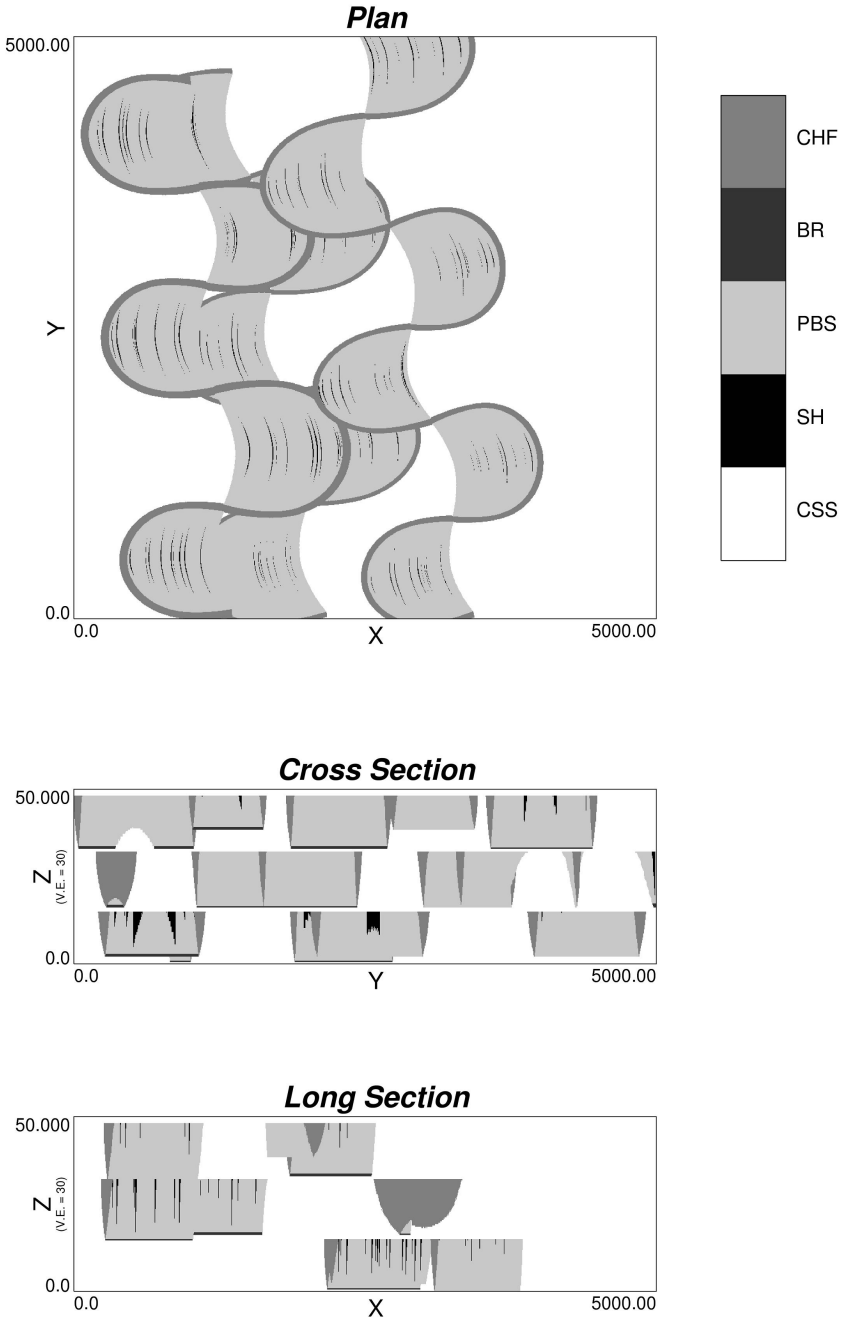

Figure 5.10: Three rasterized sections of training image for case 1-1-1-1-1 (vertical sections are exaggerated 30 times).

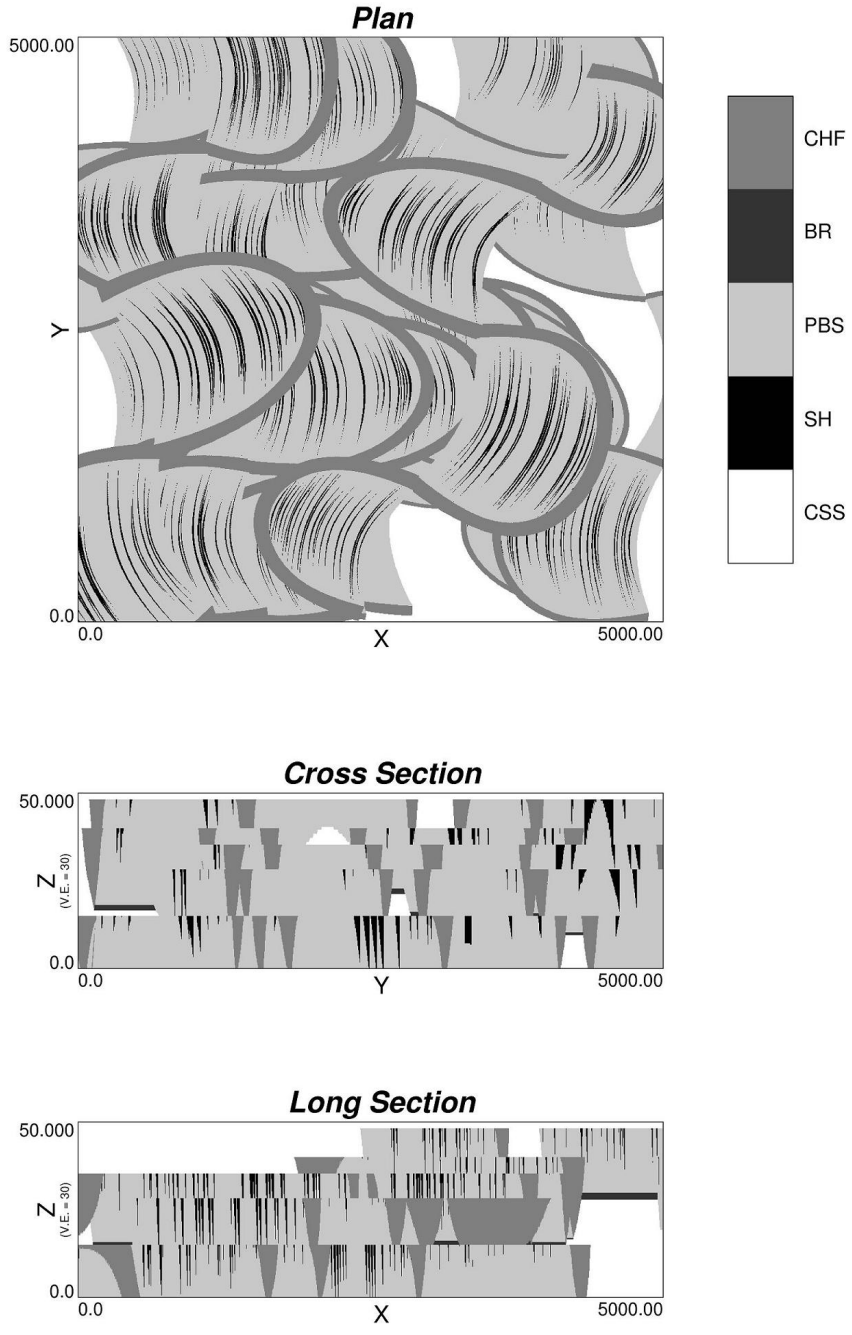

Figure 5.11: Three rasterized sections of training image for case 2-2-2-2-2 (vertical sections are exaggerated 30 times).

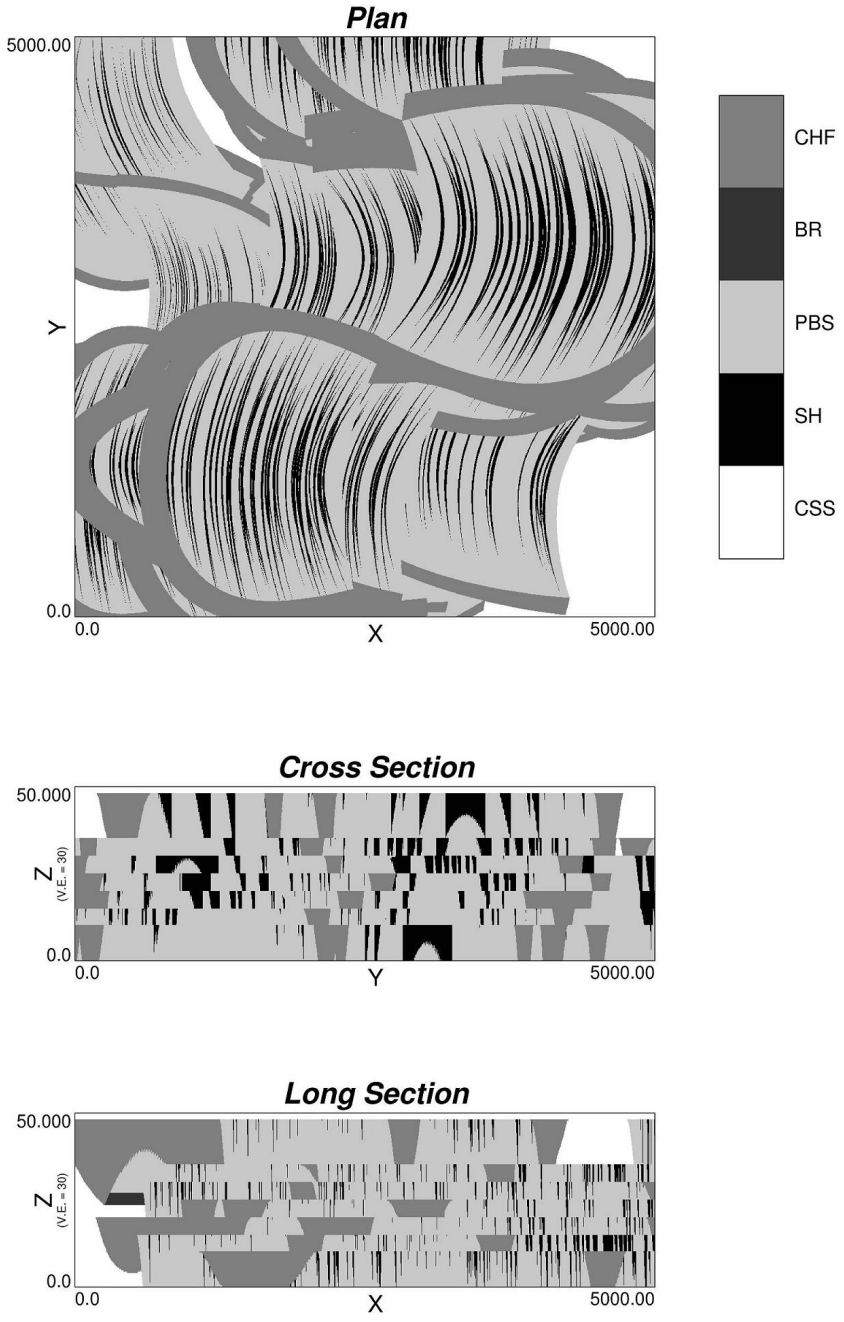

Figure 5.12: Three rasterized sections of training image for case 3-3-3-3-3 (vertical sections are exaggerated 30 times).

Chapter 6

Comparative Case Study

This Chapter provides an illustration of the grid-free facies modelling technique applied to real McMurray Formation data.

Section 6.1 explains the setting of the comparative case study. Section 6.2 presents a data set that is acquired from the McMurray Formation of Northern Alberta for this study. Section 6.3 to 6.8 documents details of the geostatistical modelling. Both the novel grid-free and the classical SIS techniques are applied. The performance of the two models are then evaluated through thermal flow simulation. This step is explained in Section 6.9. Finally, Section 6.10 campared the results from two different cases and conclusions are provided in Section 6.11.

6.1 Study Setting

The purposes of this study are: 1) to provide a comprehensive McMurray Formation reservoir modelling workflow using real data, 2) to show an extended example of grid-free IHS facies modelling, and 3) to evaluate and compare the effect of different facies models when processed through a transfer function such as SAGD thermal simulation. This study set up is as follows:

1) Data assembly
2) Geological analysis
3) Structural modelling

4) Stratigraphic transformation and gridding

5) Well log upscaling

6) Statistical analysis

7) Facies Modelling

8) Petrophysical property modelling

9) Flow simulation

10) Comparison of results

For the facies modelling part, two different methods are applied. Two conditional realizations of grid-free facies modelling and sequential indicator simulation are generated for the whole area. Then a suitable place for the horizontal well pad is selected based on the large scale models. Facies models are generated for the pad area and petrophysical models are populated within each facies model. Then a 2D slice is picked from the pad models and thermal flow simulation is run on both the grid-free and SIS-based models. Results are compared based on the flow simulation output parameters.

6.2 Data Assembly

The Data set used for this study was released from a SAGD operator in Athabasca Oilsand area. An area with the extension of approximately two sections by two sections was considered (section is a square area of about $1.6\,km$ by $1.6\,km$). The total modelling area is a square of about $3.5\,km$ by $3.5\,km$. There are ten vertical wells within the study area. For confidentiality, the coordinates of wells were transformed to the range of 0 to $3500\,m$. Figure 6.1 shows the location map of wells within the study area. Well names start with the letter W followed by a number from one to ten.

All wells contains well logs for the McMurray Formation interval (from the top of the McMurray up to the top of Devonian Formation). Well logs include effective porosity, water saturation, and volume of shale at $0.125\,m$ intervals. Structural markers for the top and base of the McMurray Formation are also

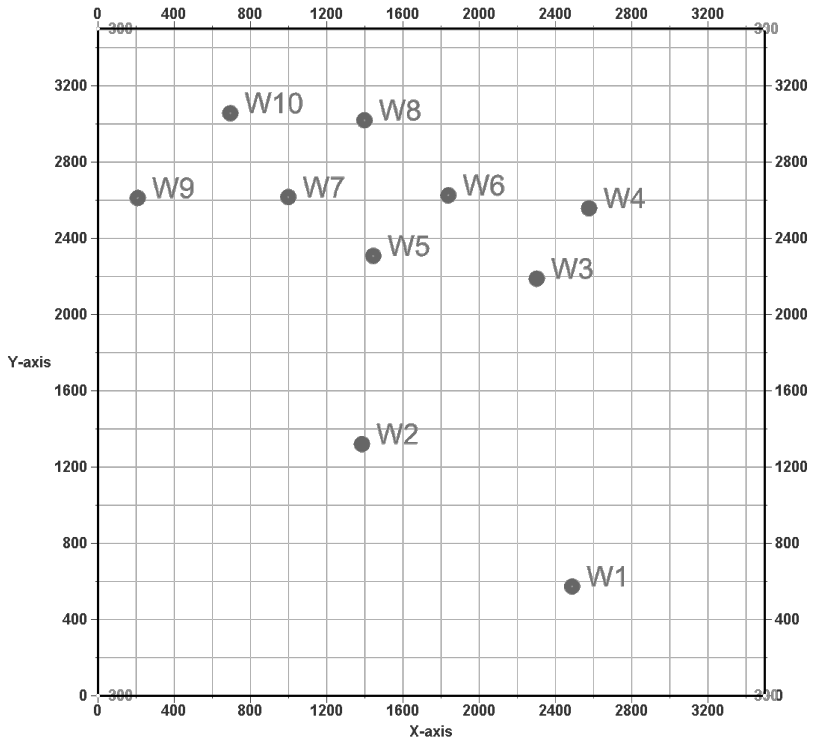

Figure 6.1: Location of vertical wells in the study area.

available for all wells.

Three pseudo-facies of clean sand (cross stratified), IHS, and mud were considered. Cutoffs were applied to the effective porosity and volume of shale to define these three facies. Table 6.1 shows the cutoffs for each facies. These cutoffs were calculated based on some expert knowledge and geological description of the McMurray Formation. In order to make the facies data and the petrophysical properties consistent, cutoffs were applied to the upscaled porosity and Vsh values. This step was performed after the data upscaling step (see Figure 6.2). In practice, the facies are likely to come from visual inspection of core; however, these log-derived facies are adequate for the purposes of demonstrating the workflow for a realistic area.

Table 6.1: Cutoffs used to generate facies data.

Facies	Cutoff
Clean Sand	$\phi > 0.28$ and $V_{sh} < 0.1$
IHS	$0.12 \leq \phi \leq 0.28$ or $\phi > 0.28$ and $V_{sh} > 0.1$
Mud	$\phi < 0.12$ or $V_{sh} > 0.6$

6.3 Geological Analysis

The McMurray Formation comprises three stratigraphic units; lower, middle and upper. Since the well markers for these units were not available in the data set, the whole McMurray Formation was considered as a single unit.

In order to get a better sense of the geology of the area, 2D trend maps of the properties were generated. Well logs including porosity, water saturation, and volume of shale were averaged up for each well. Facies codes (which were calculated based on the cutoffs in Table 6.1 at the log scale) were also averaged up for each well and facies proportions were calculated.

Global Kriging was used to generate 2D maps of upscaled properties in the modelling area. Global kriging is the general form of kriging that utilizes all conditioning data for the estimation (Isaaks and Srivastava, 1989) .

Calculation and modelling of variogram with a limited number of wells is not possible. Therefore, a Gaussian variogram with a large range ($3500\,m$) was used for all properties. This variogram model captures large scale variablity of the geological features within the modelling area and reproduces smooth maps (Deutsch and McLennan, 2005). Figure 6.3 shows 2D trends for the facies proportions and the three rock properties.

Looking at the porosity and Vsh trends suggests a SE-NW channel deposit

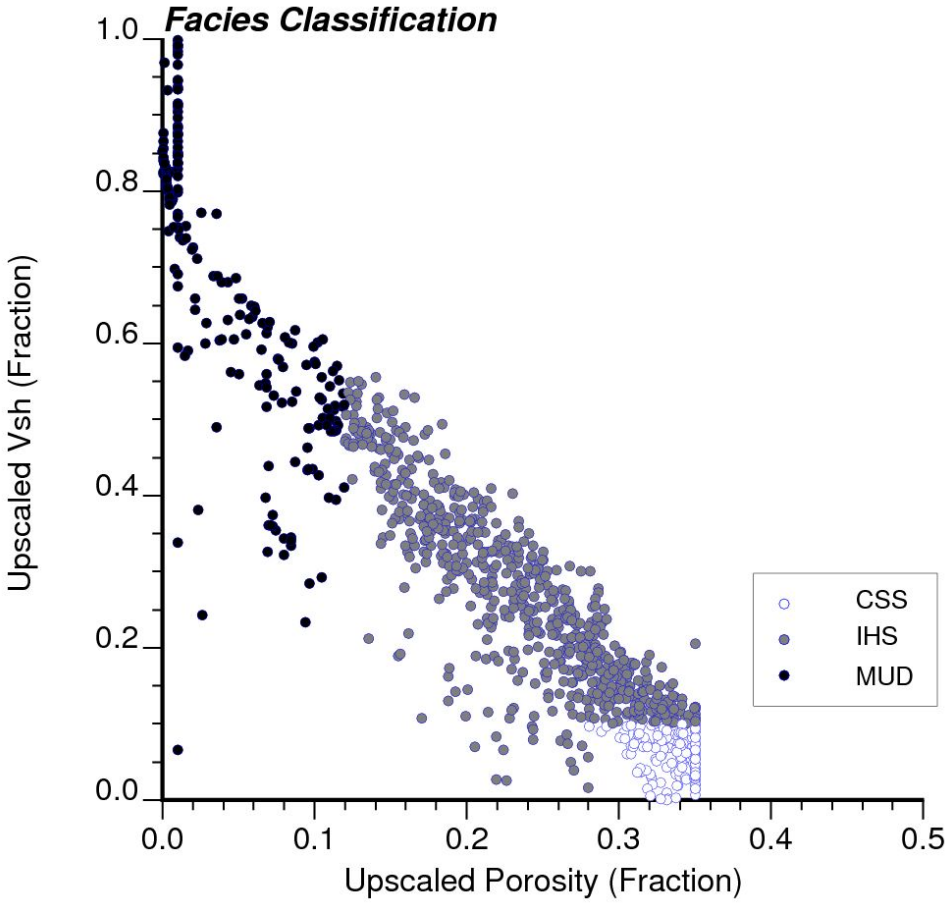

Figure 6.2: Facies data generation using porosity and Vsh cutoffs.

which has high porosity and low volume of shale (see Figure 6.4). As suggested by the mud trend, there is a package of mud on the west side of the large channel. Within the channel, the sand proportion trend shows a higher proportion of sand at the North of the study area. This suggests that the North part was probably closer to the estuarine mouth and therefore has more tidal sand bars and less muddy IHS (Lettley, 2004).

As we go from the NW to the SE the proportion of IHS facies increases. This is consistent with the idea of North side proximity to the estuarine mouth. This interpretation may not be exact since it is derived based on limited information, but at least it helps to infer the anisotropy direction in the modelling area

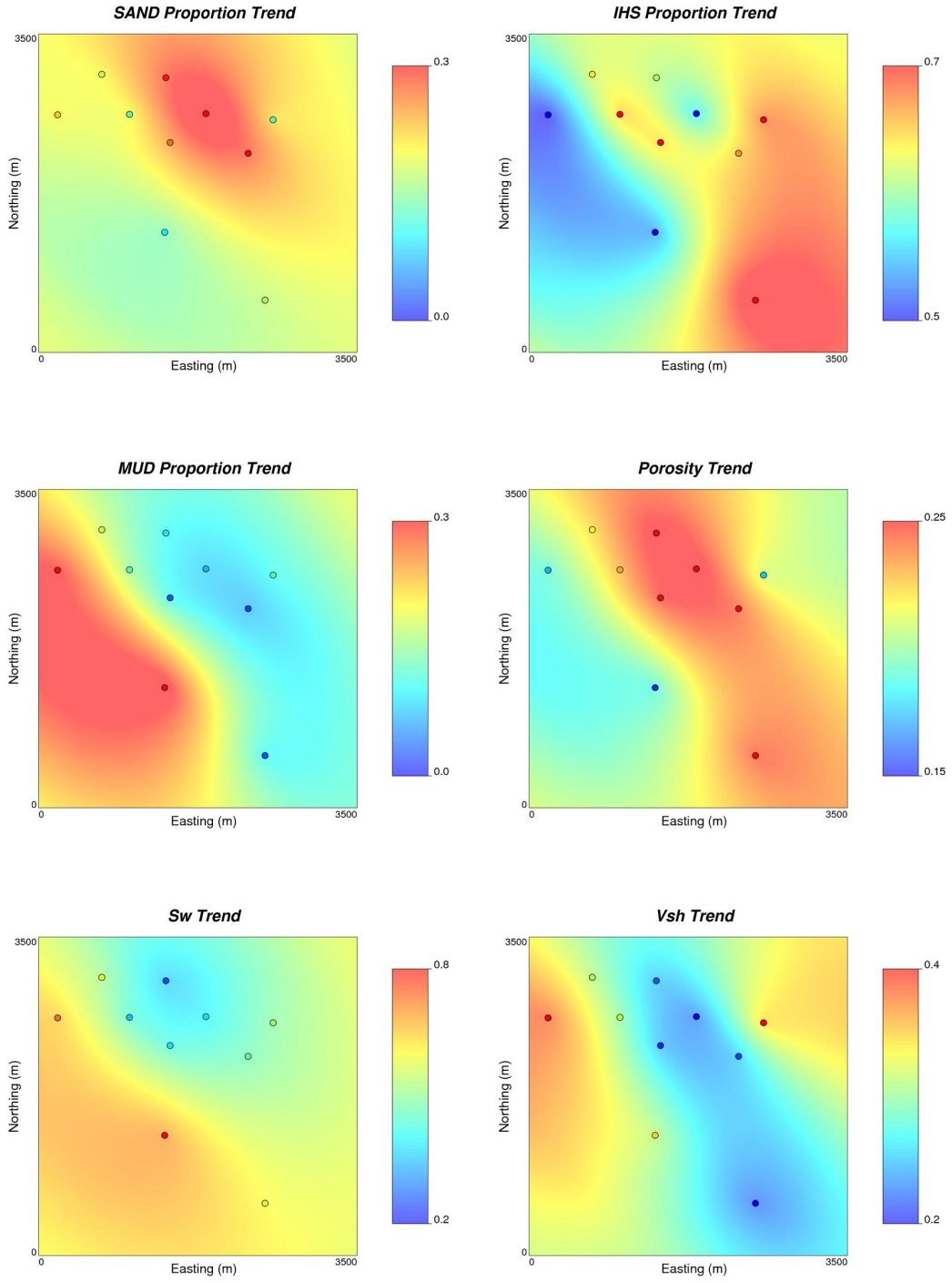

Figure 6.3: 2D trend maps of facies proportions and reservoir properties in the modelling are. The color scale unit is fraction.

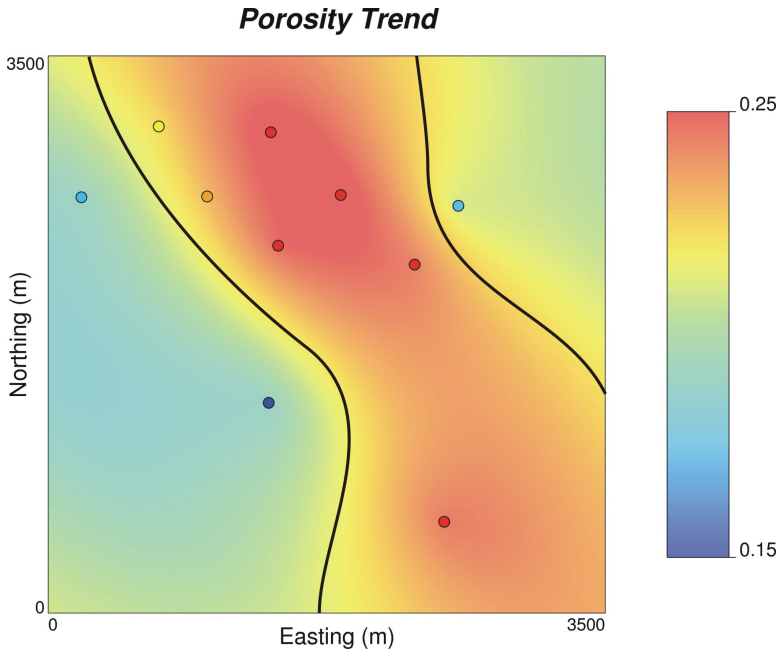

Figure 6.4: Boundary of possible SE-NW channel deposit in the study area based on the porosity trend map.

and also helps to infer some of the IHS parameters needed for grid-free facies modelling which will be discussed in the following.

6.4 Structural Modelling

There are two structural markers; top and base of the McMurray Formation. All ten wells have structural tops for both markers. Isochore thicknesses were also calculated for all ten wells. Global kriging was used to generate structural surfaces. Since calculating reasonable horizontal variograms for the tops was not possible with limited well control, a Gaussian variogram with a large range ($3500\,m$) was considered for both tops and isochore thickness. This variogram accounts for the large scale variation of structural surfaces and generates smooth maps. Figure 6.5 shows the top McMurray, Base McMurray and, the thickness maps. The SE-NW trend of the estuarine deposit is also visible on the McMurray top surface. The thickness map shows that the McMurray Formation

thickness increases from North to South of the study area varying from $51\,m$ to $84\,m$. Histograms of elevations and isochore thickness maps are also provided in Figure 6.5.

6.5 Stratigraphic Transformation and Gridding

Stratigraphic coordinate transformation is one of the essential steps in geostatistical modelling. The main goal is to establish a grid that preserves the geological structures and allows geostatistical calculations, such as variography, within each layer that is conform to the natural geological correlations (Deutsch, 2002).

For the application of McMurray Formation modelling, to preserve the erosional base surface (unconformity Devonian top surface) in the model, the vertical coordinate which was in measured depth (MD) was transformed to a stratigraphic coordinate system relative to the top McMurray surface. The new vertical coordinate was defined as the difference between the McMurray depth and log measured depth. In other words, the McMurray top surface was set to zero elevation and all the log reading below that got a negative elevation value.

A grid with size of $50\,m$ (Easting) by $50\,m$ (Northing) by $0.5\,m$ (vertical) was generated. This grid size was chosen based on the required geological details and also based on previous geostatistical modelling studies of the McMurray Formation (McLennan and Deutsch, 2004; Deutsch and McLennan, 2005). This results in 70 by 70 by 168 cells with total of $823,200$ cells. Note that, the number of cells in the vertical direction varies relative to the thickness of the Formation.

6.6 Well Log Upscaling

The well log data that was vertically transformed to the stratigraphic coordinates were upscaled to the generated grid. Arithmetic averaging was used for upscaling of porosity, Vsh, and water saturation. All the statistical analyses

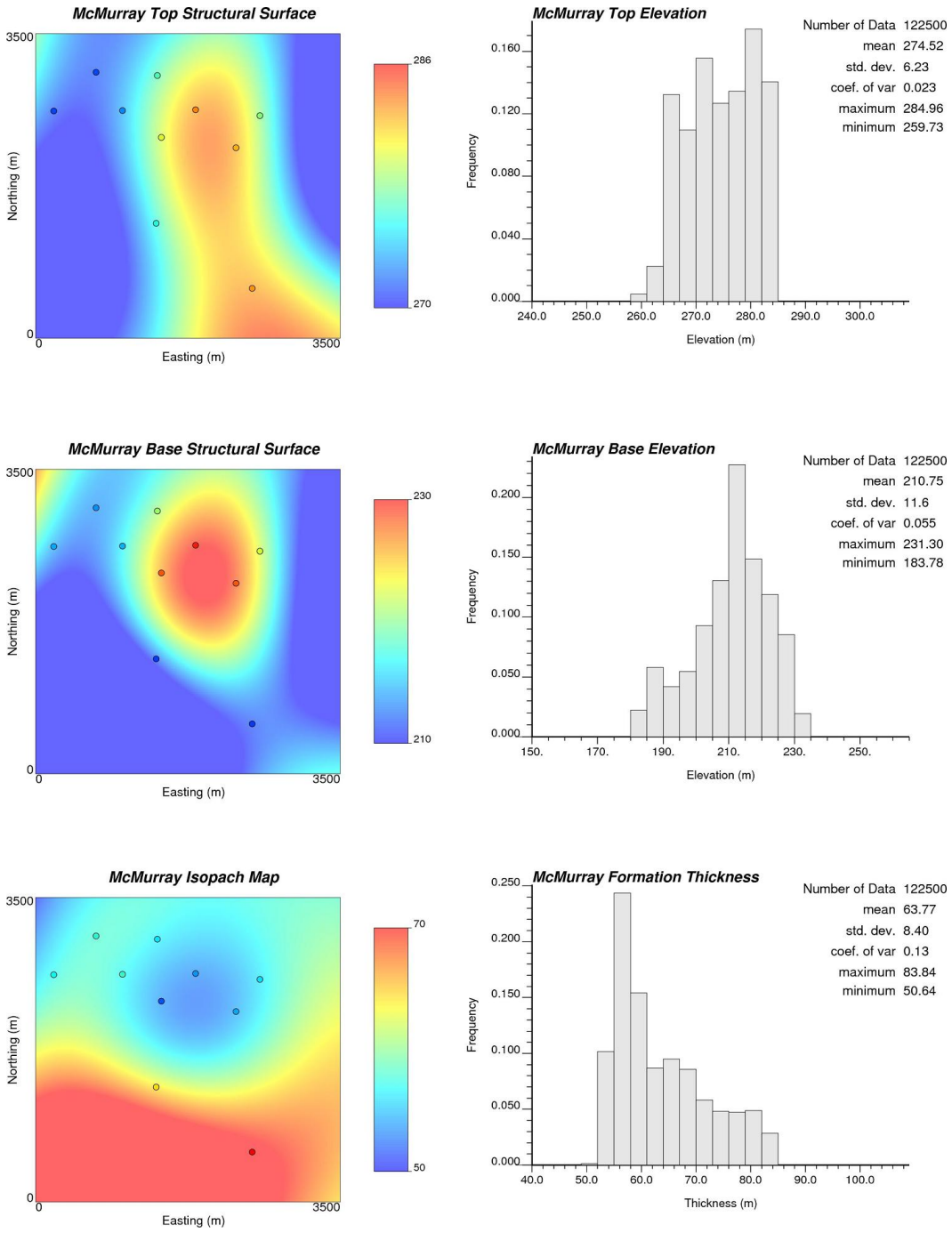

Figure 6.5: Structural surfaces of the McMurray Formation in the modelling area (left) and associated histogram of elevations(rigth). The color scale unit is meters.

were performed on the upscaled data. The effect of upscaling was checked for all variables to make sure that the difference in the statistical parameters between log-scale ($0.125\,m$) to grid-scale ($0.5\,m$) is not significant. Figure 6.6 shows Q-Q plots of log-scale and upscaled porosity, water saturation, and volume of shale. As shown in the Q-Q plots, statistics of all variables were preserved during the upscaling.

As mentioned earlier, facies data was generated after the upscaling step. Cutoffs were applied on the upscaled porosity and volume of shale and the corresponding facies code was assigned at the grid scale. The example well section in Figure 6.7 shows porosity and Vsh logs and the facies log that was calculated for Well 5.

All upscaled data were then transformed to normal score units. The normal score transformed data were used for the experimental variogram calculation.

6.7 Statistical Data Analysis

Histogram of all upscaled variables were generated both globally and by-facies. Figure 6.8 and Figure 6.9 show the global and the by-facies histograms. Summary statistics are also provided in Table 6.2.

The variography was performed for porosity and Sw globally and by-facies. Variables were first transformed from original units to the normal score units. The normal score variograms were then calculated at three directions (two horizontal and vertical). The horizontal variograms were calculated along the direction of the apparent main channel (approximately azimuth of -30.0) and perpendicular to the main channel (azimuth of 60.0).

The indicator variograms were also calculated for CSS, IHS, and Mud along and across channel and vertical direction. The variogram sill for each indicator variogram was set based on the global facies proportions.

All continuous variable and indicator variograms were modelled. Figure 6.10 to Figure 6.12 show the experimental variogram points (black dots) and

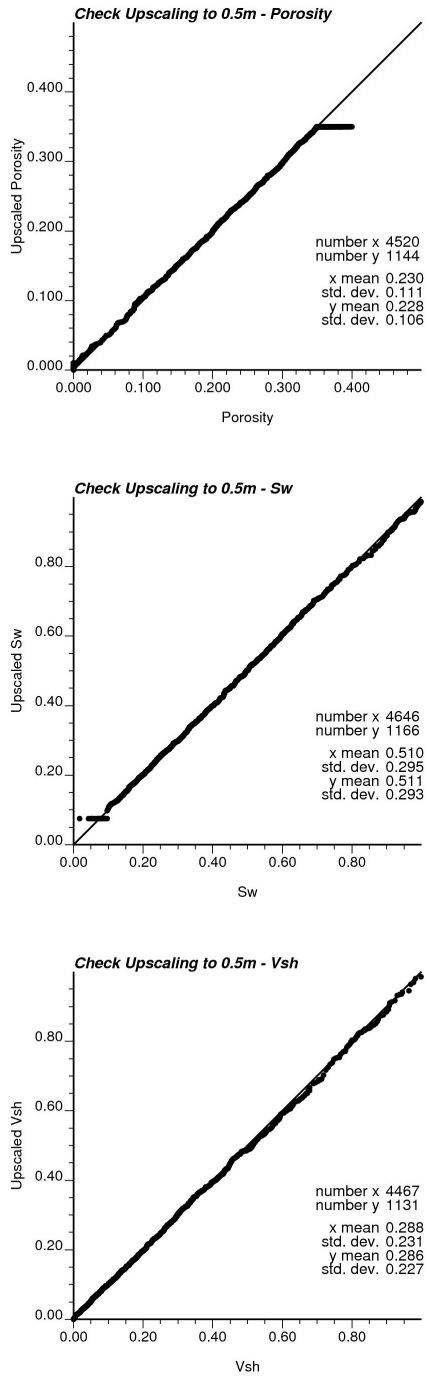

Figure 6.6: Q-Q plots used to check the quality of data upscaling from $0.125\,m$ to $0.5\,m$.

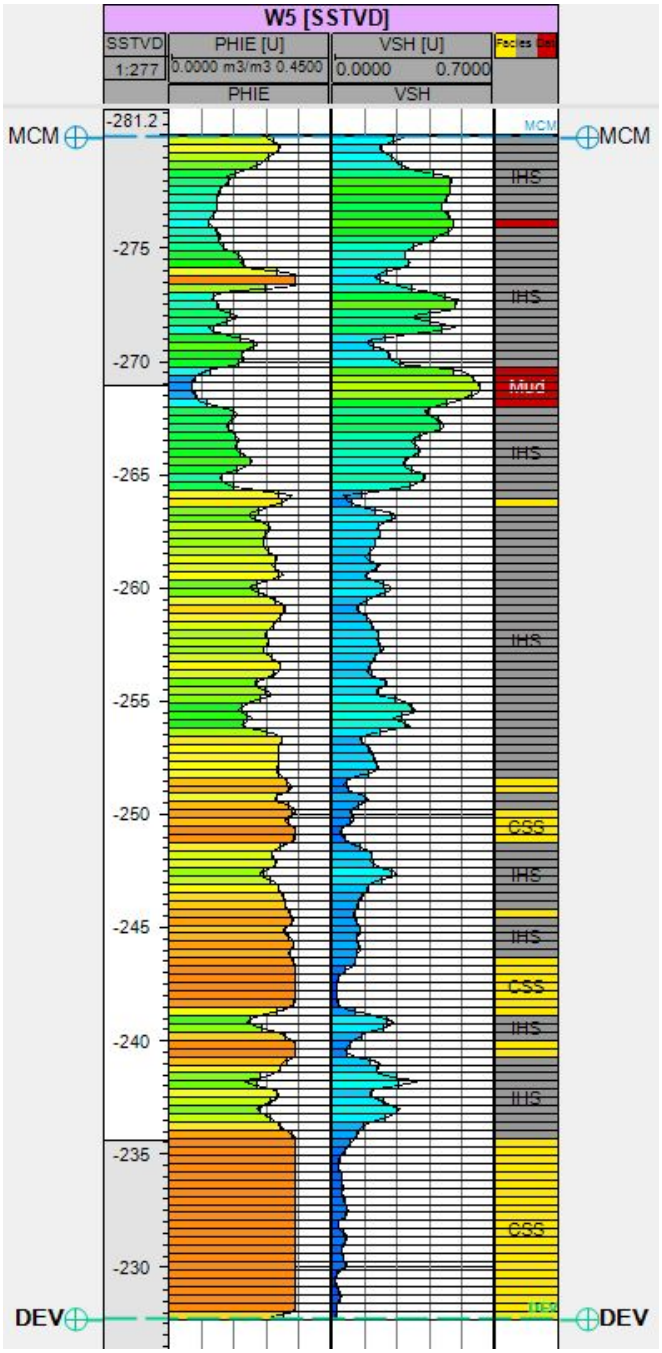

Figure 6.7: A well section for Well 5 showing porosity log (left track), Vsh log (middle track), and the calculated facies log (right track). Horizontal lines show vertical cells along Well 5.

Table 6.2: Summary statistics of the data set in the McMurray Formation.

	Variable	No. of Data	Mean	Std. Dev.	Min.	Max.
Global	*Porosity*	1120	0.23	0.11	0.0003	0.35
	Sw	1166	0.51	0.29	0.075	1.0
	Vsh	1096	0.29	0.23	0.0	1.0
CSS	*Porosity*	249	0.34	0.01	0.28	0.35
	Sw	249	0.36	0.29	0.075	1.0
	Vsh	249	0.06	0.025	0.0	1.0
IHS	*Porosity*	685	0.24	0.06	0.12	0.35
	Sw	685	0.44	0.21	0.075	1.0
	Vsh	685	0.26	0.12	0.016	1.0
Mud	*Porosity*	195	0.046	0.041	0.0003	0.12
	Sw	195	0.90	0.16	0.27	1.0
	Vsh	195	0.66	0.19	0.065	1.0

the fitted models (solid line).

As mentioned earlier, calculating and modelling of horizontal variograms with the limited data coverage was challenging. Therefore, in all cases, the 3D variogram was modelled based on the experimental variogram in the vertical direction. This is because of higher resolution data in the vertical direction that makes the variography easier. A horizontal-to-vertical anisotropy ratio of 150:1 and 100:1 were applied to generate variogram models in the maximum and minimum horizontal continuity directions, respectively. These ratios were picked based on the approximate size of the interpreted channel within the modelling area.

6.8 Facies Modelling

Facies modelling was performed in two steps. First, the large scale facies models were generated for the whole area. Then a representative area for the thermal flow simulation was picked and facies models were built at a smaller pad scale. The reason to perform two-steps facies modelling was to capture the large scale

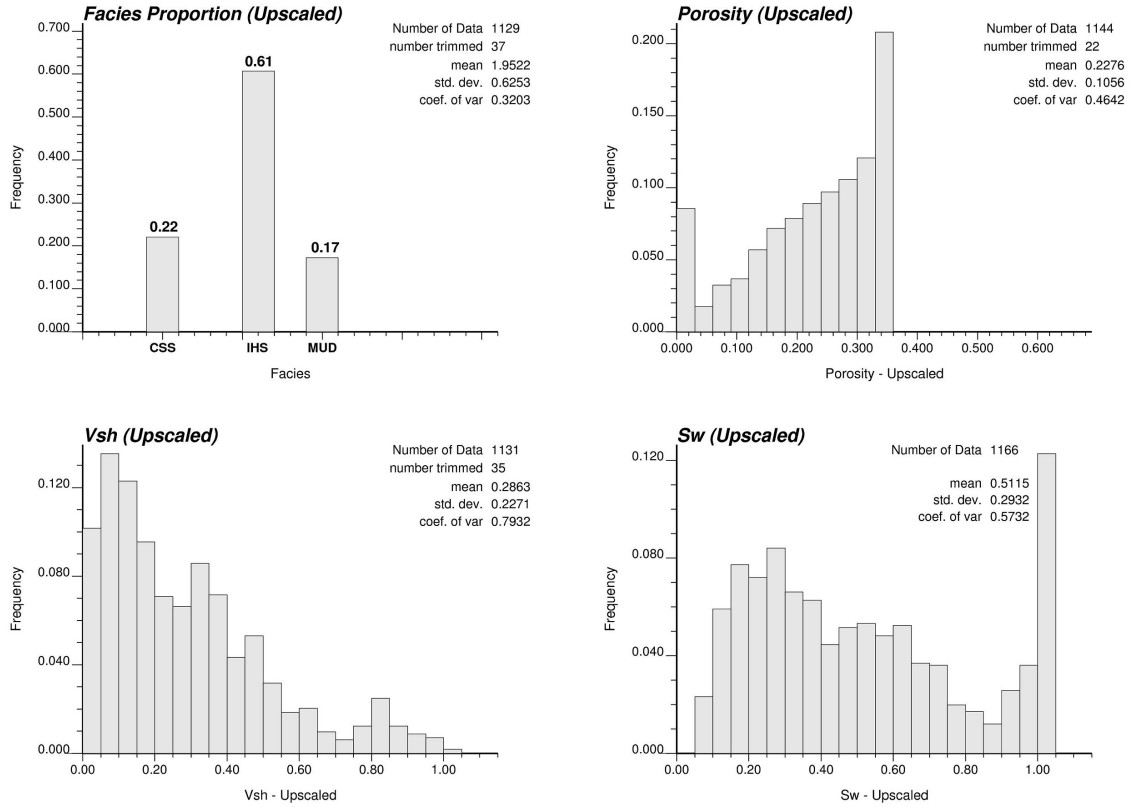

Figure 6.8: Global histograms of facies, porosity, Vsh, and Sw.

geological features such as point bars especially for the grid-free modelling purpose.

6.8.1 Large Scale Facies Modelling

The `SISIM` program of `GSLIB` was used to generate a large scale conditional indicator simulation realization. Upscaled facies data and indicator variogram models were used. Figure 6.13 shows 3D view of the SIS realization.

The program `IHSSIM` was used to generate large scale conditional grid-free realization. Parameters for the `IHSSIM` program were selected based on the previous studies in the McMurray Formation (Mossop and Flach, 1983; Crerar and Arnott, 2007) and the geological interpretations presented earlier in this

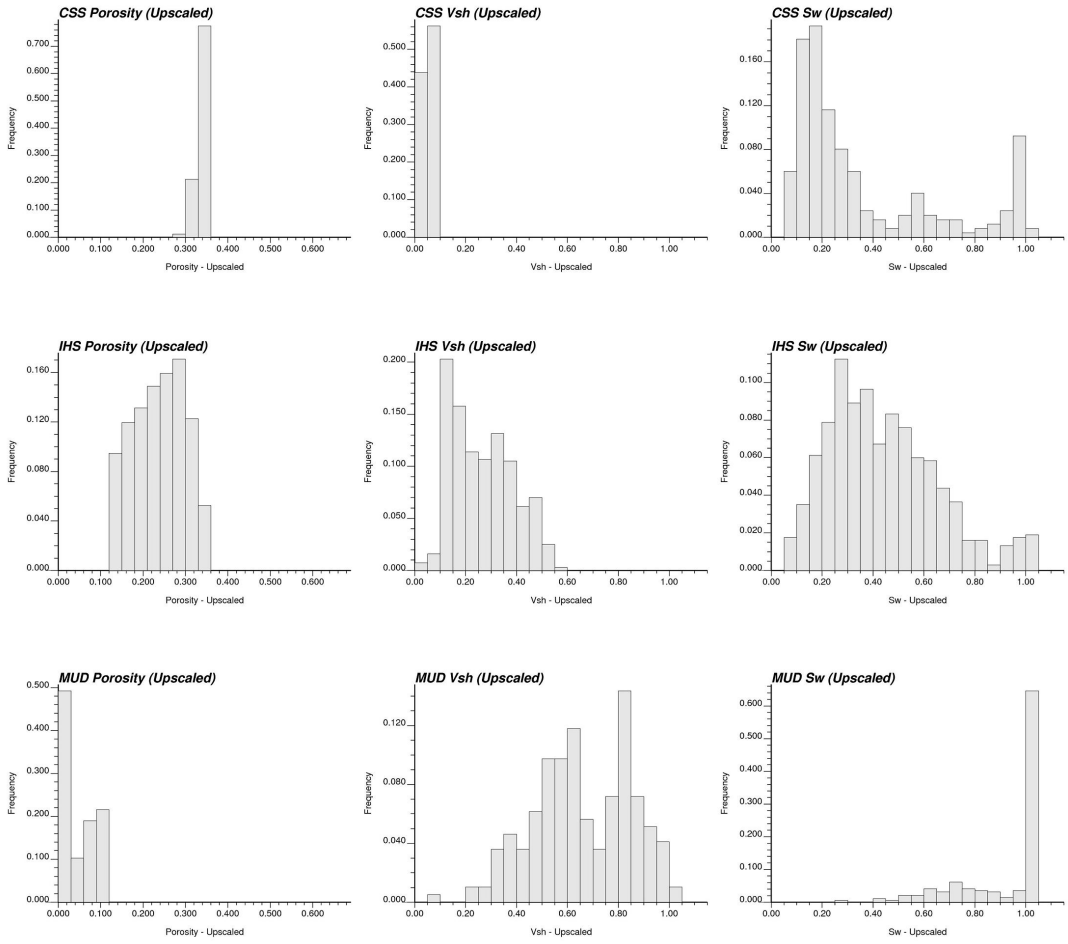

Figure 6.9: By-facies histograms of porosity, Sw, and Vsh in CSS(top), IHS(middle), and mud (bottom).

chapter. Table 6.3 summarizes these parameters. High standard deviation value was considered for most of the parameters to make it easier for the program to select object for the conditioning.

For grid-free conditioning, facies data has been converted to the intervals. Only IHS and Mud facies were considered as conditioning data and CSS was assumed as the background facies. IHS was considered as PBS element and mud was considered as CHF element. Intervals with more than $4\,m$ mud thickness were considered as conditioning data for channel fill element (CHF). IHS

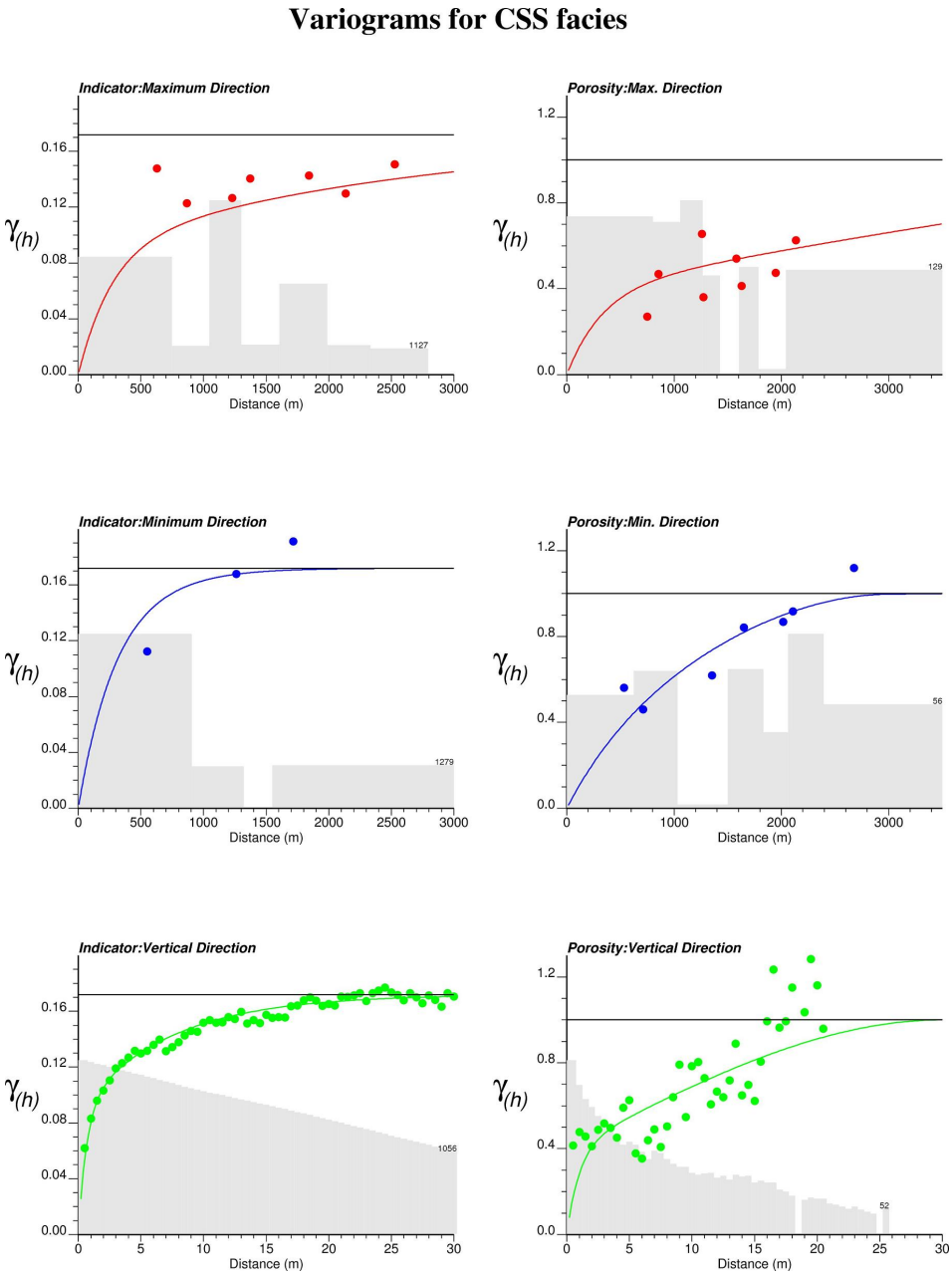

Figure 6.10: Experimental variogram (bullet) and variogram model (solid line) for CSS facies (left) and porosity within CSS facies(right). The red color refers to the maximum direction, the blue refers to the minimum direction, and the green refers to the vertical direction. Gray bars show the number of pairs for each lag separation distance.

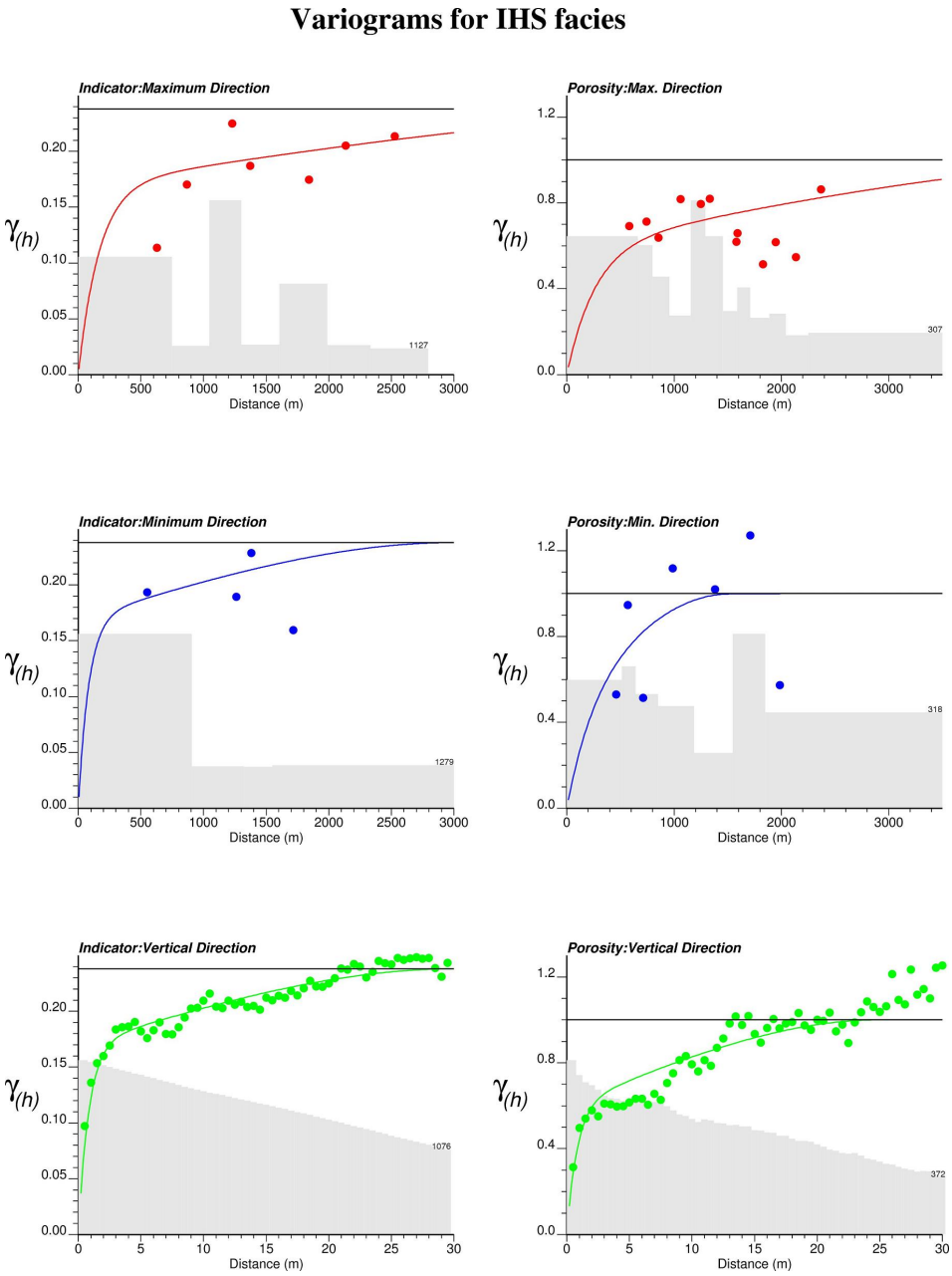

Figure 6.11: Experimental variogram (bullet) and variogram model (solid line) for IHS facies (left) and porosity within IHS facies(right). The red color refers to the maximum direction, the blue refers to the minimum direction, and the green refers to the vertical direction. Gray bars show the number of pairs for each lag separation distance.

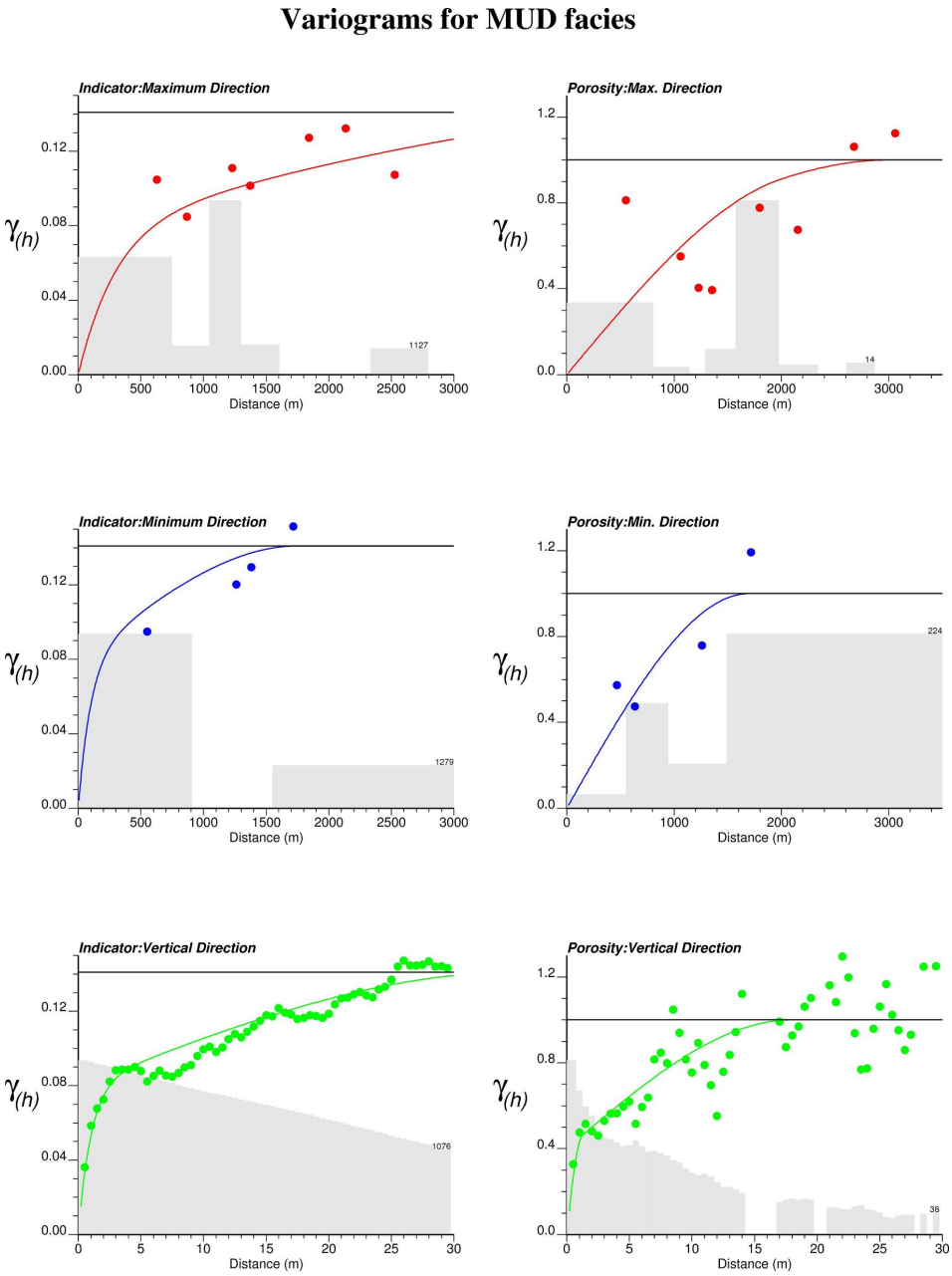

Figure 6.12: Experimental variogram (bullet) and variogram model (solid line) for MUD facies (left) and porosity within MUD facies(right). The red color refers to the maximum direction, the blue refers to the minimum direction, and the green refers to the vertical direction. Gray bars show the number of pairs for each lag separation distance.

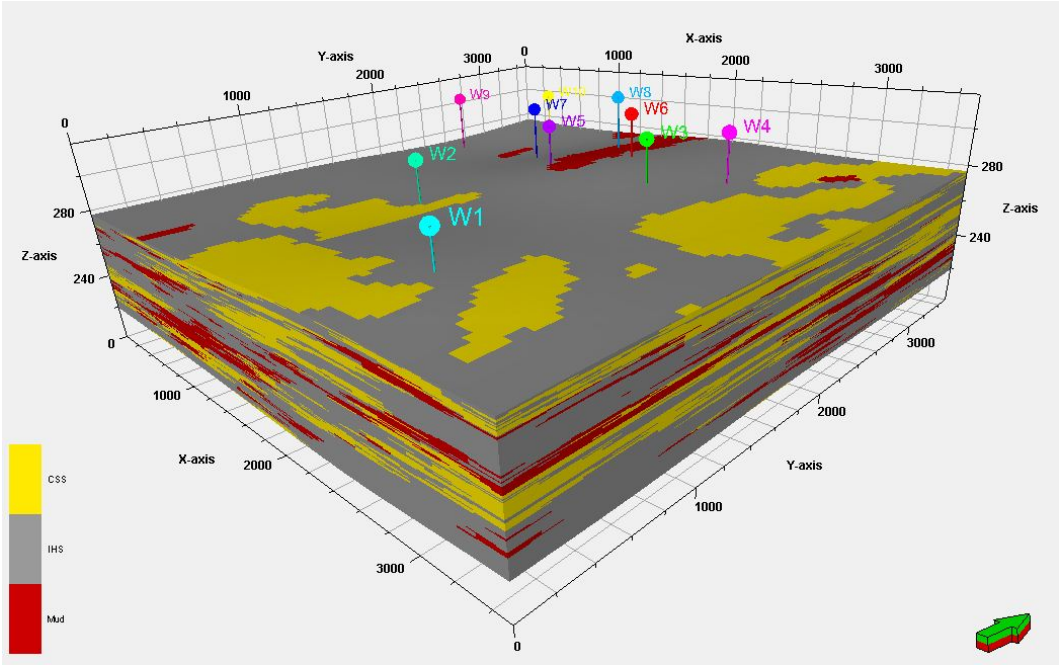

Figure 6.13: 3D view of conditional facies models generated with SIS technique for the study area. Model is exaggerated 10 times in the vertical direction.

intervals greater than 30 m thickness were also divided into sub intervals. The data set for grid-free conditioning contains 51 facies intervals including 42 IHS intervals and 9 mud intervals.

Conditioning the grid-free model to the centimeter scale shale drapes was not part of this work. Shale drapes were randomly populated within the IHS facies based on the `IHSSIM` input parameters. The frequency of shale drapes was selected so that more shally IHS were populated at the top and bottom of the model. Five aggradational levels were considered. The elevation of these five levels selected based on the conditioning facies data. Among the 51 facies intervals, only one interval was not matched. The computation time for conditional grid-free simulation for this data set was less than a minute on a 2.33GHz machine.

The grid-free model was rasterized to the grid specification mentioned above. The `IHSRAST` program was used for rasterization. Since the main purpose of the

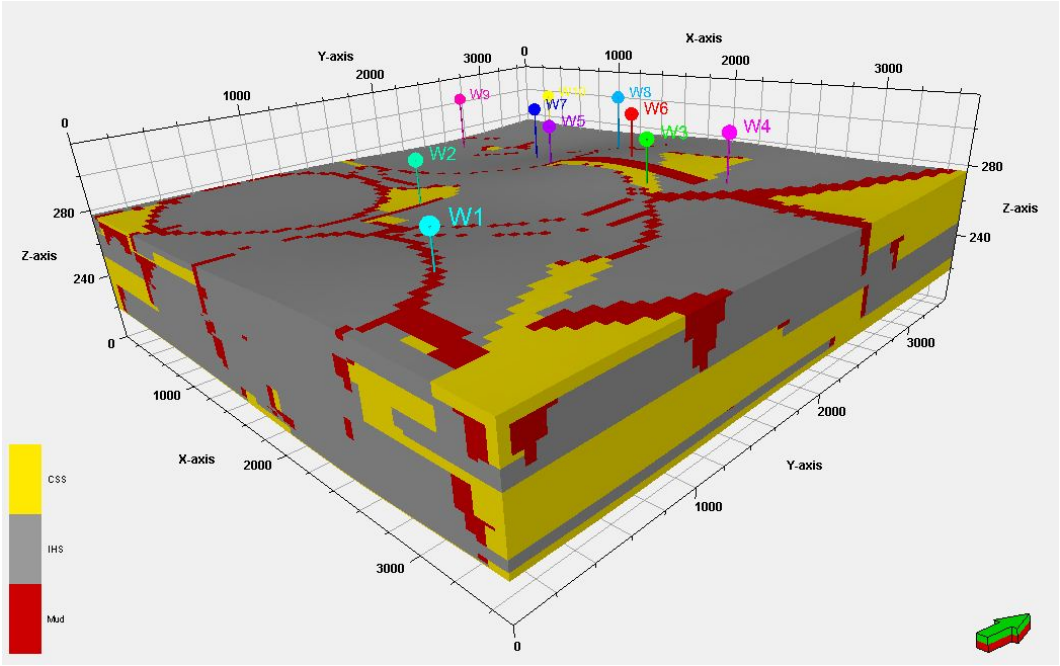

Figure 6.14: 3D view of conditional facies models generated with grid-free technique for the study area. Model is exaggerated 10 times in the vertical direction.

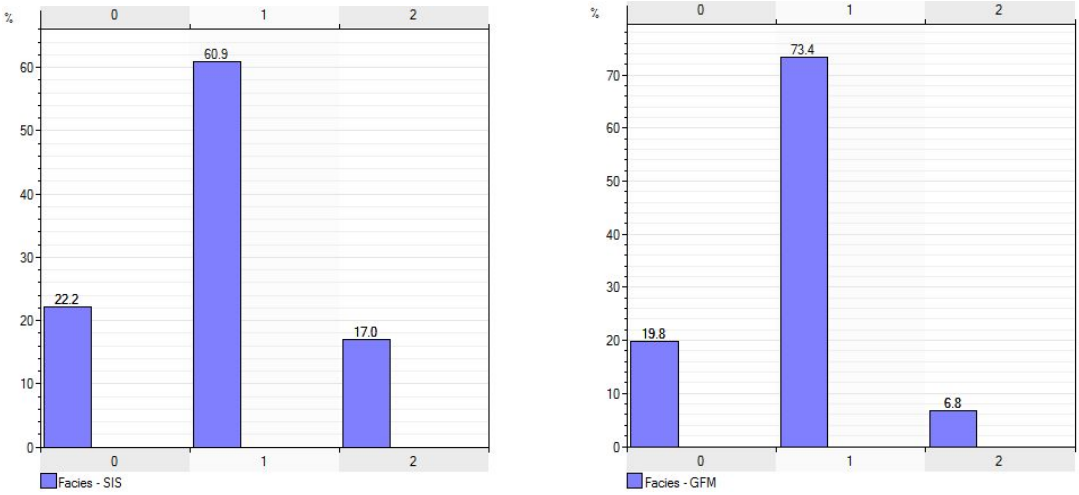

Figure 6.15: Histograms of large scale facies model generated with SIS (left) and grid-free method (right). The facies code 0 represents CSS, 1 represents IHS, and 2 represents mud facies.

Table 6.3: Parameters that were used in the `IHSSIM` program to generate grid-free facies model of the McMurray Formation.

Parameter	**Value**	
	Mean	Std. dev.
Channel Azimuth Angle	$-45°$	25
IHS Length	$1200\,m$	$100\,m$
IHS Width	$1300\,m$	$200\,m$
IHS Thickness	$15\,m$	$5.5\,m$
IHS Dip Angle	$15°$	1

large scale modelling was to capture the large scale geological features such as point bars, rasterization of shale drapes was not considered for this step of the modelling. Note that the shale drapes, that were simulated in the previous step, are stored in the grid-free model and will be rasterized in the pad scale modelling step (next section). Figure 6.14 shows a 3D view of rasterized grid-free model.

Histograms of the proportions for both the SIS-based and the grid-free based facies models are shown in Figure 6.15. The facies model generated with the SIS technique reproduced the input distribution but did not reproduce the conceptual geological geometries of facies associations in the McMurray Formation. On the other hand, the grid-free model reproduced geometries of architectural elements in the McMurray Formation, but did not reproduce the input facies data distribution as closely. The proportion of the CSS facies is 19.8% instead of 22%. The IHS facies proportion is higher and the mud facies proportion is lower than the conditioning data. There are some reasons for this. First of all there is no direct control on the facies proportion in the grid-free facies modelling algorithm. Secondly, shale drapes were not added into the grid-free model in this stage, so it is expected to get lower IHS and higher mud facies proportion after simulating shale drapes inside IHS facies.

6.8.2 Pad Scale Modelling

A rectangular area of $700\,m$ by $900\,m$ was selected as a drainage area for the SAGD thermal simulation. Figure 6.16 shows the location of the pad imposed on top of the two facies realizations generated in previous steps. In general, several factors such as reservoir quality, oil-in-place, thief zones, structural surfaces, and surface facilities may be considered in the SAGD pad placement (Kumar and Deutsch, 2010). In this study, the pad was placed in a high reservoir quality area that was detected based on the porosity trend map (Figure 6.4).

As mentioned earlier, flow simulation will be used as a transfer function to evaluate the SIS-based and the grid-free based realizations. In order to avoid the effect of upscaling on the comparison study, pad-scale models were generated directly on the flow simulation grids. In general, flow simulation grid cells are larger than what is used in the geostatistical modelling. For this study, grid cells with size of $2\,m$ (Easting) by $50\,m$ (Northing) by $0.5\,m$ (vertical) were considered. This results in 350 by 18 by 120 cells with total of $756,000$ cells. Similar to the large scale modelling, the grid is generated relative to the top McMurray Surface. This grid was chosen based on the common practices in the SAGD flow simulation (Butler et al., 1994; Butler, 1994; McLennan and Deutsch, 2004; Gates and Chakrabarty, 2006). It has been shown that the cell size along the horizontal well direction (in this case, Northing) does not have significant impact on the results of thermal flow simulation (Shin et al., 2012) therefore, choosing a larger grid along horizontal well direction will reduce the flow simulation run time.

An indicator simulation realization for the pad area was generated in the same way as the large scale modelling step. All the well data were used for the pad modelling. The large scale gird-free facies model was re-rasterized at the pad scale grid. This time shale drapes were rasterized within the IHS facies. The computational time for rasterization of the pad was around 30 minutes. Figure 6.18 shows both SIS and grid-free facies models at the pad scale.

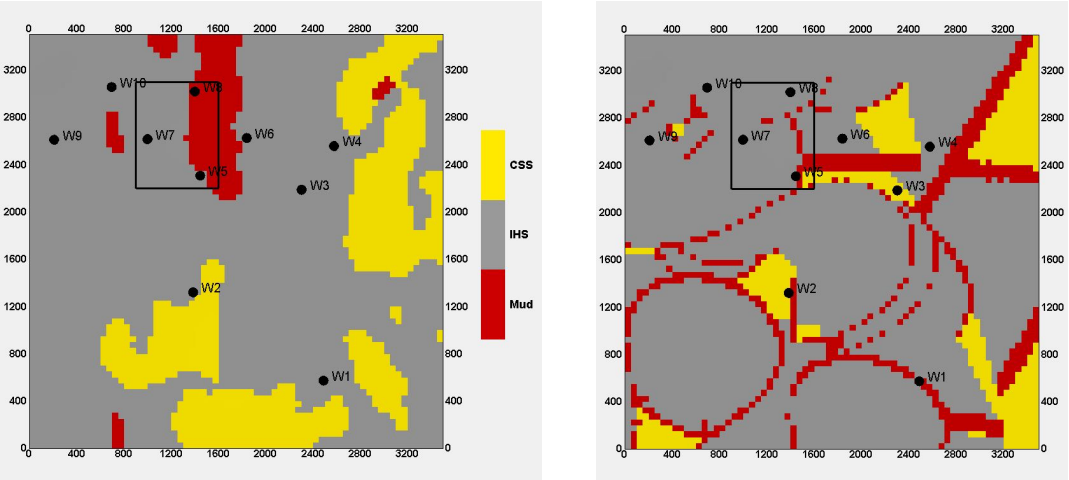

Figure 6.16: Location of SAGD pad imposed on top of SIS (left) and grid-free (right) models.

To compare the two facies realizations, histograms of both models were generated. Figure 6.17 shows both histograms. Similar to the large scale modelling, the SIS-generated facies model reproduced the conditioning data facies proportions. The grid-free model also reproduced the proportions with less than 10% error. Also a well section through well 5, 7, and 8 was generated to compare two models at the well locations (Figure 6.19). The well section shows the original facies data that was used in both SIS and grid-free modelling (left track), extracted SIS realization at the well locations (middle track), and extracted grid-free model at the well locations (right track). A visual inspection of 3D models and the well section reveals that, the SIS realization reproduced the original facies data at $0.5\,m$ scale and the grid-free model reproduced the conditioning facies intervals and also the geometry of the IHS facies association at large scale and small scale.

6.9 Property Modelling

Reservoir property models such as porosity, permeability, and saturations are required for the flow simulation study. Sequential Gaussian simulation (SGS)

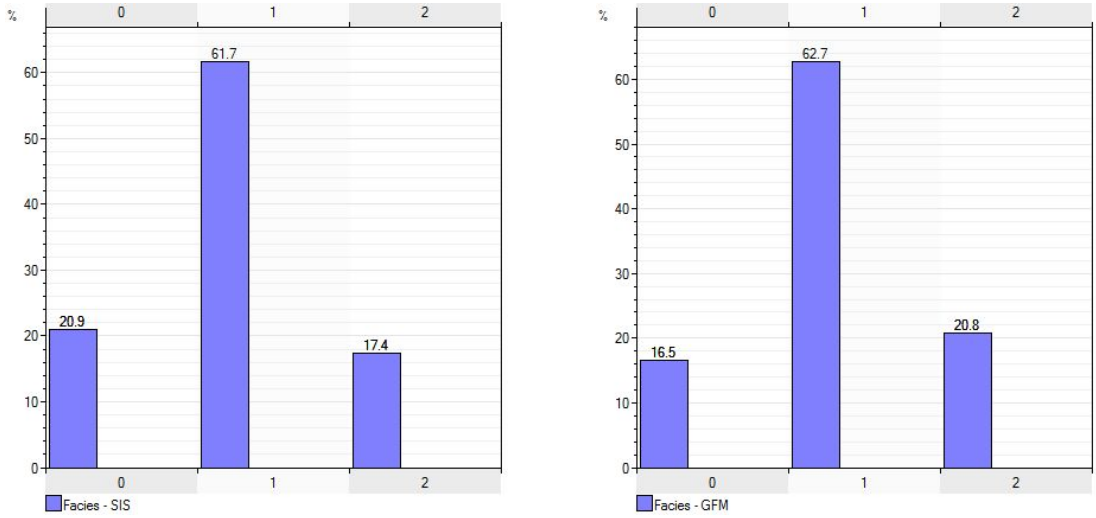

Figure 6.17: Histograms of pad scale facies model generated with SIS (left) and grid-free method (right). zero represents CSS, one represents IHS and two represents mud facies.

was applied to generate porosity models at the pad scale. The program `SGSIM` from the `GSLIB` was used for this simulation. A porosity realization was generated for each facies. Well data and by-facies variogram models were used for the simulation. By-facies porosity models were combined using the SIS facies and grid-free models. So two realizations of porosity, each related to one facies model, were generated. Figure 6.20 shows a 3D view of both models. These two realizations are similar in terms of global statistics (mean and standard deviation) however, since they were conditioned to the facies models, there are differences in spatial distribution of porosity values. For example, the grid-free based porosity model shows area of low porosity around well 7 while the SIS-based porosity model shows high porosity values in the same area.

Since there was no permeability data available for this study, synthetic permeability models were generated using the porosity realizations. In order to do that, a porosity versus permeability relationship was required. Only one correlation was considered for all facies because facies was already classified based on the porosity cutoffs. Deutsch (2010) provided a porosity versus horizontal

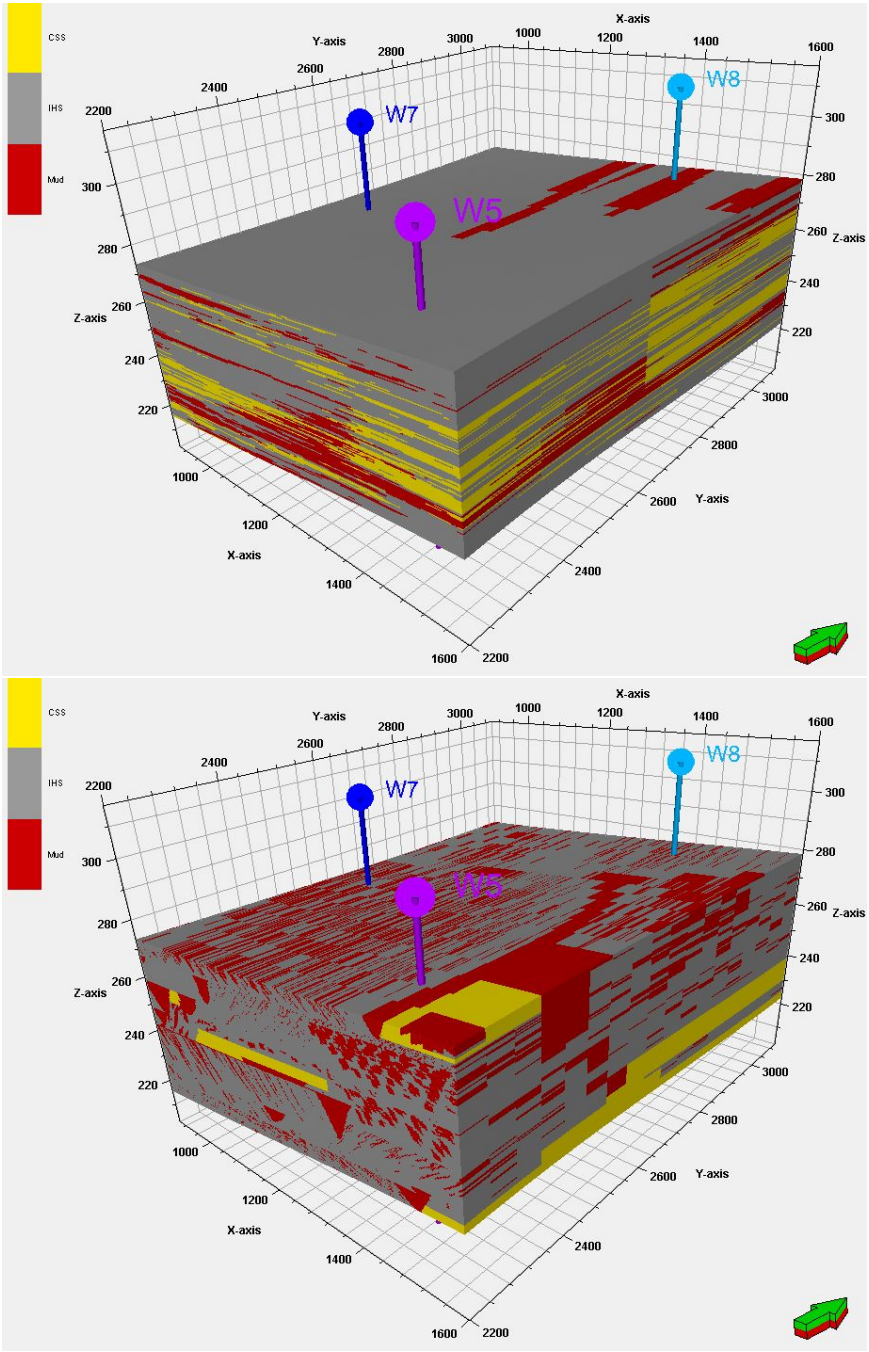

Figure 6.18: 3D view of conditional facies models generated with SIS (top) and the grid-free technique (bottom) at the pad scale. Model is exaggerated 5 times in the vertical direction.

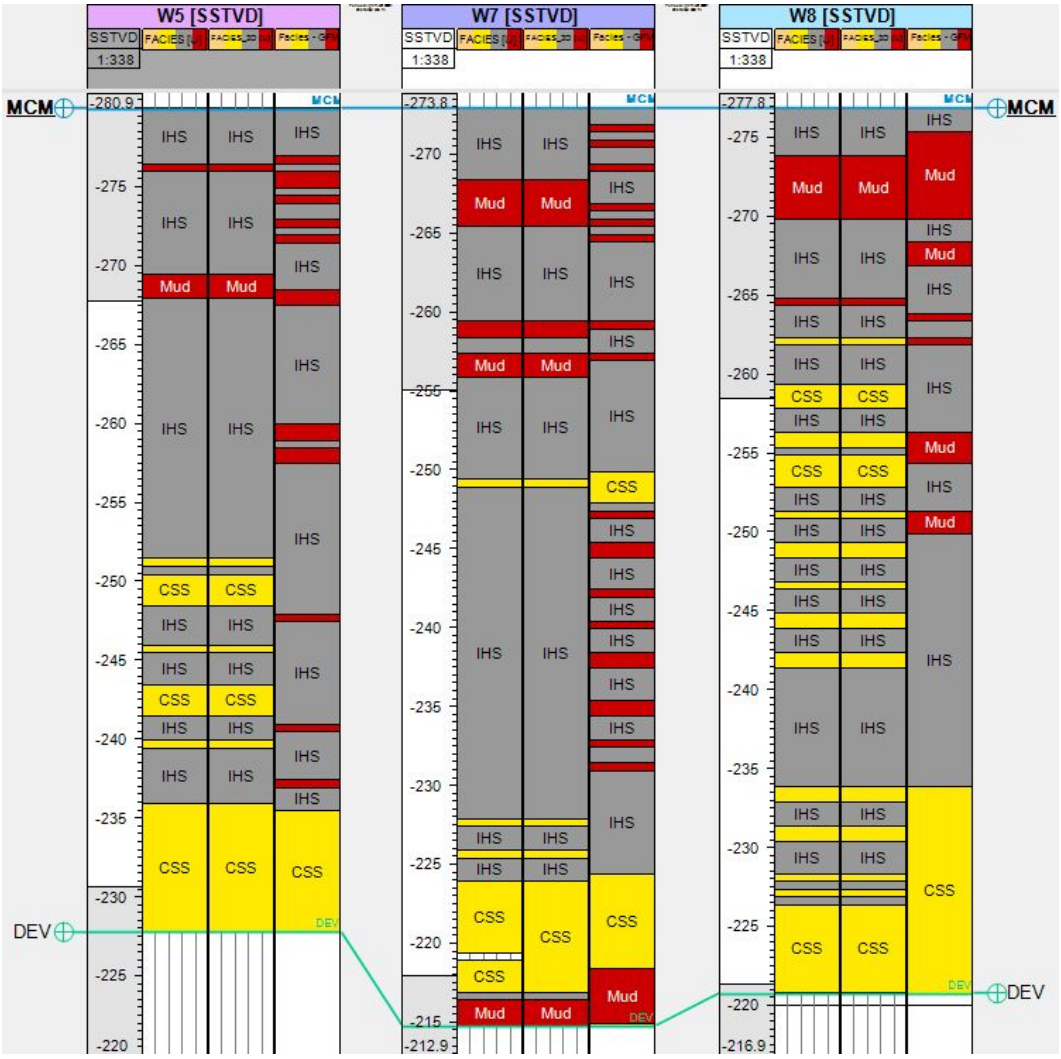

Figure 6.19: Well cross section of well 5, 7, and 8 showing facies data reproduction for two facies realizations. For each well the left track is the original facies data, the middle is the SIS and the right track is the grid-free model.

permeability relationship for the McMurray Formation:

$$log(k_h) = a_0 + a_1\phi + a_2\left(1 - e^{(\frac{-3\phi}{\phi c})}\right) \tag{6.1}$$

where $a_0 = -2.0$, $a_1 = 3.67$, $a_2 = 4.15$, and $\phi_c = 0.35$. This equation was used to generate horizontal permeability models for the McMurray Formation. In order to avoid the unrealistic linear relationship between permeability versus

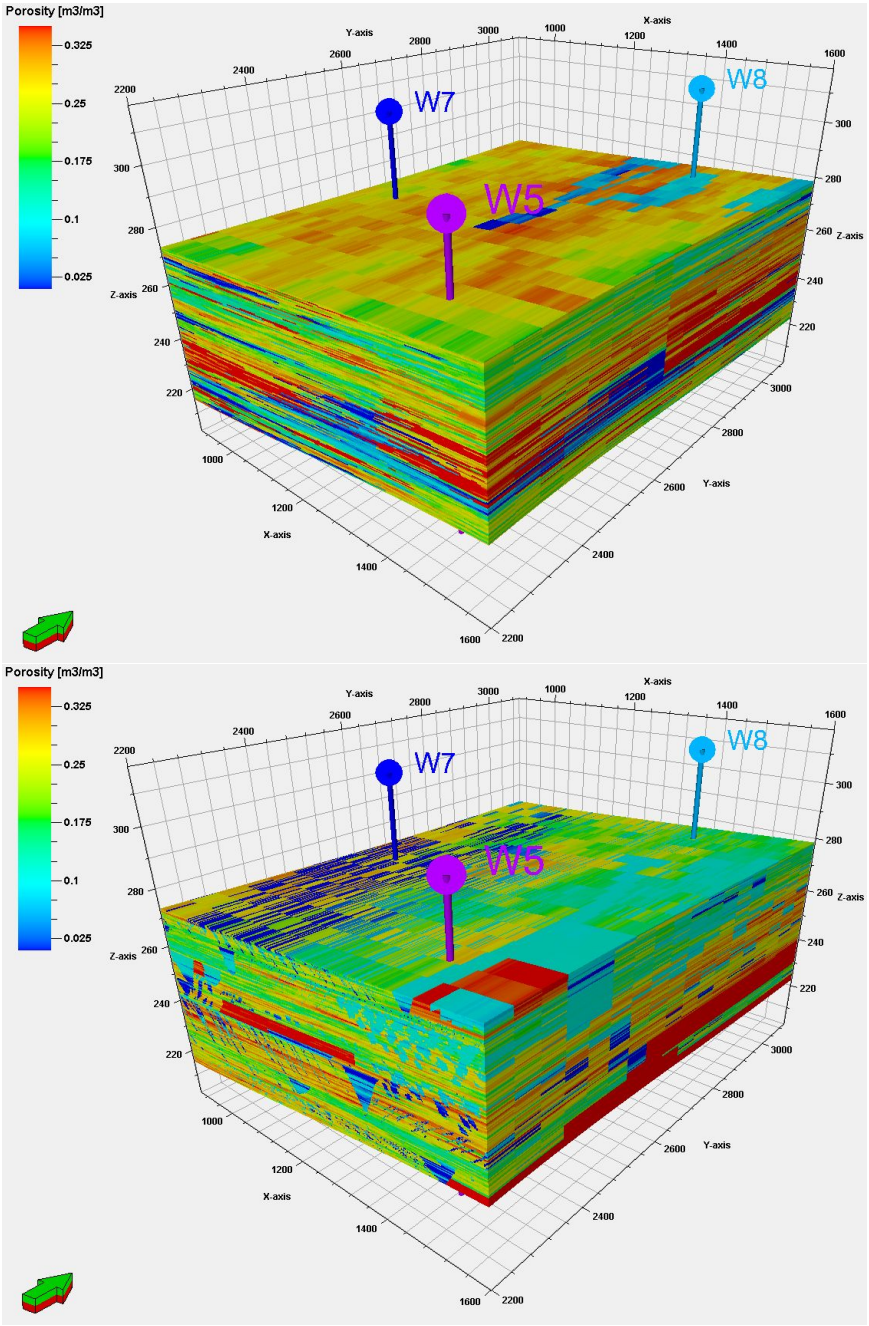

Figure 6.20: 3D view of by-facies porosity models generated for SIS (top) and the grid-free model (bottom) at the pad scale. Model is exaggerated 5 times in the vertical direction.

porosity and to account for the statistical variation of permeability, a cloud transformation technique was applied (Kolbjørnsen and Abrahamsen, 2005). In this technique, the variability of permeability was modelled with a normal distribution with mean of 1 and a standard deviation defined as a function of porosity:

$$log(k_h^*) = log(k_h^f) \cdot Normal(1, 0.2 \cdot \phi) \tag{6.2}$$

where k_h^* is the estimated permeability and k_h^f is permeability calculated with Equation 6.1. Figure 6.21 shows the cross plot of porosity versus horizontal permeability values for the grid-free and the SIS-based models. As shown in the plot, a higher permeability variation was generated at higher permeability values. This accounts for the proportional effect of the permeability model (Joumel and Huijbregts, 1978).

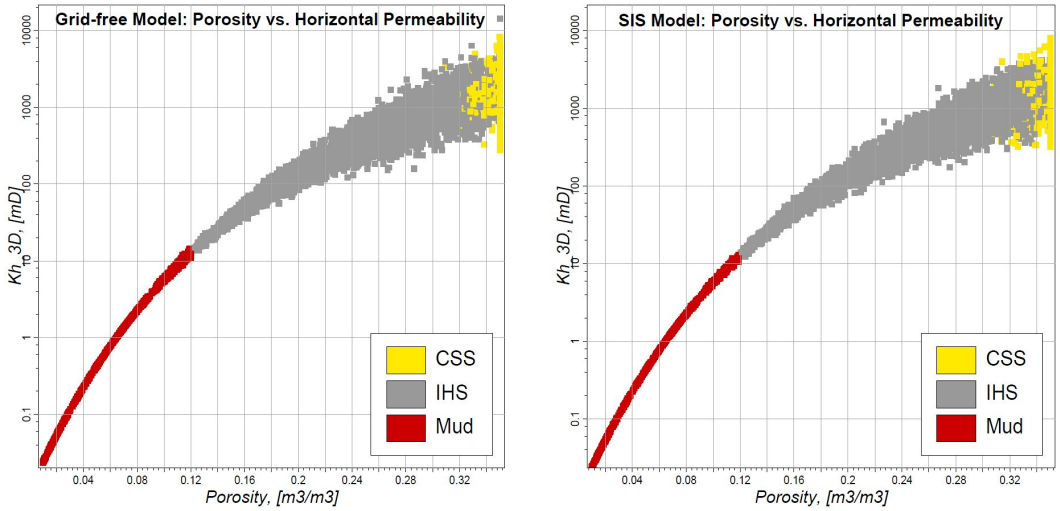

Figure 6.21: The cross plot of porosity versus horizontal permeability for the grid-free based model (left) and the SIS-based model (right).

Vertical to horizontal permeability ratios of 0.1 , 0.5 , and 0.8 were considered for mud, IHS, and clean sand facies, respectively. These ratios were picked from the cross plot provided in Deutsch (2010). Vertical permeability models were generated by multiplying these ratios to horizontal permeability models.

6.10 Flow Simulation

SAGD thermal simulations were run on the SIS and grid-free based models using CMG STARS^{TM} thermal simulator. For simplicity and reducing the computational time, the simulation was run on a 2D slice that was extracted from each generated models. The 2D slice was picked along the $x - z$ direction around well $W8$.

Four horizontal well pairs were placed at the bottom of the reservoir layer. Well pairs are $140\,m$ apart from each other. The injector (top) and producer (bottom) wells were placed $5\,m$ apart from each other (Butler et al., 1994; Butler, 1994).

In order to have similar amount of oil-in-place for both SIS and GFM based models, a constant initial oil saturation of 0.8 was applied to CSS and IHS facies. Oil saturation for mud facies was set to zero. This resulted in $2.52 \times 10^6\,bbl$ of oil-in-place for the grid-free model and 2.48×10^6 for the SIS model. The difference is small enough to be neglected for the comparison study. Figure 6.22 shows initial oil saturation maps and location of four well pairs for the SIS and the grid-free models.

Thermal simulation parameters used for this simulation study were gathered from the literature (Kisman and Yeung, 1995; Gates and Chakrabarty, 2006; Fenik, 2010). Table 6.4 summarizes these parameters. A heavy oil model with two components of oil and water was considered. Note that, no top gas or bottom aquifer was considered in this study. Thermal flow simulation was run for 5040 days (about 14 years). All the simulation parameters and initial and boundary conditions were set the same for both cases.

6.11 Comparison of Results

Oil saturation maps are shown in time lapses of 120, 720, 2160, 3600, and 5040 days in Figure 6.23 and Figure 6.24. Comparing two cases visually shows

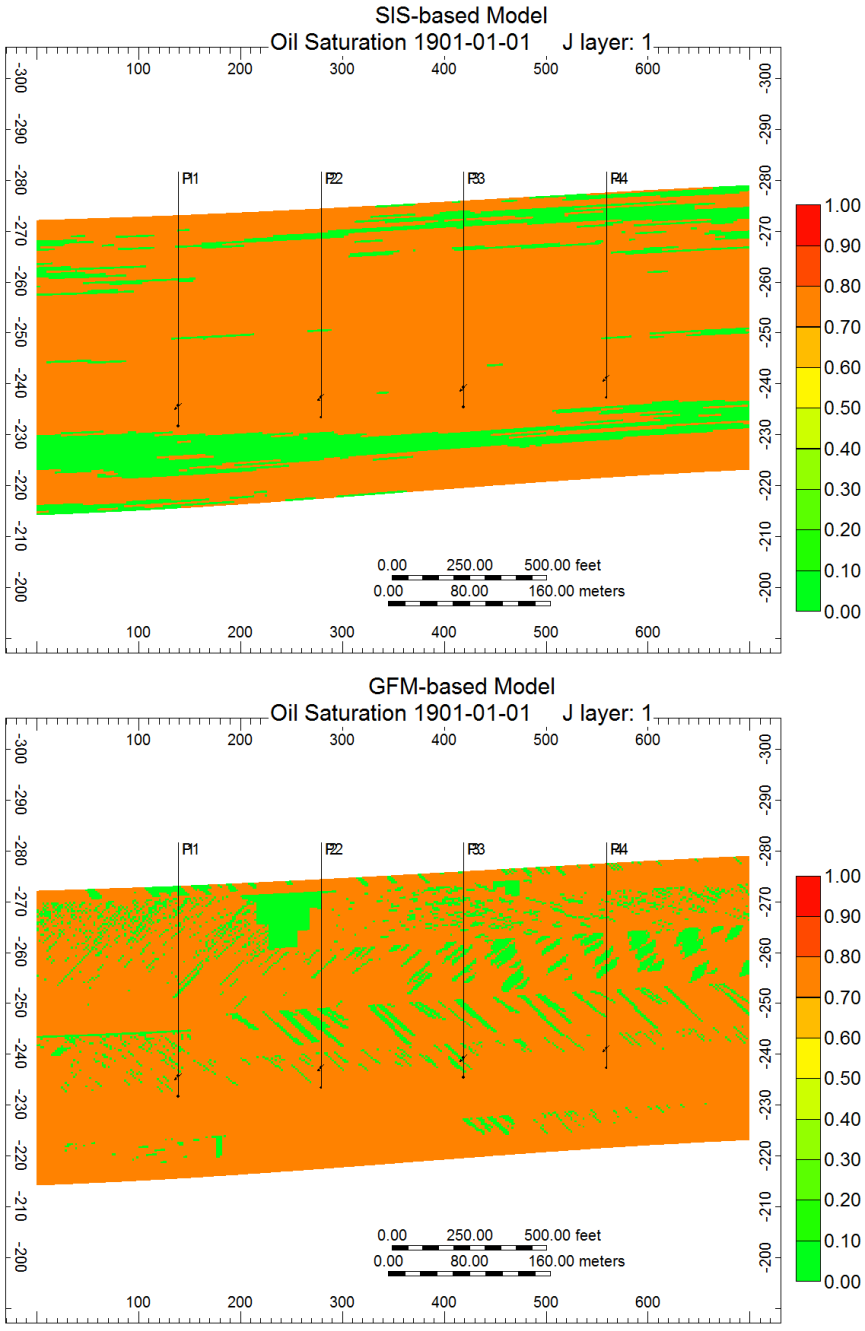

Figure 6.22: Initial oil saturation maps for the SIS model (top) and the grid-free model (bottom).

Table 6.4: Thermal simulation parameters used for SAGD simulations of the grid-free and the SIS based models.

Parameter	**Value**
Initial Reservoir Pressure, kPa	3000
Initial Reservoir Temperature, $^{\circ}C$	12
Rock Compressibility (all facies), kPa^{-1}	9.6×10^{-6}
Volumetric Heat Capacity (all facies), $\text{kJ}/(\text{m}^3\ ^{\circ}C)$	2347
Rock Thermal Conductivity (all facies), $\text{kJ}/(\text{m day}^{\circ}C)$	660
Bitumen Thermal Conductivity, $\text{kJ}/(\text{m day}^{\circ}C)$	11.5
Water Thermal Conductivity, $\text{kJ}/(\text{m day}^{\circ}C)$	53.5
Gas Thermal Conductivity, $\text{kJ}/(\text{m day}^{\circ}C)$	0.14
Bitumen Viscosity at $12^{\circ}C$, cp	2.0×10^5
Steam Temperature, $^{\circ}C$	224

that steam chamber has grown more evenly in the SIS based model after 5040 days. This has been confirmed by comparing the steam chamber volume for both cases; $69,825\,m^3$ for the SIS case and $29,254\,m^3$ for the grid-free case. As a result, the SIS model produced more oil compared to the grid-free model. The cumulative produced oil was $622,808\,bbl$ for the SIS model and $393,732\,bbl$ for the grid-free model (See Figure 6.25). The field cumulative steam oil ratio (CSOR) and the instantaneous steam oil ratio for both cases are also shown in Figure 6.25. The grid-free model has higher CSOR (5.35) as opposed to the SIS model (4.22).

These difference in results of SAGD simulation for the SIS and the grid-free model are mainly due to the distribution of mud facies (shale drapes). This has been shown in the oil saturation maps in Figures 6.23 and 6.24. In the grid-free model, shale drapes placed above the well pairs significantly reduced the steam

chamber growth and resulted lower oil production and higher CSOR. On the other hand, in the SIS case, less shale barriers existed above well pairs and this resulted in better steam chamber growth and more oil production.

6.12 Concluding Remarks

A comparative case study was performed on a real data set in the McMurray Formation. SIS and grid-free facies models were generated and processed through a thermal flow simulation transfer function. Although this illustration may not be general for all cases, some points may be concluded.

- The distribution of shale drapes has significant effect in the performance of SAGD. Shale drapes above well pairs act as flow barriers and reduce productivity of SAGD. Proper modelling of shale barriers is required for accurate flow performance prediction.
- SIS facies modelling may not properly reproduce complex geological heterogeneity of the McMurray Formation and as a result the SAGD performance will be overestimated in the thermal flow simulation.
- Grid-free facies modelling technique reproduces geological heterogeneity of the McMurray Formation. However, a good understanding of reservoir geology is required to properly choose the input parameters.

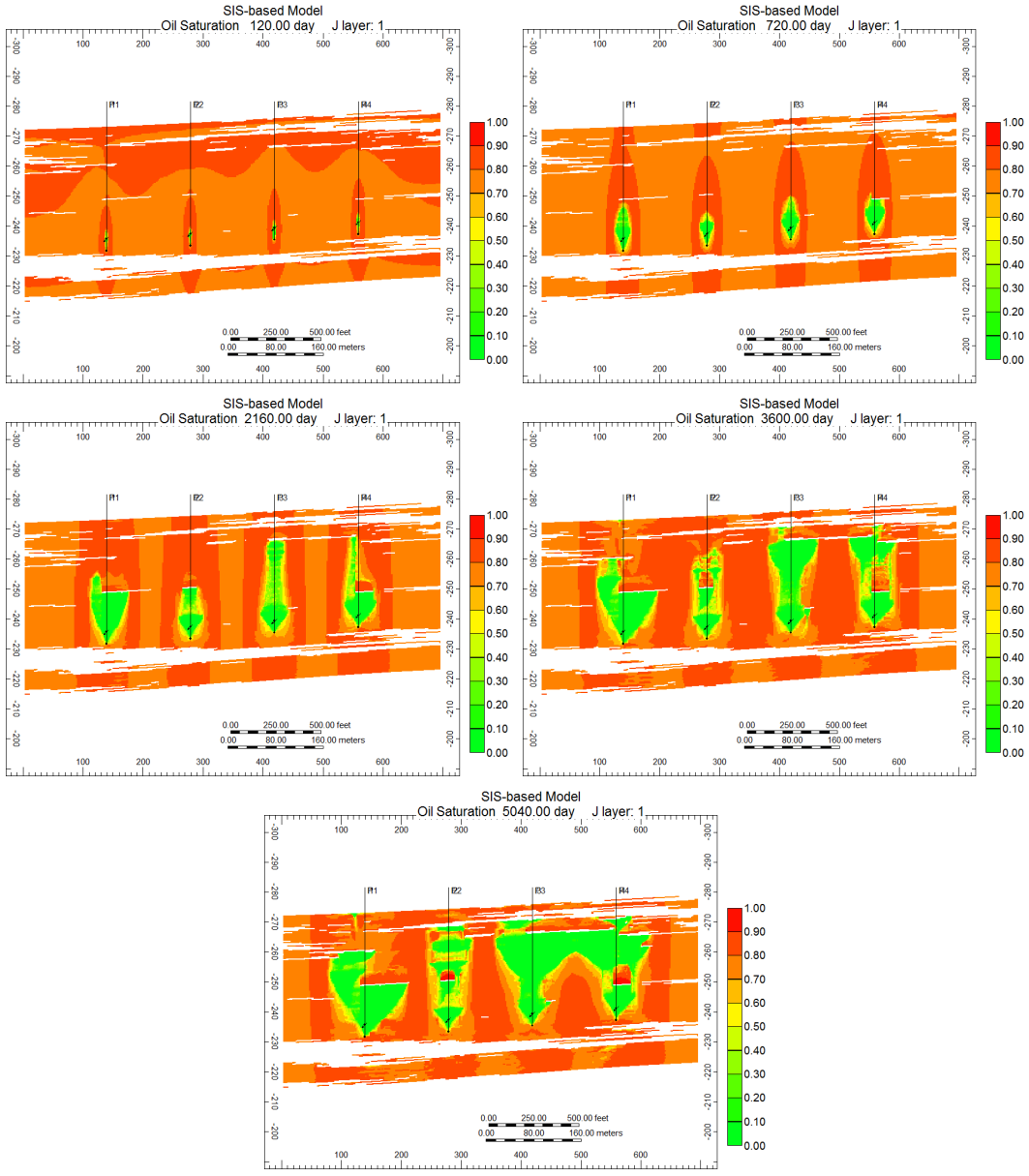

Figure 6.23: Oil saturation map for SIS-based model at different time steps; 120 days (top left), 720 days (top right), 2160 days (middle left), 3600 days (middle right), and 5040 days (bottom). The MUD facies is shown in white color.

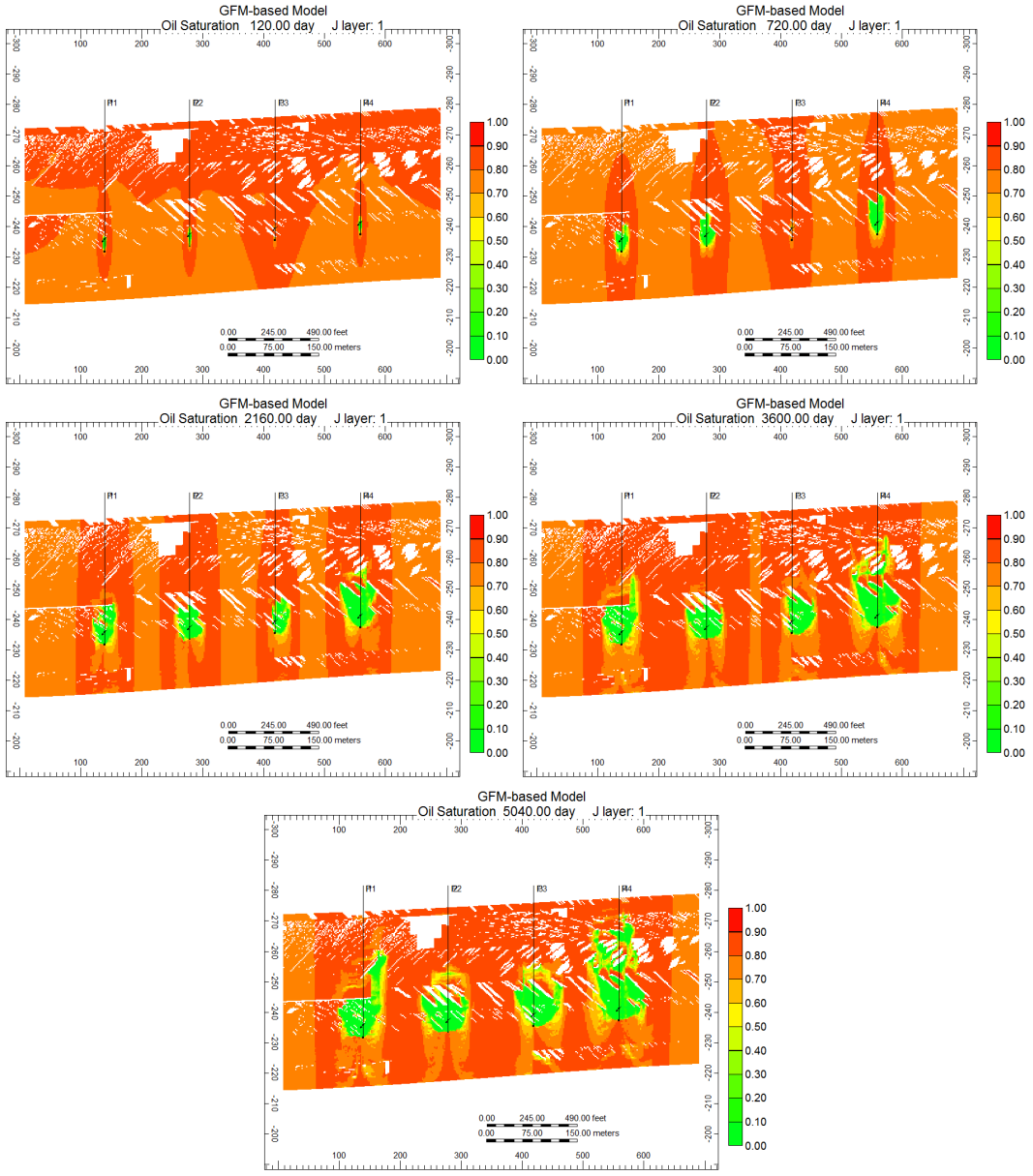

Figure 6.24: Oil saturation map for grid-free based model at different time steps; 120 days (top left), 720 days (top right), 2160 days (middle left), 3600 days (middle right), and 5040 days (bottom). The MUD facies is shown in white color.

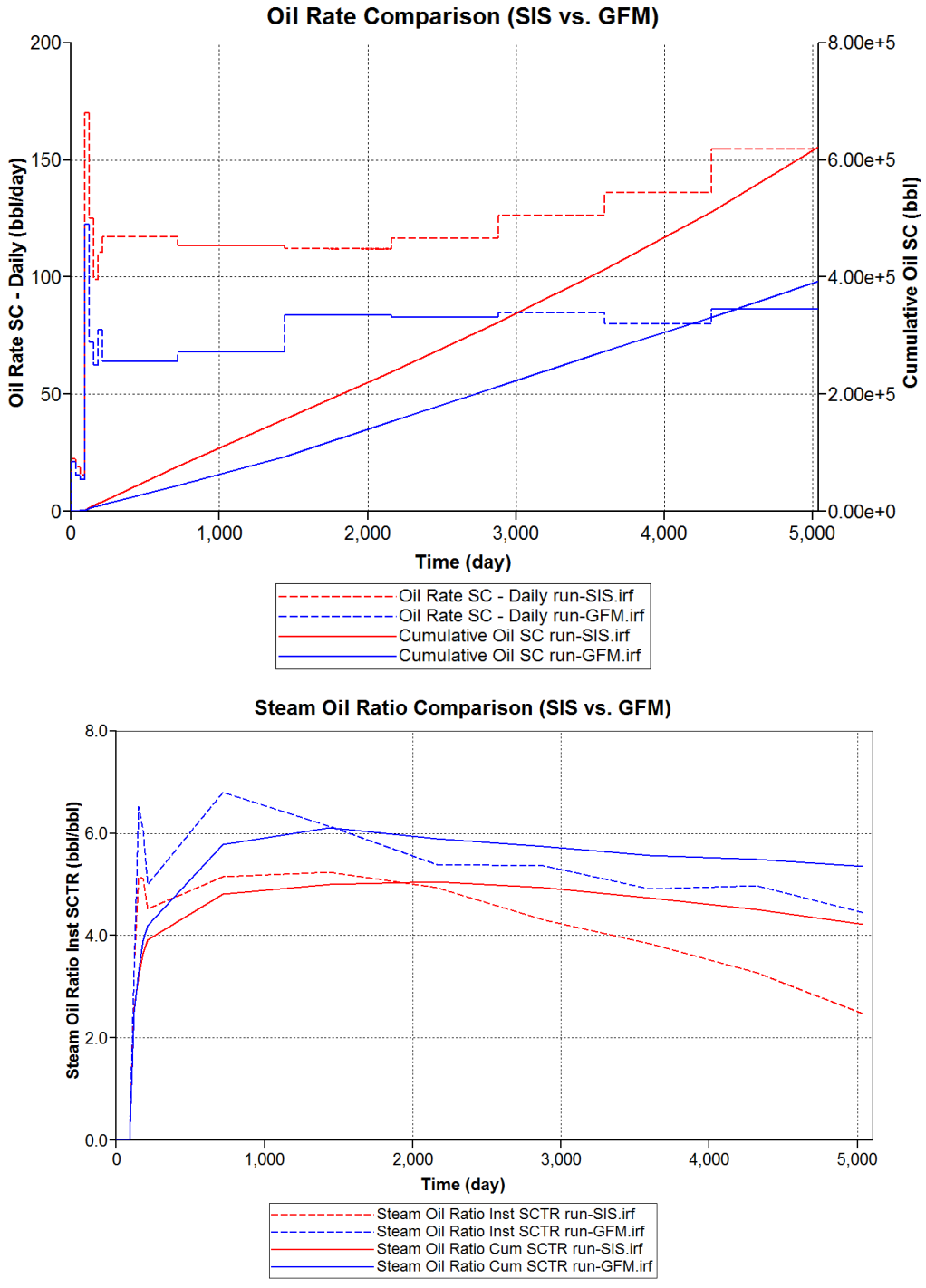

Figure 6.25: Comparison of thermal flow simulation performance for the SIS (red) and the grid-free models (blue). Daily oil rate and cumulative produced oil(top), and instantaneous and cumulative steam oil ratio comparison graph (bottom).

Chapter 7

Concluding Remarks

Geological conceptual models contain important information about the depositional processes and geometry of geological architectural elements. Conventional geostatistical facies modelling techniques incompletely integrate this geological information. Object-based techniques overcome this limitation by parametrizing geological bodies with mathematical functions and stochastically populating them in the model.

Generally, due to the uniqueness of architectural elements in each depositional environment, the object-based techniques are customized for a specific geological setting. In the fluvial-estuarine system of the McMurray Formation, a number of geological architectural elements have been detected. IHS facies association is the most common elements in the McMurray Formation that is deposited as part of kilometre scale channels and contains centimetre scale geological features.

In this dissertation, methodologies have been developed to model the geometry of multi-scale geological architectural elements in the McMurray Formation.

7.1 Summary of Contributions

There are number of contributions of this dissertation; an algorithm for modelling geometry of tidal channelized system, a framework for grid-free object-

based modelling, and algorithm for grid-free object-based facies modelling of McMurray Formation, and an estuarine training image library.

7.1.1 Tidal Channel Modelling

Chapter 3 presented a methodology to create a numerical model that mimics the geometry of tidal channels. The method is an object/event based technique that enables generation of multiple realizations of tidal network channels based on the channel centreline simulation and mimicking the evolution process based on the pre-defined geological parameters.

The ESTUSIM algorithm is applicable in the modelling of tidal channels in the McMurray Formation. The required input parameters for modelling can be borrowed from the outcrops, modern analogs, and sequence stratigraphy interpretations. The static model can be used as a training image in the multipoint geostatistical methods (MPS). Conditioning of the model to well data can also be achieved with MPS techniques.

7.1.2 Grid-free Facies Modelling Framework

A framework for implementing object-based facies modelling in the grid-free mode was presented in Chapter 4. Tow main components of this framework are the simulation and the rasterization engines. These two components are generally integrated in a single component in the traditional OBM or EBM techniques leading to immediate rasterization of geo-objects and missing important information and parameters. In the grid-free framework, however, all objects are first simulated and placed in the model and then rasterized as needed.

There are many advantages for the facies modelling in the grid-free framework. First, it allows fast simulation of geological objects because rasterization of objects are not required. Second, since geo-objects are represented with mathematical functions it is possible to introduce both small scale features (such as the centimetre scale shale drapes) and large scale features (kilometre long

meandering channels) in the same model. However, in the conventional OBM the objects smaller than the modelling grid size may not be captured in the final model. They could only be represented in another model or as effective properties within the chosen grid size.

Preserving the geo-object parameters also allows the user to visualize these geometries and apply them to any gridding scheme for local grid refinements, exact down-scaling and up-scaling, and within facies trend models.

7.1.3 Grid-free Modelling of McMurray Formation

The grid-free modelling framework was extended to the estuarine environment of the McMurray Formation. The main advantage of the grid-free facies modeling is the ability to reproduce geo-objects with different scales in the same model and to interrogate and interact with these models. Geometry of centimeter- to meter-scale shale drapes in the estuarine point bar of McMurray Formation were reproduced with a detail parameterization in the grid-free mode.

The conditional algorithm was very fast for the examples presented in this dissertation. However, more mismatches and more computational time are expected when closely spaced data set is used.

7.1.4 Estuarine Training Image Library

A set of 248 grid-free training images was generated based on the typical size, shape, shale intensity, and facies components of the architectural elements in the McMurray Formation. These grid-free training images can be rasterized to any grid resolution using the program that was explained in Section 5.1.2.

There are many anticipated applications for the grid-free estuarine training image library. Training images may be either used directly as a typical facies model of the McMurray Formation or they can be used in a multiple-point geostatistical technique. Also the variety of training images enables practitioners to perform scenario-based uncertainty analysis to improve decision making.

7.2 Future Work

There are number of research ideas that may be considered to improve the methodologies presented in this dissertation.

Conditioning the tidal channel modelling algorithm to well data and trend models can be considered as a future work. Also, dynamic implementation of the ESTUSIM algorithm that result in generation of inclined heterolithic strata would be an additional improvement to the methodology. More research is required to gather information about the geological events and processes in the estuarine systems and to numerically model those processes. Two simple possible algorithms for this purpose were suggested in Chapter 3.

The grid-free framework can be applied to any object-based modelling algorithm. One challenge in implementation of the grid-free modelling is the 3D visualization of the grid-free model. Some useful tools were introduced in Section 4.1.4 however, further research in this area is required. Three-dimensional vector-based visualization of grid-free models is a future direction of research that would abandon the need to rasterize the grid-free model for visualization.

The grid-free modelling of IHS facies could be improved. The parametrization of IHS facies association can be modified to include multiple connected channel lines instead of one single straight channel line. This will generate more geologically realistic models and include large scale channel sinuosity. This would also add more flexibility in the conditioning algorithm when bypass of conditioning well is required.

The conditioning algorithm can also be modified to integrate areal and vertical trend models. Trend models, that are usually provided in gridded format, are utilized in the object-based methods to control the object placement. In the grid-free framework however, no grid system is defined. One simple approach is to transform gridded trend maps into coordinate system that is understandable for grid-free simulator.

Future improvement in the conditioning algorithm can be considered. Multi-

scale conditioning is one possible research idea in which IHS sets are honored in the large scale model and then small scale features are conditioned inside the IHS packages. Also conditioning to seismic attributes and FMI logs needs to be more investigated.

Another possible research idea is to modify the rasterization algorithm to rasterize the grid-free model to unstructured grids. Unstructured grids are utilized to accommodate more accurate flow response prediction in flow simulation. Geometrical parameters of objects that are stored in a grid-free model may be used to design the unstructured grid. Small-scale objects in the model can be rasterized to smaller cells which will result in better preservation. The unstructured grid that is designed based on the geological features may be used directly in petrophysical property modelling and flow simulation (Manchuk, 2010).

Bibliography

Allen, J. (1963). The classification of cross-stratified units, with notes on their origin. *Sedimentology*, 2(2):93–114.

Anderton, R. (1985). Clastic facies models and facies analysis. *Geological Society London Special Publications*, 18(1):31.

Babak, O., Manchuk, J. G., and Deutsch, C. V. (2013). Accounting for non-exclusivity in sequential indicator simulation of categorical variables. *Computers & Geosciences*, 51(0):118 – 128.

Bagdan, C. A. (2005). Stratigraphy, sedimentology and ichnology of the McMurray Formation; Northeastern Alberta, Canada. Master's thesis, University of Alberta.

Bailleul, J., Delhaye-Prat, V., and Parize, O. (2006). Facies analysis and architectural elements within a fluvio-estuarine sedimentary system: The lower cretaceous bituminous sandstones of the macmurray formation, alberta (canada). In *SPE Annual Technical Conference and Exhibition*, San Antonio, Texas, USA. Society of Petroleum Engineers.

Bakke, S. and Øren, P. (1997). 3-d pore-scale modelling of sandstones and flow simulations in the pore networks. *SPE Journal*, 2(2):136–149.

Barwis, J. (1978). Sedimentology of some South Carolina tidal-creek point bars, and a comparison with their fluvial counterparts. *Fluvial Sedimentology*, pages 129–160.

Boisvert, J. (2007). Mineral deposit modeling with pseudo-genetically constructed training images. M.sc. thesis, University of Alberta, Canada. 72 p.

Boisvert, J., Manchuk, J., Neufeld, C., Niven, E., and Deutsch, C. (2012). Micro-modeling for enhanced small scale porosity-permeability relationships. *Geostatistics Oslo 2012*, pages 159–171.

Brekke, H. and Evoy, R. (2004). Use of dipmeter data in the definition of the internal architecture of point bar deposits in the Athabasca Oilsands: implications for the Middle McMurray Formation in the Hangingstone area, Alberta. In *AAPG Annual Meeting 2004*.

Bridge, J. (1993). Description and interpretation of fluvial deposits: a critical perspective. *Sedimentology*, 40(4):801–810.

Butler, R. (1994). Steam-assisted gravity drainage: concept, development, performance and future. *Journal of Canadian Petroleum Technology*, 33(2).

Butler, R., Dargie, B., and of CIM., P. S. (1994). *Horizontal wells for the recovery of oil, gas and bitumen*. Petroleum Society, Canadian Institute of Mining, Metallurgy & Petroleum.

Calverley, A. (1984). *Sedimentology and geomorphology of the modern epsilon cross-stratified point bar deposits in the Athabasca upper delta plain*. Geography (1984), University of Calgary.

Capilla, J., Gómez-Hernández, J., and Sahuquillo, A. (1997). Stochastic simulation of transmissivity fields conditioning to both transmissivity and piezometric data - 2. demonstration in a synthetic aquifer. *Journal of Hydrology*, 203:175–188.

Carrigy, M. (1959). Geology of the McMurray Formation, Part III, general geology of the McMurray area. *Alberta Research Council, Memoir*, 1:130.

Cojan, I., Fouché, O., Lopéz, S., and Rivoirard, J. (2005). Process-based reservoir modelling in the example of meandering channel. *Geostatistics Banff 2004*, pages 611–619.

Crerar, E. E. (2003). Sedimentology and stratigraphic evolution of a tidally-influenced marginal-marine complex: the Lower Cretaceous McMurray Formation, Athabasca Oil Sands Deposit, northeastern Alberta. Master's thesis, University of Ottawa and the Ottawa-Carleton Geoscience Centre.

Crerar, E. E. and Arnott, R. W. C. (2007). Facies distribution and stratigraphic architecture of the Lower Cretaceous McMurray Formation, Lewis Property, northeastern Alberta. *Bulletin of Canadian Petroleum Geology*, 55(2):99–124. 10.2113/gscpgbull.55.2.99.

Dalrymple, R. W., Zaitlin, B. A., and Boyd, R. (1992). Estuarine facies models; conceptual basis and stratigraphic implications. *Journal of Sedimentary Research*, 62(6):1130–1146.

Daly, L. and Brutzman, D. (2008). X3D: extensible 3D graphics standard. In *ACM SIGGRAPH ASIA 2008 courses*, pages 1–6. ACM.

Derakhshan, S., Babak, O., and Deutsch, C. (2010). Accounting for nonexclusivity in sequential indicator simulation of categorical variables. Technical Report 12, Paper 111, Centre for Computational Geostatistics, University of Alberta.

Deutsch, C. and Tran, T. (1999). Simulation of Deepwater Lobe Geometries with Object Based Modelling: LOBESIM.

Deutsch, C. V. (1992). *Annealing Techniques Applied to Reservoir Modeling and the Integration of Geological and Engineering (Well Test) Data*. PhD thesis, Stanford University.

Deutsch, C. V. (2002). *Geostatistical Reservoir Modeling*. Oxford University Press, Oxford, N.Y.

Deutsch, C. V. (2010). Estimation of vertical permeability in the mcmurray formation. *Journal of Canadian Petroleum Technology*, 49(12):10–18.

Deutsch, C. V. and Journel, A. G. (1998). *GSLIB: Geostatistical Software Library and User's Guide*. Oxford University Press, New York, 2nd edition.

Deutsch, C. V. and McLennan, J. A. (2005). *Guide to SAGD (Steam Assisted Gravity Drainage) Reservoir Characterization Using Geostatistics*. Centre for Computational Geostatistics, University of Alberta, guidebook series vol. 3 edition.

Deutsch, C. V. and Tran, T. T. (1998). Fluvsim: A program for object-based stochastic modeling of fluvial depositional systems. *Computers & Geosciences*, page submitted.

Deutsch, C. V. and Wang, L. (1996). Hierarchical object-based stochastic modeling of fluvial reservoirs. *Mathematical Geology*, 28(7):857–880. M3: 10.1007/BF02066005.

Dorjes, J. and Howard, J. (1975). Estuaries of the Georgia coast, USA: sedimentology and biology. IV. *Fluvial-marine transition indicators in an estuarine environment, Ogeechee River-Ossabaw Sound: Senckenbergiana Maritima*, 7:137–179.

Dunbar, C. and Rodgers, J. (1957). *Principles of stratigraphy*, volume 752. Wiley New York.

ERCB (2012). ST98-2012: Albertas energy reserves 2011 and supply/demand outlook 2012-2021. Energy Resources Conservation Board, available online at : `http://www.ercb.ca/sts/ST98/ST98-2012.pdf`.

Evensen, G. (2009). *Data Assimilation: the ensemble Kalman filter*. Springer, Bergen.

Fagherazzi, S., Bortoluzzi, A., Dietrich, W. E., Adami, A., Lanzoni, S., Marani, M., and Rinaldo, A. (1999). Tidal networks 1. automatic network extraction and preliminary scaling features from digital terrain maps. *Water Resour. Res.*, 35(12):3891–3904.

Fagherazzi, S. and Furbish, D. (2001). On the shape and widening of salt marsh creeks. *Journal of Geophysical Research*, 106(C1):991–1003.

Fagherazzi, S., Gabet, E. J., and Furbish, D. J. (2004). The effect of bidirectional flow on tidal channel planforms. *Earth Surface Processes and Landforms*, 29(3):295–309. CP: Copyright 2004 John Wiley & Sons, Ltd.; PN: 0197-9337.

Fenik, D. R. (2010). Practical use of multiple geostatistical realizations in petroleum engineering. Master's thesis, University of Alberta, Edmonton, Alberta.

Ferguson, R. I. (1976). Disturbed periodic model for river meanders. *Earth Surface Processes*, 1(4):337–347. CP: Copyright 1976 John Wiley & Sons, Ltd; PN: 0360-1269.

Flach, P., Matthie, J., Survey, A. G., and Services, A. R. C. G. (1984). *Oil Sands Geology: Athabasca Deposit North*. Geological Survey Dept., Alberta Research Council.

Flach, P. and Mossop, G. (1985). Depositional environments of the Lower Cretaceous McMurray Formation. *Athabasca oil sands, Alberta: AAPG Bulletin*, 69(8):1195–1207.

Fox, A. J. (1988). The Lower Cretaceous McMurray Formation in the subsurface of Syncrude Oil Sands lease 17, Athabasca Oil Sands, northeastern Alberta

a physical sedimentological study in an area of exceptional drill core control. Master's thesis, University of Alberta.

Fustic, M. (2007). Stratigraphic dip analysis - a novel application for detailed geological modeling of point bars, and predicting bitumen grade, McMurray Formation, Muskeg River mine, northeast Alberta. *Natural Resources Research*, 16(1):31–43.

Galli, A., Beucher, H., Le Loch, G., and Doligez, B. (1994). The pros and cons of the truncated Gaussian method. *Geostatistical simulations*, pages 217–233.

Gates, I. and Chakrabarty, N. (2006). Optimization of steam assisted gravity drainage in mcmurray reservoir. *Journal of Canadian Petroleum Technology*, 45(9).

Georgsen, F. and Omre, H. (1993). *Combining Fibre Process and Gaussian Random Functions for Modeling Fluvial Reservoirs*, volume 2 of *Geostatistics Troiae*, pages 425–440. Kluwer.

Gómez-Hernández, J. (2005). Geostatistics. *Hydrogeophysics*, pages 59–83.

Gómez-Hernández, J., Sahuquillo, A., and Capilla, J. (1997). Stochastic simulation of transmissivity fields conditioning to both transmissivity and piezometric data -1. theory. *Journal of Hydrology*, 203:162–174.

Government of Alberta, . (2008). Alberta's oil sands: *Opportunity, Balance.* available online at: `http://www.environment.alberta.ca/documents/Oil_Sands_Opportunity_Balance.pdf`.

Grabau, A. (1913). *Principles of stratigraphy.* AG Seiler and company.

Guardiano, F. and Srivastava, R. (1993). *Multivariate geostatistics: Beyond bivariate moments*, pages 133–144. Kluwer Academic.

Haldorsen, H. and Lake, L. (1984). A new approach to shale management in field-scale models. *Old SPE Journal*, 24(4):447–457.

Haldorsen, H. and MacDonald, C. (1987). Stochastic modeling of underground reservoir facies (smurf). In *SPE Annual Technical Conference and Exhibition*.

Hatloy, A. S. (1995). *Numerical Facies Modeling Combining Deterministic and Stochastic Method*, pages 109–120. Stochastic Modeling and Geostatistics: Principles, Methods and Case Studies. AAPG Computer Applications in Geology.

Hauge, R., Holden, L., and Syversveen, A. (2007). Well conditioning in object models. *Mathematical geology*, 39(4):383–398.

Hayes, M. (1979). Barrier island morphology as a function of tidal and wave regime. *Barrier islands*, pages 1–28.

Hein, F. and Cotterill, D. (2006). The Athabasca Oil Sands–a regional geological perspective, Fort McMurray area, Alberta, Canada. *Natural Resources Research*, 15(2):85–102.

Hein, F. J., Cotterill, D. K., and Berhane, H. (2000). An atlas of lithofacies of the McMurray Formation Athabasca Oil Sands deposit, northeastern Alberta: Surface and subsurface. Technical Report 2000-07, Alberta Energy and Utilities Board.

Holden, L., Hauge, R., Skare, Ø., and Skorstad, A. (1998). Modeling of fluvial reservoirs with object models. *Mathematical Geology*, 30(5):473–496.

Hosseini, A. and Deutsch, C. (2010). Conditional simulation of subseismic megakarstic features. Technical Report 12, Paper 210, Centre for Computational Geostatistics, University of Alberta.

Hosseini, A., Leuangthong, O., and Deutsch, C. (2008). An integrated approach to permeability modeling using micro-models. In *International Thermal Operations and Heavy Oil Symposium*.

Howard, A. (1992). Modeling channel migration and floodplain sedimentation in meandering streams. In Carling, P. A. and Petts, G., editors, *Lowland Floodplain Rivers: geomorphological Perspectives*. John Wiley & Sons Ltd.

Howard, A. (1996). *Modelling channel evolution and floodplain morphology*, pages 15–62. Floodplain Processes. John Wiley & Sons Ltd.

Hu, L. and Jenni, S. (2005). History matching of object-based stochastic reservoir models. *SPE Journal*, 10(3):312–323.

Hubbard, S., Smith, D., Nielsen, H., Leckie, D., Fustic, M., Spencer, R., and Bloom, L. (2011). Seismic geomorphology and sedimentology of a tidally influenced river deposit, lower cretaceous athabasca oil sands, alberta, canada. *AAPG bulletin*, 95(7):1123.

Ikeda, S., Parker, G., and Sawai, K. (1981). Bend theory of river meanders. part 1. linear development. *Journal of Fluid Mechanics*, 112:363–377.

Isaaks, E. (1990). *The application of Monte Carlo methods to the analysis of spatially correlated data*. PhD thesis, Stanford University, Stanford, CA.

Isaaks, E. and Srivastava, R. (1989). *An Introduction to Applied geostatistics*, volume 561. Oxford University Press New York.

Jay, D. (1991). Green's law revisited: tidal long-wave propagation in channels with strong topography. *Journal of geophysical research*, 96(C11):20585–20.

Joumel, A. and Huijbregts, C. (1978). *Mining geostatistics*. Academic Press.

Journel, A. and Alabert, F. (1989). Non-Gaussian data expansion in the earth sciences. *Terra Nova*, 1:134.

Journel, A., Gundeso, R., Gringarten, E., and Yao, T. (1998). Stochastic modelling of a fluvial reservoir: a comparative review of algorithms. *Journal of Petroleum Science and Engineering*, 21(1):95–121.

Journel, A. and Zhang, T. (2006). The necessity of a multiple-point prior model. *Mathematical Geology*, 38(5):591–610.

Journel, A. G. (1983). Non-parametric estimation of spatial distributions. *Mathematical Geology*, 15(3):445–468.

Kirwan, M. and Murray, A. (2007). A coupled geomorphic and ecological model of tidal marsh evolution. *Proceedings of the National Academy of Sciences*, 104(15):6118.

Kisman, K. and Yeung, K. (1995). Numerical study of the SAGD process in the burnt lake oil sands lease. In *SPE International Heavy Oil Symposium*.

Kolbjørnsen, O. and Abrahamsen, P. (2005). Theory of the cloud transform for applications. *Geostatistics Banff 2004*, pages 45–54.

Krige, D. (1951). *A statistical approach to some mine valuation and allied problems on the Witwatersrand*. Univ. of the Witwatersrand.

Kumar, A. and Deutsch, C. V. (2010). Optimal drainage area and surface pad positioning for SAGD development. Technical Report 12, paper 12, Centre for Computational Geostatistics, University of Alberta.

Langenberg, C. W., Hein, F. J., Lawton, D., and Cunningham, J. (2002). Seismic modeling of fluvial-estuarine deposits in the athabasca oil sands using ray-tracing techniques, steepbank river area, northeastern alberta. *Bulletin of Canadian Petroleum Geology*, 50(1):178–204. 10.2113/50.1.178.

Lanzoni, S. and Seminara, G. (1998). On tide propagation in convergent estuaries. *Journal of Geophysical Research*, 103(C13):30793.

Le Loch, G. and Galli, A. (1997). Truncated plurigaussian method: theoretical and practical points of view. *Geostatistics wollongong*, 96:211–222.

Lettley, C. D. (2004). Elements of a genetic framework for inclined heterolithic strata of the McMurray Formation, northeast Alberta. Master's thesis, University of Alberta.

Lopez, S., Galli, A., and Cojan, L. (2001). Fluvial meandering channelized reservoirs: a stochastic and process-base approach. In *2001 Annual Conference of the IAMG, Cancun, Mexico, SPE*.

Lyster, S. (2009). *Simulation of Geologic Phenomena Using Multiple-Point Statistics in a Gibbs Sampler Algorithm*. PhD thesis, University of Alberta.

Maharaja, A. (2008). Tigenerator: Object-based training image generator. *Computers & Geosciences*, 34(12):1753–1761.

Mallet, J. (2002). *Geomodeling*. Oxford University Press, USA.

Manchuk, J. G. (2010). *Geostatistical Modeling of Unstructured Grids for Flow Simulation*. PhD thesis, University of Alberta, Edmonton, Alberta.

Marani, M., Lanzoni, S., and Zandolin, D. (2002). Tidal meanders. *Water Resour. Res.*, 38(11):1225.

Marciano, R., Wang, Z., Hibma, A., de Vriend, H., and Defina, A. (2005). Modeling of channel patterns in short tidal basins. *Journal of geophysical research*, 110(F01001):1–13.

Matheron, G. (1962). Traité de Géostatistique Appliquée. Vol. 1 et 2. *Techip. París*.

Matheron, G., Beucher, H., de Fouquet, C., Galli, A., Guerillot, D., and Ravenne, C. (1987). Conditional simulation of the geometry of fluvio-deltaic

reservoirs. In *SPE Annual Technical Conference and Exhibition*, Dallas, Texas. 1987 Copyright 1987, Society of Petroleum Engineers.

McLean, F. H. (1917). Athabasca river section, Alberta. Technical report, Geological Survey of Canada.

McLennan, J., Deutsch, C., Garner, D., Mus, E., Wheeler, T., and Richy, J. (2006). SAGD Permeability Modeling Using Geostatistics and Minimodels. In *SPE Annual Technical Conference and Exhibition*.

McLennan, J. A. and Deutsch, C. V. (2004). SAGD reservoir characterization using geostatistics: Application to the Athabasca Oil Sands, Alberta, Canada. Technical Report 6, paper 204, Centre for Computational Geostatistics, University of Alberta.

Miall, A. (1985). Architectural-element analysis: a new method of facies analysis applied to fluvial deposits. *Earth-Science Reviews*, 22(4):261–308.

Millar, R. (2000). Influence of bank vegetation on alluvial channel patterns. *Water Resources Research*, 36(4):1109–1118.

Mossop, G. D. and Flach, P. D. (1983). Deep channel sedimentation in the Lower Cretaceous McMurray Formation, Athabasca oil sands, Alberta. *Sedimentology*, 30(4):493–509.

Musial, G., Reynaud, J.-Y., Gingras, M., Fenies, H., Labourdette, R., and Parize, O. (2012). Subsurface and outcrop characterization of large tidally influenced point bars of the Cretaceous McMurray Formation (Alberta, Canada). *Sedimentary Geology*, 279:156 – 172.

Oliver, D. (2002). Conditioning channel meanders to well observations. *Mathematical geology*, 34(2):185–201.

Ømre, H. (1992). Heterogeneity models. In *SPOR Monograph: Recent Advances in Improved Oil Recovery Methods for North Sea Sandstone Reservoirs, Norway*. Norwegian Petroleum Directorate.

Øren, P. and Bakke, S. (2002). Process based reconstruction of sandstones and prediction of transport properties. *Transport in Porous Media*, 46(2):311–343.

Pemberton, S., Flach, P., and Mossop, G. (1982). Trace fossils from the Athabasca oil sands, Alberta, Canada. *Science*, 217(4562):825.

Pyrcz, M. (2004). *The Integration of Geologic Information into Geostatistical Models*. PhD thesis, University of Alberta.

Pyrcz, M., Boisvert, J., and Deutsch, C. (2009). Alluvsim: A program for event-based stochastic modeling of fluvial depositional systems. *Computers & Geosciences*, 35(8):1671–1685.

Pyrcz, M., Catuneanu, O., and Deutsch, C. (2005). Stochastic surface-based modeling of turbidite lobes. *AAPG bulletin*, 89(2):177.

Pyrcz, M. and Deutsch, C. (2004). Stochastic modeling of inclined heterolithic stratification with the bank retreat model. In *Proceedings of the 2004 Canadian Society of Petroleum Geologists. Canadian Well Logging Society and Canadian Heavy Oil Association Joint Convention (ICE2004), Calgary, Canada*.

Pyrcz, M., McHargue, T., Clark, J., Sullivan, M., and Strebelle, S. (2012). Event-based geostatistical modeling: Description and applications. *Geostatistics Oslo 2012*, pages 27–38.

Pyrcz, M. and Strebelle, S. (2008). Event-based geostatistical modeling. In Ortiz, J. and Emery, X., editors, *Geostatistics Santiago 2008*. Springer, Netherlands.

Quint, A. (2003). Scalable vector graphics. *Multimedia, IEEE*, 10(3):99–102.

Rahmani, R. (1988). Estuarine tidal channel and nearshore sedimentation of a Late Cretaceous epicontinental sea, Drumheller, Alberta, Canada. *Tide-influenced sedimentary environments and facies*, pages 433–471.

Ranger, M. and Gingras, M. (2003). Geology of the Athabasca oil sands, field guide and overview. *Canadian Society of Petroleum Geologists, Calgary*, 123.

Ranger, M. and Pemberton, S. (1997). Elements of a stratigraphic framework for the McMurray Formation in South Athabasca area, Alberta. *Petroleum Geology of the Cretaceous Mannville Group, Western Canada. SG Pemberton and DP James (eds.). Canadian Society of Petroleum Geologists, Memoir*, 18:263–291.

Rider, M. (1986). *The geological interpretation of well logs*. John Wiley and Sons, Inc., New York, NY.

Schafmeister, M., Makowski, K., and Tetzlaff, D. (2010). Geologic object modeling with hierarchical attachment probabilities applied to a glacial environment. In *IAMG 2010 Meeting, Budapest*.

Schroeder, W., Martin, K., Martin, K., and Lorensen, B. (1998). *The visualization toolkit*. Prentice Hall PTR.

Shin, H., Hwang, T., and Chon, B. (2012). Optimal grid system design for SAGD simulation. In *SPE Heavy Oil Conference Canada*, Calgary, Alberta, Canada.

Shmaryan, L. and Deutsch, C. (1999). Object-based modeling of fluvial/deepwater reservoirs with fast data conditioning: methodology and case studies. In *SPE Annual Technical Conference and Exhibition*.

Slatt, R. (2006). *Stratigraphic Reservoir Characterization for Petroleum Geologists, Geophysicists, and Engineers*. Elsevier, Oxford.

Smith, D. (1985). Modern analogues of the mcmurray formation channel deposits, sedimentology of meso-tidal-influenced meandering river point bars with inclined beds of alternating mud and sand. *Alberta Oil Sands Technology and Research Authority, Final Rept. for Research Project*.

Smith, D. (1987). Meandering river point bar lithofacies models: modern and ancient examples compared. *Recent Developments in Fluvial Sedimentology: SEPM, Special Publication*, 39:83–91.

Smith, D. (1988). Modern point bar deposits analogous to the Athabasca oil sands, Alberta, Canada. *Tide-influenced sedimentary environments and facies*, pages 417–432.

Stewart, G., MacCallum, G., and of Petroleum Geologists, C. S. (1978). *Athabasca Oil Sands Guide Book*. Canadian Society of Petroleum Geologists.

Strebelle, S. (2002). Conditional simulation of complex geological structures using multiple-point statistics. *Mathematical Geology*, 34(1):1–21.

Strebelle, S. and Journel, A. (2000). Sequential simulation drawing structures from training images. In Kleingeld, W. and Krige, D., editors, *6th International Geostatistics Congress*, page 12 p.

Sun, T., Meakin, P., Jøssang, T., and Schwarz, K. (1996). A simulation model for meandering rivers. *Water Resour. Res.*, 32(9):2937–2954.

Teichert, C. (1958). Concepts of facies. *AAPG Bulletin*, 42(11):2718.

Tetzlaff, D. (1990). Limits to the predictive ability of dynamic models the simulation clastic sedimentation. *Quantitative Dynamic Stratigraphy*, pages 3–20.

Tetzlaff, D. and Harbaugh, J. (1989). *Simulating clastic sedimentation*. New York, NY; Van Nostrand Reinhold Co. Inc.

Thomas, R. G., Smith, D. G., Wood, J. M., Visser, J., Calverley-Range, E. A., and Koster, E. H. (1987). Inclined heterolithic stratificationterminology, description, interpretation and significance. *Sedimentary Geology*, 53(1-2):123–179.

Viseur, S., Shtuka, A., and Mallet, J. (1998). New fast, stochastic, boolean simulation of fluvial deposits. In *SPE Annual Technical Conference and Exhibition*.

Waite, M., Johansen, S., Betancourt, D., and Acharya, U. (2004). Modeling of Scale-Dependent Permeability Using Single-Well Micro-Models: Application to Hamaca Field, Venezuela. In *SPE International Thermal Operations and Heavy Oil Symposium and Western Regional Meeting*.

Wen, R. (2004). 3d modeling of stratigraphic heterogeneity in channelized reservoirs: Methods and applications in seismic attribute facies classification: Cseg recorder, p38-45.

Wen, X., Deutsch, C., and Reza, Z. (2005). Integration of production data in generating reservoir models. Technical report, Centre for Computational Geostatistics, University of Alberta.

Wightman, D., of Energy. External Relations, A. D., Communications, Survey, A. G., and Council, A. R. (1995). *Resource characterization of the McMurray/Wabiskaw Deposit in the Athabasca Oil Sands Area: a synthesis*. Alberta Dept. of Energy, External Relations and Communications.

Wightman, D. M. and Pemberton, S. G. (1997). The Lower Cretaceous (Aptian) McMurray Formation; an overview of the fort McMurray area, northeastern Alberta. *Memoir - Canadian Society of Petroleum Geologists*, 18:312–344. ID: georef;1999035126.

Xie, Y., Cullick, A. S., and Deutsch, C. V. (2001). Surface-geometry and trend

modeling for integration of stratigraphic data in reservoir models. In *SPE Western Regional Meeting*, Bakersfield, California.